University of Alberta

Analysis of Energy Detection in Cognitive Radio Networks

by

Saman Udaya Bandara Atapattu

A thesis submitted to the Faculty of Graduate Studies and Research
in partial fulfillment of the requirements for the degree of

Doctor of Philosophy
in
Communications

Department of Electrical and Computer Engineering

Fall 2013
Edmonton, Alberta

Dedicated to my parents...

Abstract

Cognitive radio is one of the most promising technologies to address the spectrum scarcity problem. Cognitive radio requires spectrum sensing, which is used by unlicensed users to opportunistically access the licensed spectrum. Spectrum sensing using energy detection offers low-cost and low-complexity. In this thesis, a comprehensive performance analysis of energy detection based spectrum sensing is developed. Detection performance over composite (fading and shadowing) channels is first investigated using the K and K_G channel models. To further facilitate analysis of energy detection over different wireless channels, a unified channel model based on a mixture gamma distribution is developed. The unified model can accurately represent most existing channel models. A single-value performance metric, the area under the receiver operating characteristic curve, is proposed to measure the overall detection capability, and is investigated over various wireless fading channels. The energy detection based cooperative spectrum sensing is also studied, which can largely improve the detection performance. Since spectrum sensing is required to identify activities of licensed users at a very low signal-to-noise ratio (SNR), performance of energy detection with low SNR is also analyzed in this thesis.

$\sim$

Acknowledgement

I greatly appreciate my co-supervisors, Dr. Chintha Tellambura and Dr. Hai Jiang, for their excellent and prompt feedback, which has allowed me to perform my research timely and efficiently. Their expertise on wireless communications is significantly influential on my research. I wish to thank them for not only being as research supervisors but also for their constant support of my personal life.

My thanks go to members of my PhD candidacy committee and PhD examining committee, Dr. Witold Krzymień, Dr. Peter Hooper, Dr. Scott Dick, Dr. Xiaodai Dong (external examiner-University of Victoria), Dr. Yindi Jing, and Dr. Majid Khabbazian. I would like to express my gratitude to the faculty and the staff of the Department of Electrical and Computer Engineering for their full support. I am especially thankful to Dr. Nandana Rajatheva who introduced me to Dr. Chintha Tellambura. I greatly appreciate his constant research collaboration.

I gratefully acknowledge the funding sources that made my research work possible. I was funded by the Alberta Innovates Technology Futures (AITF) and the Killam Trusts in the form of AITF Graduate Scholarship and Izaak Walton Killam Memorial Scholarships, respectively.

I am grateful to my fellow lab-mates who always create a pleasant lab environment. I thank to Hans and Frieda who provide accommodation and make my life enjoyable in Edmonton. I also thank to all teachers, relatives, and friends who help me in numerous ways.

Finally, I would like to express my deep gratitude and respect to my family who gives me unequivocal supports throughout my life.

Thank you !!!

~

Table of Contents

1 Introduction **1**

1.1 Wireless Communications 1

1.2 Cognitive Radio 3

1.2.1 Standardization and Applications of Cognitive Radio 4

1.2.2 Dynamic Spectrum Access 5

1.2.3 Spectrum Sensing 6

1.2.4 Spectrum Sensing Techniques 7

1.3 Motivation 8

1.4 Problem Statements 9

1.5 Thesis Outline 10

2 Background **13**

2.1 Mobile Radio Channel 13

2.1.1 Small-Scale Fading and Large-Scale Fading 14

2.1.2 Composite Fading 15

2.2 System Model of Spectrum Sensing 16

2.3 Spectrum Sensing via Energy Detection 17

2.4 Test Statistic of Energy Detector 18

2.4.1 Signal Models 19

2.4.2 Distribution of Test Statistics 20

2.4.3 CLT Approach 22

2.5 Design Parameters 24

2.5.1 Threshold 24

2.5.2 Number of Samples 24

2.6 IEEE 802.22 Standard 25
2.7 Cooperative Spectrum Sensing 26

3 Energy Detection over Composite Fading and Shadowing Channels 28
3.1 Introduction 28
3.2 Average Detection Probability 29
3.2.1 With No-Diversity Reception 30
3.2.2 With Diversity Reception 34
3.3 Numerical and Simulation Results 36
3.4 Conclusion 40

4 A Mixture Gamma Distribution to Model the SNR of Wireless Channels 42
4.1 Introduction 42
4.2 Mixture Gamma Distribution 44
4.3 MG Distribution for Typical mobile radio channels 45
4.3.1 Nakagami-lognormal Channel 46
4.3.2 K and K_G Channels 46
4.3.3 η-μ Channel 47
4.3.4 Nakagami-q (Hoyt) Channel 49
4.3.5 κ-μ Channel 49
4.3.6 Nakagami-n (Rician) Channel 50
4.3.7 Rayleigh and Nakagami-m Channels 51
4.4 Determination of the Number S 51
4.4.1 Accuracy of MG Distribution to Approximate mobile radio channel SNR 52
4.4.2 Moment Matching 54
4.4.3 Complexity of Determining S 55
4.5 MG Channel Performance Analysis 55
4.6 Numerical Results 58
4.7 Conclusions 60

5 Area under the ROC Curve of Energy Detection **61**

5.1 Introduction 61

5.2 AUC for Instantaneous SNR 63

5.2.1 Complementary AUC 64

5.2.2 Partial AUC 65

5.3 Average AUC over Fading Channels 65

5.3.1 No-Diversity Reception 66

5.3.2 Diversity Reception 68

5.4 Numerical and Simulation Results 70

5.5 Conclusions 73

6 Energy Detection based Cooperative Spectrum Sensing **74**

6.1 Introduction 74

6.2 Non-Cooperative

Cases 76

6.3 Data Fusion 78

6.3.1 Cooperative Scheme 78

6.3.2 Analysis of Average Detection Probability 80

6.3.3 Multi-hop cooperative Sensing 82

6.4 Decision Fusion 84

6.4.1 k-out-of-n Rule 84

6.4.2 Multi-hop Cooperative Sensing 86

6.5 Numerical and Simulation Results 86

6.6 Conclusion 90

7 Energy Detection in Low SNR **91**

7.1 Introduction 91

7.2 Low-SNR Model 93

7.3 Performance Analysis at a Low SNR 94

7.3.1 Average Missed-Detection Probability 96

7.3.2 Average AUC 99

7.4 Threshold Selection 100

7.5 Numerical/Simulation Results and Discussion 106
7.6 Conclusion 113

8 Conclusion and Future Work **115**

Bibliography **118**

A Proofs for Chapter 3 **133**
A.1 Derivation of $\overline{P_d^K}$ 133
A.2 Derivation of $\overline{P_d^{K_G}}$ 134

B Proofs for Chapter 5 **135**
B.1 Necessary Integrations 135
B.2 Derivation of $\mathcal{A}(\gamma)$ in (5.7) 136
B.3 Derivation of $\bar{\mathcal{A}}_{Nak}$ in (5.13) 137

C Expressions for Chapter 6 **138**
C.1 Calculation of Residue 138
C.2 Cascaded BSC 139

D Proofs for Chapter 7 **140**
D.1 Proof of Theorem 7.1 140
D.2 Optimal Threshold for AWGN Channel 141

List of Tables

3.1 Number of terms required to get the accuracy up to four decimal points. 37

4.1 The selected value of S and the nearest integer values of the first three moments of both exact and approximated SNR distributions of κ-μ channel. 54

7.1 AUC approximations (the numbers in front of the brackets) versus the area under the simulated curves (the numbers in the brackets) for AWGN, Rayleigh, Nakagami-4 channels in Fig. 7.2 and SLC ($L = 2, 3$) in Fig. 7.3. 109

7.2 Numerically calculated normalized threshold values ($\hat{\lambda}_f^*$, $\hat{\lambda}_{md}^*$, $\hat{\lambda}_e^*$, $\hat{\lambda}^*$) and numerically calculated error probabilities (P_f, P_{md}, P_e) at $\hat{\lambda}_e^*$ for AWGN, Rayleigh and Nakagami-4 channels, SLC, and cooperative spectrum sensing when $N = 2 \times 10^6$ and $\bar{\gamma} = -20$ dB. The numbers in brackets are approximated $\hat{\lambda}_{\text{md}}^*$ and $\hat{\lambda}_e^*$ for Rayleigh fading channels based on (7.22) and (7.25). 110

7.3 The regions of N for different cases of $\lambda_f^*, \lambda_{md}^*, \lambda_e^*$, the minimal sensing time τ_{min} at $f_s = 1$ MHz, and the minimal sampling rate $f_{s,\text{min}}$ at $\tau = 2$ seconds. 113

List of Figures

1.1 Radio spectrum allocated for wireless communications 1

1.2 A basic cognitive radio network architecture 5

2.1 The conventional energy detectors: (a) analog and (b) digital 17

2.2 The exact and approximated (CLT) CDFs of the test statistic for **S1** and **S2** with $2\sigma_w^2 = 1$ and $\gamma = 5$dB 23

2.3 Cooperative spectrum sensing in a cognitive radio network. 26

3.1 Energy detection with MRC 34

3.2 (a) Comparison of analytical expressions (3.4) and (3.6) with numerical approximations by the Gaussian-Legendre method, and Monte Carlo simulations ($N = 2$, $k = 5.5$ and $\bar{\gamma} = 10$ dB); (b) Comparison of exact I_K with approximation in (3.9). 37

3.3 (a) ROC curves for the K channel model with different k ($N = 1$, $\bar{\gamma} = 0,\ 5,\ 15$ dB); (b) ROC curves for K_G channel model with different fading parameters, m ($k = 5.5$, $N = 1$, $\bar{\gamma} = 5,\ 10$ dB). . . . 38

3.4 ROC curves for L-branch MRC and SC diversity receptions with K channel model ($N = 3$, $k = 6$, $\bar{\gamma} = 5$ dB) 39

3.5 Comparison of K channel model with Rayleigh-lognormal channel . 40

4.1 (a) The MSE versus S when the GL distribution is approximated by K_G, $\mathcal{G}$, Gamma, Log-normal and MG for $m = 2.7$, $\lambda = 1$, $\mu = 0$, and the average SNR = 0 dB; (b) The KL divergence ($\mathcal{D}_{KL}$) versus S when the GL distribution is approximated by K_G, $\mathcal{G}$, Gamma, Log-normal and MG for $m = 2.7$, $\lambda = 1$, $\mu = 0$, and the average SNR = 0 dB. 51

4.2 (a) The exact CDF of GL distribution and the CDFs of the K_G, $\mathcal{G}$, Log-normal, Gamma and MG approximations. The parameter values are $m = 2.7$, $\lambda = 1$, $\mu = 0$, and the average SNR = 0 dB. The number of components in the MG model is $S = 5$; (b) Exact SNR distributions of K_G, Nakagami-q (Hoyt), η-μ (Format 1), Rician and κ-μ channel models and their MG approximations. . 53
4.3 The average capacity of an SISO channel versus average SNR over different fading channels 58
4.4 (a) The outage probability of an SISO channel versus average SNR over different fading channels for $\gamma_{th} = 0$ dB; (b) The SER of an SISO channel versus average SNR over different fading channels for BPSK and QAM. 59

5.1 Energy Detection with SLC 69
5.2 The average AUC versus the average SNR for different $N = 1, 3, 5$ with no diversity reception under Nakagami-2 fading channel 70
5.3 (a) The average AUC versus the average SNR for different $m = 1, 3, 5$ with no diversity reception under Nakagami-m fading channel; (b) The average CAUC versus the average SNR for different $m = 1, 3, 5$ with no diversity reception under Nakagami-m fading channel. 71
5.4 (a) The average CAUC versus the average SNR for different fading channels based on the MG model; (b) The average CAUC versus the average SNR for different $L = 1, 2, 3$ with diversity reception under Rayleigh fading channel. 72

6.1 Illustration of a multiple-cooperative node network 78
6.2 ROC curves of an energy detector over Rayleigh and Rayleigh-lognormal fading channels 87
6.3 (a) ROC curves for different number of cooperative nodes over Rayleigh fading channels $\overline{\gamma}$ = 5 dB; (b) ROC curves with the direct link over Rayleigh fading channels. 88

6.4 (a) ROC curves for OR, AND and Majority fusion rules with error-free reporting channels; (b) ROC curves for OR, AND and the Majority fusion rules with Rayleigh faded reporting channels. 89
6.5 ROC curves for a multi-hop cooperative network 90

7.1 The exact and approximated (low-SNR) CDFs of the test statistic which is modeled using the CLT, with $\sigma = 1$ and $N = 2 \times 10^3$. **S1** is considered as an example. The exact CDF is based on (7.1) and approximated CDF is based on (7.2). 95
7.2 Approximated (low-SNR analysis) ROC curves (represented by solid lines) and simulated ROC curves (represented by discrete marks) of AWGN, Rayleigh and Nakagami-4 fading channels for $N = 2\times10^3$ and $N = 2 \times 10^5$ at -20 dB average SNR. 106
7.3 Approximated (low-SNR analysis) ROC curves (represented by solid lines) and simulated ROC curves (represented by discrete marks) of SLC when $L = 2, 3$ and cooperative spectrum sensing when $K = 2, 3$ for $N = 2 \times 10^3$ and $N = 2 \times 10^6$ over Rayleigh fading at -20 dB average SNR. 107
7.4 Approximated total error rate (represented by solid lines) and simulated total error rate (represented by discrete marks) versus normalized threshold of (a) AWGN, Rayleigh and Nakagami-4 channels and cooperative spectrum sensing ($K = 2$) over Rayleigh fading; (b) SLC ($L = 3$) over Rayleigh fading, for $N = 2 \times 10^6$ at -20 dB average SNR. 109
7.5 Analytical error rates (represented by lines) and simulated error rates (represented by discrete marks) at the optimal threshold value (total error: P_e^*; false alarm: P_f^*; and missed-detection: P_{md}^*) versus the number, N, of samples at -20 dB average SNR for (a) AWGN; (b) Rayleigh; (c) Nakagami-4 fading channels. 111

7.6 Analytical error rates (represented by lines) and simulated error rates (represented by discrete marks) at the optimal threshold value (total error: P_e^*; false alarm: P_f^*; and missed-detection: P_{md}^*) versus the number, N, of samples at -20 dB average SNR for (a) SLC when $L = 2, 3$; (b) cooperative spectrum sensing when $K = 2, 3$, over Rayleigh fading. 112

List of Abbreviations

Abbreviation	Definition
ADC	analog-to-digital converter
AF	amplify-and-forward
AM	amplitude modulation
AUC	Area Under the receiver operating characteristic Curve
AWGN	additive white Gaussian noise
BER	bit error rate
BPSK	binary phase shift keying
BSC	binary symmetric channel
CAUC	complementary AUC
CDF	cumulative distribution function
CLT	central limit theorem
CSCG	circularly symmetric complex Gaussian
CSI	channel-state information
DSA	dynamic spectrum access
EGC	equal gain combining
FCC	Federal Communications Commission
GL	gamma-lognormal
i.i.d.	independent and identically distributed
KL	Kullback-Leibler
LTE	long term evolution
MG	mixture gamma
MGF	moment generating function
MIMO	multiple-input multiple-output

Abbreviation	Definition
MRC	maximal ratio combining
MSE	mean square error
NL	Nakagami-lognormal
OFDM	orthogonal frequency division multiplexing
PDF	probability density function
PSK	phase shift keying
RL	Rayleigh-lognormal
ROC	receiver operating characteristic
RV	random variable
SC	selection combining
SER	symbol error rate
SISO	single-input single-output
SLC	square-law combining
SNR	signal-to-noise ratio
TV	television
UWB	ultra-wideband
WLAN	wireless local area network
WRAN	wireless regional area network

List of Symbols

- Basic arithmetic, set, and calculus notations have standard definitions.

Elementary & Special Functions

Notation	Definition
$\lceil \cdot \rceil$	ceiling function
$\Gamma(\cdot)$	Gamma function
$\Gamma(\cdot, \cdot)$	upper incomplete Gamma function
$\gamma(\cdot, \cdot)$	lower incomplete Gamma function
$\mathrm{Erfc}(\cdot)$	Gauss error function
${}_1F_1(\cdot;\cdot;\cdot)$	confluent hypergeometric function of the first kind
${}_2F_1(\cdot;\cdot;\cdot)$	Gaussian hypergeometric function
${}_1\tilde{F}_1(\cdot;\cdot;\cdot)$	regularized confluent hypergeometric function of the first kind
${}_2\tilde{F}_1(\cdot;\cdot;\cdot)$	regularized Gaussian hypergeometric function
$G_{m,n}^{p,q}$	Meijer-G function
$\mathcal{I}_\nu(\cdot)$	modified Bessel function of the first kind of order ν
$\mathcal{K}_\nu(\cdot)$	modified Bessel function of the second kind of order ν
$\ln(\cdot)$	natural logarithm
$\log_2(\cdot)$	logarithm to base 2
$Q(\cdot)$	Gaussian-Q function
$Q_N(\cdot, \cdot)$	generalized Marcum-Q function
$U(\cdot;\cdot;\cdot)$	confluent hypergeometric function of the second kind

Probability & Statistics

Let X be a random variable, and $\mathcal{D}$ be an arbitrary event.

Notation	Definition
$\mathbb{E}\{\cdot\}$	expectation
$f_X(\cdot)$	probability density function (PDF) of X
$f_{X\|Y}(\cdot)$	PDF of X given Y

$F_X(\cdot)$	cumulative distribution function (CDF) of X
$\mathcal{M}_X(\cdot)$	moment generating function (MGF) of X
$\mathcal{P}\left[\mathcal{D}\right]$	probability of $\mathcal{D}$
$X \sim \mathcal{CN}(\cdot, \cdot)$	circularly symmetric complex Gaussian (CSCG) random variable X
$X \sim \mathcal{N}(\cdot, \cdot)$	Gaussian random variable X
$\mathbb{V}\text{ar}\{\cdot\}$	variance

Miscellaneous

Notation	**Definition**
$\lvert\mathbf{a}\rvert$	absolute value of **a**
$k!$	factorial of k
$\binom{n}{k}$	binomial coefficient n choose k
$(x)_s$	pochhammer symbol
$\arg\min_i (a_i)$	index i corresponding to the smallest a_i
$\mathcal{H}_i$	Hypothesis i
$\lim_{x \to a} f(x)$	the limit of function $f(x)$ as x tends to a
$\max(a_1, a_2)$	maximum of scalars a_1 and a_2
$\max(a_1, \ldots, a_n)$	maximum of all scalars a_i for relevant i; also $\max_i (a_i)$
$\min(a_1, a_2)$	minimum of scalars a_1 and a_2
$\min(a_1, \ldots, a_n)$	minimum of all scalars a_i for relevant i; also $\min_i (a_i)$
$\mathcal{O}(x^n)$	the remainder in a series of a function of x after the x^n term
$\text{Res}(g; a)$	residues of function $g(z)$ at $z = a$

Chapter 1

Introduction

1.1 Wireless Communications

"In the new era, thought itself will be transmitted by radio."

~ Guglielmo Marconi [1931]

Radio communications have grown tremendously since the early development in the late 19th and early 20th century, and now have impacted people's lives in every corner of the globe. As a precious resource, the radio spectrum must be carefully managed to mitigate spectrum pollution, maximize the utilization, and minimize the interference. In different countries, wireless systems (commercial or government operated) have been allocated (licensed) chunks of spectrum by the regulatory agencies. For instance, the radio spectrum allocated for different radio transmissions and applications is shown in Fig. 1.1.

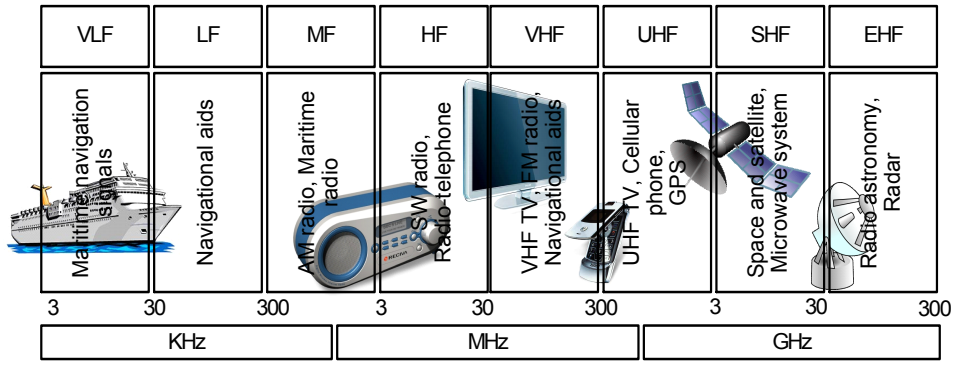

Figure 1.1: Radio spectrum allocated for wireless communications.

Dramatically rising demand for wireless communications has increased the de-

mand for radio spectrum. To meet the rising demand, new broadband communication technologies have been introduced to utilize radio spectrum effectively. Some key novel technologies are as follows.

- Multiple-input multiple-output (MIMO) communications: MIMO systems allow higher data throughput without additional bandwidth or power increase. IEEE 802.11n (Wi-Fi) uses MIMO to achieve the maximum data rate up to 600 Mbps at 2.4 GHz [1]. For a single-user MIMO network with $n_T(\geq 1)$ transmit and $n_R(\geq 1)$ receive antennas, the capacity of a single link increases linearly with $\min(n_T,\ n_R)$. This increase also motivates a *multi-user MIMO* network which achieves the similar capacity scaling when an access point with n_T transmit antennas communicates with n_R users [2]. And larger diversity gain can be achieved when each user has multiple antennas. Multi-user MIMO will be implemented in IEEE 802.11ac (in early 2014) which enables multi-station wireless local area network (WLAN) with throughput of at least 1 Gbps [3]. In addition, a very large MIMO system, known as *massive MIMO*, which includes large-scale antenna arrays, is capable of shrinking the cell size and reducing the transmit power and overhead for channel training (when channel reciprocity is exploited) [4].

- Cooperative communications: This helps reliable transmission and improves data rate by exploiting spatial diversity in a multi-user environment, by using cooperative techniques such as relaying, cooperative MIMO, and multi-cell MIMO. Relaying facilitates the signal transmission between the source and the destination utilizing less power [5]. Cooperative MIMO, which forms a distributed antenna system employing antennas of different users, is effective for poor line-of-sight propagation and for cell-edge users. Cooperative MIMO utilizes the advantages of both MIMO and cooperative communications techniques [6]. Further, the larger number of users/antennas in MIMO networks and the universal frequency reuse (e.g., in long term evolution (LTE)-advanced) cause high levels of co-channel interference. Such interference can be mitigated by using multi-cell cooperation which is re-

ferred to as *multi-cell MIMO* [7]. The cooperation among base stations can be established via high-capacity wired backhaul links.

- Heterogeneous networks: As node density in cellular networks increases and data traffic demand for the nodes also increases rapidly, the network capacity must grow significantly. Since these demands cannot be achieved with traditional cellular networks, heterogeneous networks have been envisaged. These include a disparate mix of base stations and cells such as lower-power base station in pico-cells (250 mW - 2 W) and femto cells (100 mW or less), and high-speed WLANs. A user may be switched among the macro-cells, pico-cells, femto cells, and WLANs [8].

Despite these advanced technologies, when new service providers request new frequency bands, spectrum scarcity has created challenges for the Federal Communications Commission (FCC) in the United States and spectrum regulatory bodies in other countries. A promising solution is *cognitive radio* technology [9, 10].

1.2 Cognitive Radio

What has motivated cognitive radio technology, an emerging novel concept in wireless access, is spectral usage experiments done by FCC. These experiments show that at any given time and location, much of the licensed (pre-allocated) spectrum (between 80% and 90%) is idle because licensed users (termed primary users) rarely utilize all the assigned frequency bands at all time [10]. Such unutilized bands are called spectrum holes, resulting in spectral inefficiency. These experiments suggest that the spectrum scarcity is caused by poor spectrum management rather than a true scarcity of usable frequency.

The key features of a cognitive radio transceiver are radio environment awareness and spectrum intelligence. Intelligence can be achieved through learning the spectrum environment and adapting transmission parameters [10].

1.2.1 Standardization and Applications of Cognitive Radio

The radio spectrum allowed for television (TV) broadcasting (e.g., 54–806 MHz in US) is allocated for different TV operators. In the TV band, the frequencies not being used by operators are called *white spaces*. White spaces may include guard bands, free frequencies due to analog TV to digital TV switchover (e.g., 698–806 MHz in US), and free TV bands created when traffic in digital TV is low and can be compressed into fewer TV bands. Since the use of white spaces by unlicensed users is allowed by the FCC, the IEEE 802.22 standard has been released with medium access control and physical layer specifications for a wireless regional area network (WRAN). This standard focuses on broadband access in general mobile networks by using cognitive radio techniques on a non-interfering basis [11–13]. Other standardization activities of cognitive radio include ECMA 392 [14], IEEE SCC41 [15], and IEEE 802.11af [16].

Some other applications of cognitive radio technology are as follows [17, 18].

- Smart grid networks: Currently, the traditional power grids are being transformed to smart grids with smart meters for billing. Since smart meters transfer information between premises and a network gateway (with a distance from a few hundred meters to a few kilometers), a reliable communication system is required. Conventional options such as power line communications support only low data rate and shorter distance, and the cellular networks may not have enough bandwidth. Therefore, IEEE 802.15.4g Smart Utility Networks (SUN) Task Group, which provides a global standard for smart grid networks, seeks cognitive radio solutions which offer advantages in terms of bandwidth, coverage range and overhead [19].

- Public safety networks: Public services such as police, fire, and medical services largely use wireless devices. The allocated radio spectrum for the public services can be highly congested in some emergency conditions, which may cause a delayed response to victims. In addition to fixed allocated radio spectrum, public services can use unlicensed radio spectrum (for example, the TV white spaces) to ensure sufficient capacity so as to achieve efficient com-

munications on time [18]. For example, the US Department of Homeland Security concerns the National Emergency Communications Plan to improve the quality of service of public services [20].

- Cellular networks: The current cellular networks are overloaded with the traffic growth. As the National Broadband Plan [21], the TV white spaces may be available for the cellular operators in future to use cognitive radio techniques. However, integration of cognitive radio technologies and current cellular networks, e.g., LTE and WiMAX, remains to be investigated.

1.2.2 Dynamic Spectrum Access

The dynamic spectrum access (DSA) allows the operating spectrum of a radio network to be selected dynamically from the available spectrum [22]. DSA is applied in cognitive radio networks, which has a hierarchical access structure with primary and secondary users as shown in Fig. 1.2. The basic idea of DSA is to open li-

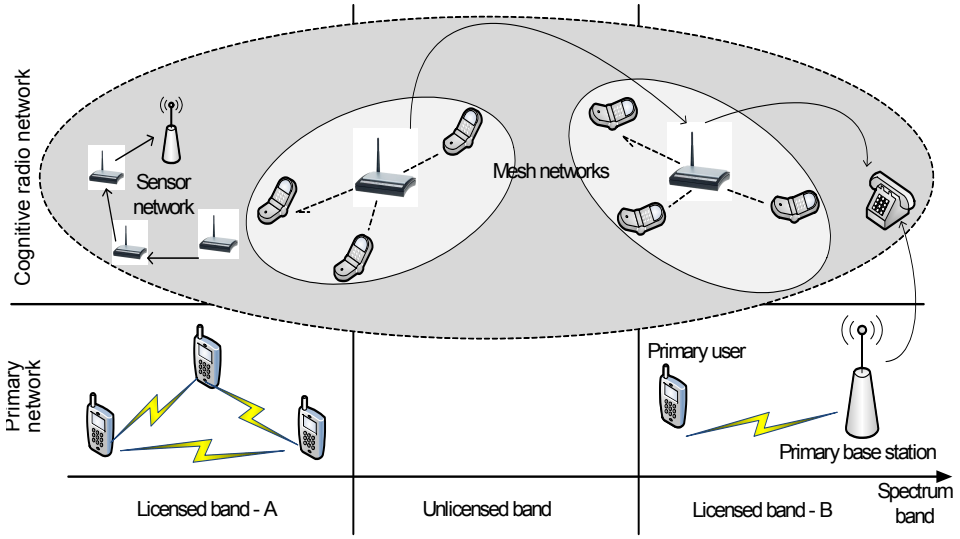

Figure 1.2: A basic cognitive radio network architecture.

censed spectrum to secondary users (which are unlicensed users) while limiting the interference received by primary users (which are licensed users). This allows secondary users to operate in the best available channel opportunistically. Therefore, DSA requires opportunistic spectrum sharing, which is implemented via two strategies [23].

1. *Spectrum overlay* does not necessarily impose strict constraints on the transmit power of secondary users, but rather on their transmission time. Consequently, a secondary user accesses a spectrum hole assigned via DSA.

2. *Spectrum underlay* imposes strict constraints on the transmit power of secondary users. This power at a certain portion of the spectrum is then low enough to be regarded as noise by the primary users. Both primary and secondary users may thus transmit simultaneously in the same channel assigned via DSA, and this assignment may minimize the mutual interference.

In spectrum overlay cognitive radio, the secondary (cognitive) users are allowed to opportunistically access spectrum which has already been allocated to primary users. As this opportunistic access may create interference, secondary users transmit only if primary users are not active. Whenever primary users become active, secondary users must detect the presence of the primary users reliably, immediately vacate the channel, and find other free channels for continuing communication. One of the most important tasks in the spectrum overlay system is thus to identify the spectrum holes.

1.2.3 Spectrum Sensing

The purpose of spectrum sensing is to identify the spectrum holes for opportunistic spectrum access. After available channels (spectrum holes) are detected successfully, they may be used for communications by a secondary transmitter and a secondary receiver [24]. Spectrum sensing is performed based on the received signal from the primary users. Primary users have two states, idle or active. With the presence of the noise, primary signal detection at a secondary user can be viewed as a binary hypothesis testing problem in which Hypothesis 0 ($\mathcal{H}_0$) and Hypothesis 1 ($\mathcal{H}_1$) are the primary signal absence and the primary signal presence, respectively [25]. Based on the hypothesis testing model, several spectrum sensing techniques have been developed. They are reviewed next.

1.2.4 Spectrum Sensing Techniques

Spectrum sensing techniques include energy detection, matched filter, cyclostationary feature detection, and eigenvalue detection.

- Energy detection: This measures the energy of the received signal within the pre-defined bandwidth and time period. The measured energy is then compared with a threshold to determine the status (presence/ absence) of the transmitted signal. Not requiring channel gains and other parameter estimates, the energy detector is a low-cost option. However, it performs poorly under high noise uncertainty and background interference [26].

- Matched filter: This detector requires perfect knowledge of the transmitted signal and the channel responses for its coherent processing at the demodulator. The matched filter is the optimal detector of maximizing the signal-to-noise ratio (SNR) in the presence of additive noise. Since it requires the perfect knowledge of the channel response, its performance degrades dramatically when there is lack of channel knowledge due to rapid changes of the channel conditions [27, 28].

- Cyclostationary feature detection: If periodicity properties are introduced intentionally to the modulated signals, the statistical parameters of received signal such as mean and autocorrelation may vary periodically. Such periodicity of statistical properties is used in the cyclostationary detection. Cyclostationary properties of the received signal may be extracted by its input-output spectral correlation density. The signal absence status can be identified easily, because the noise signal does not have cyclostationary properties. While this detector is able to distinguish among the primary user signals, secondary user signals, or interference. it needs high sampling rate and a large number of samples, and thus increases computational complexity as well [29–32].

- Eigenvalue detection: The ratio of the maximum (or the average) eigenvalue to the minimum eigenvalue of the covariance matrix of the received signal vector is compared with a threshold to detect the absence or the presence of

the primary signal. However, if the correlation of the primary signal samples is zero (e.g., primary signal appears as white noise), eigenvalue detection may fail - a very rare event. This detector has the advantage of not requiring the knowledge of the primary signal and the propagation channel conditions. The main drawback is the computational effort to compute covariance matrix and eigenvalue decomposition. The threshold selection is challenging as well [33–35].

1.3 Motivation

The exponential growth of wireless communications has led to spectrum scarcity. Although cognitive radio has been developed to solve the spectrum scarcity and spectrum under-utilization issues, many research problems remain open.

Reliable primary user detection via spectrum sensing is one of the critical problems, and hence spectrum sensing is one of the most challenging and difficult tasks [36]. Moreover, selecting the best available channel and reducing or eliminating interference to primary users are also essential [37, 38]. All these requirements depend on the spectrum sensing technique. Among the spectrum sensing techniques, energy detection is the most popular one due to its low complexity. Although energy detection has been well investigated for traditional wireless networks, new challenges arise when it is applied in cognitive radio networks.

- A more reliable energy detector (than those in traditional networks) is needed to minimize interference.

- A much wider spectrum bandwidth needs to be sensed to identify spectrum holes. Since different spectrum holes experience different signal propagation conditions, the design and analysis of energy detection is challenging.

- Many transmission environments must be considered. Activities from multiple licensed wireless applications must be detected. Different applications may have different population of users, with different mobility patterns, which have a great impact on the signal reception, and thus, affect energy detection.

Thus, to address these research challenges, this thesis focuses on energy detection for spectrum sensing, and related research problems.

1.4 Problem Statements

Specifically, this thesis addresses five problems, **P1-P5**, which are related to the spectrum sensing via energy detection in cognitive radio networks.

P1: *Energy detection under channels with both multipath fading and shadowing:* Spectrum holes must be correctly detected by the energy detector, whose performance can be quantified by the false-alarm and detection probabilities. While the performance of energy detectors on multipath fading has been analyzed extensively, wireless signals also undergo shadowing which severely impacts the detection capability. Multipath fading superimposed on shadowing occurs in practical communication channels. Due to the analytical intractability of composite fading models, the shadowing effect has been neglected in the literature.

P2: *A unified channel model for performance analysis of wireless communications:* Analytical intractability of different propagation models, and the resulting mathematically complicated expressions do not facilitate rapid evaluation of energy detection and other wireless network performance. Therefore, a simple analytical framework is vital, and thus, a unified channel model which represents typical channel models in various spectrum bands and various scenarios is desirable.

P3: *A generalized and simplified performance metric for energy detection:* The detection capability of an energy detector depends on many parameters, and is traditionally characterized through the receiver operating characteristic (ROC) curve, which is not flexible when more than one parameters change concurrently. Further, visual examination of ROC curves to compare different energy detectors is unreliable. Thus, a generalized and simplified single-valued

performance metric, which facilitates energy detector design and analysis, is desired.

P4: *Reliability improvement of energy detector:* Spectrum sensing in cognitive radio may suffer from the notorious hidden terminal problem, which happens when close by secondary and primary transmitters are blocked by a disturbance (e.g., a high building). Although the cooperative spectrum sensing has been identified as a solution, an extensive performance analysis has been lacking.

P5: *Spectrum sensing in very low SNR:* The US FCC and the IEEE 802.22 standard have determined that cognitive devices must detect with very low false alarm and missed-detection probabilities within a very short sensing time at low SNR and low receiver sensitivity. This inherent conflict between low false alarm and missed-detection probabilities and short sensing time poses critical challenges to the energy detector design in very low SNR. Little attention was paid to this research problem in the past because of analytical intractability of traditional frameworks.

1.5 Thesis Outline

Chapters 2–7 provide background knowledge, detailed treatment and new ideas in order to address the problems **P1–P5**, which are briefly outlined as follows.

- Chapter 2 contains background knowledge for topics related to this thesis. The wireless communication channel and its fading are considered throughout the thesis. The conventional energy detection and its system model are reviewed to gain further insights of the already existing literature.

- Chapter 3 addresses problem **P1**, in which the performance of an energy detector for channels with both multipath fading and shadowing is analyzed by the adoption of the K channel and generalized-K (denoted as K_G) channel. Multipath fading and shadowing effects are shown by using the ROC curves based on analytical expressions of the average detection probability.

The ROC curves are presented for different degrees of multipath fading and shadowing.

- Composite fading (i.e., multipath fading and shadowing together) has increasingly been analyzed by means of the K channel and related models. Nevertheless, these models do have computational and analytical difficulties as pointed out in problem **P2**. Motivated by this context, Chapter 4 proposes a mixture gamma (MG) distribution for the SNR of mobile radio channels. Not only is it a more accurate model for composite fading, but is also a versatile approximation for any fading SNR. With this model, performance metrics such as the average channel capacity, the outage probability, the symbol error rate (SER) of general wireless communication networks, and the detection capability of an energy detector are readily derived. Note that the analysis is not limited to cognitive radio networks.

- As pointed out in problem **P3**, a simple figure of merit to describe the performance of an energy detector is desired. Such a measure is the Area Under the receiver operating characteristic Curve (AUC). In Chapter 5, the AUC is analyzed for an energy detector with no-diversity reception and with several popular diversity schemes.

- As a solution to problem **P4**, a cooperative spectrum sensing cognitive radio network with much improved reliability is designed based on energy detection, in which multiple cognitive relays in a secondary network can help forward received primary signals to a fusion center such that detection performance at the fusion center is significantly improved. The detection performance of an energy detector used for cooperative spectrum sensing in a cognitive radio network is investigated over channels with both multipath fading and shadowing in Chapter 6. The analysis focuses on two fusion strategies: data fusion and decision fusion. The results are extended to multi-hop networks as well.

- The IEEE 802.22 WRAN requires spectrum-sensing techniques to identify

primary signals with an SNR as low as -20 dB and receiver sensitivity as low as -116 dBm, which is identified as a challenging problem as in problem **P5**. In Chapter 7, under such low-SNR levels, the detection performance of an energy detector used for spectrum sensing in cognitive radio networks is investigated, and analytical expressions for performance metrics are derived. Further, the detection threshold is also optimized to minimize the total error rate.

$\sim$

Chapter 2

Background

This chapter reviews relevant topics for this thesis. For analysis of energy detection, the wireless channel models which represent small-scale fading, large-scale fading and composite fading are important. The test statistic of the energy detector and its distribution depend on the signal model (e.g., Gaussian signal) and the network (e.g., cooperative networks). Parameters of the energy detector also need to be carefully designed to achieve target performance metrics. The IEEE 802.22 standard and the cooperative spectrum sensing are also reviewed.

2.1 Mobile Radio Channel

The mobile radio channel refers to the transmission medium between the transmitter and the receiver. Fundamental mobile radio channel propagation effects include path loss, microscopic (small scale or fast) fading, and macroscopic (large scale or slow) fading. These effects are modeled as a complex channel gain, $\mathbf{h}$. Additive thermal noise, with a flat power spectral density, is called the additive white Gaussian noise (AWGN). Including these factors, the received signal may be generically represented as

$$\mathbf{y} = \mathbf{h}\mathbf{s} + \mathbf{w} \tag{2.1}$$

where $\mathbf{s}$ is the transmitted signal and $\mathbf{w}$ is the AWGN term.

The path loss can model the attenuation of signal strength with distance, wavelength, and antenna heights. In the thesis, while the small-scale fading and the large-scale fading are considered, the path loss effect is neglected due to analytical

difficulties.

2.1.1 Small-Scale Fading and Large-Scale Fading

The small-scale fading, which occurs in indoor environments and also both macrocellular and microcellular outdoor environments, results from multipath propagation due to the reflections and scatters. The constructive and destructive effects of the multiple signals distort both amplitude and phase of the received signal with time, which is called the envelope fading, given by Rayleigh, Nakagami-m and Rician fading models [39]. For Rayleigh fading, the magnitude of the channel gain, $|\mathbf{h}|$, has Rayleigh distribution given by

$$f_{|\mathbf{h}|}(x) = \frac{2x}{\Omega} e^{-\frac{x^2}{\Omega}}, \quad 0 \leq x \leq \infty \tag{2.2}$$

where Ω is the average envelope power. The Nakagami-m fading is a generalized model for the non-line of sight small-scale fading, which is given as

$$f_{|\mathbf{h}|}(x) = \frac{2m^m x^{2m-1}}{\Omega^m \Gamma(m)} e^{-\frac{mx^2}{\Omega}}, \quad 0 \leq x \leq \infty \tag{2.3}$$

where $0.5 \leq m < \infty$ is the fading severity parameter, and $\Gamma(\cdot)$ is the Gamma function. The Rician channel model fits well with a channel having a dominant line-of-sight component. If real and imaginary components of $\mathbf{h}$ have the mean a and the variance b, the distribution is given as

$$f_{|\mathbf{h}|}(x) = \frac{x}{b} e^{-\frac{x^2+s^2}{2b}} I_0\left(\frac{sx}{b}\right), \quad 0 \leq x \leq \infty \tag{2.4}$$

where $s = \sqrt{2}a$, which is the non-centrality parameter, and $I_0(\cdot)$ is the zeroth-order modified Bessel function of the first kind.

The large-scale fading, which occurs due to the shadowing effect by buildings, foliage and other objects, can significantly impact satellite channels, point-to-point long distance microwave links and macrocellular outdoor communications [40]. The mean-squared amplitude, Ω, represents the shadowing effect which is typically modeled with the log-normal distribution as [39]

$$f_{\Omega}(x) = \frac{\xi}{x\sqrt{2\pi\sigma^2_{\Omega\text{dB}}}} e^{-\frac{(10\log_{10}(x)-\mu_{\Omega\text{dB}})^2}{2\sigma^2_{\Omega\text{dB}}}}, \quad 0 \leq x \leq \infty \tag{2.5}$$

where $\xi = \frac{10}{\ln 10}$, and $\mu_{\Omega\text{dB}}$ and $\sigma_{\Omega\text{dB}}$ are mean and standard deviation of $10\log_{10}(\Omega)$, respectively.

2.1.2 Composite Fading

Both microscopic fading and macroscopic fading are modeled by composite shadowing/fading distributions. The Rayleigh-lognormal (RL) and Nakagami-lognormal (NL) are two most common models [39]. But the probability density function (PDF) of these two composite models are not in closed form, making performance analysis of some applications difficult or intractable. Therefore, the K distribution and generalized-K or K_G distribution have been introduced, by using a gamma distribution to approximate the lognormal distribution of the shadowing to model channels with composite multipath fading and shadowing. In [41], the K distribution, a mixture of Rayleigh distribution and gamma distribution, is used to approximate the Rayleigh-lognormal distribution, referred to as the K channel model, in which the fading amplitude undergoes multipath fading as a Rayleigh distribution and shadowing as a gamma distribution. Therefore, the average power of the fading amplitude, which represents the shadowing effect, follows the gamma distribution. The PDF of the fading amplitude, denoted as $f_{|\mathbf{h}|}(x)$, follows a K distribution which is given as [42]

$$f_{|\mathbf{h}|}(x) = \frac{4}{\Gamma(k)\sqrt{\Omega}} \left(\frac{x}{\sqrt{\Omega}}\right)^k K_{k-1}\left(\frac{2}{\sqrt{\Omega}}x\right), \ \ 0 \leq x \leq \infty \tag{2.6}$$

where $K_\nu(\cdot)$ is the modified Bessel function of the second kind of order ν, k is the shaping parameter and Ω represents the mean signal power.

In [43], the K_G distribution, a mixture of the Nakagami distribution and gamma distribution, is presented to approximate the NL distribution, referred to as the K_G channel model. The K_G distribution is given as [44]

$$f_{|\mathbf{h}|}(x) = \frac{4m^{\frac{\beta+1}{2}}x^\beta}{\Gamma(m)\Gamma(k)\Omega^{\frac{\beta+1}{2}}} K_\alpha\left[2\left(\frac{m}{\Omega}\right)^{\frac{1}{2}}x\right], \ \ 0 \leq x \leq \infty \tag{2.7}$$

where m is the fading parameter, $\alpha = k - m$, and $\beta = k + m - 1$. The K_G distribution reduces to a K distribution when $m = 1$. Moreover, as $m \to \infty$ and $k \to \infty$, the K_G model tends to a non-fading case, i.e., the AWGN channel. The accuracy of the approximation is verified by comparison of their moment generating function (MGF) [42, 44]. The K_G model includes special cases, such as the K

model, and can also approximate the Nakagami-m model, the RL distribution and the Suzuki model [41].

Moreover, several other composite models have been developed including the $\mathcal{G}$- distribution, the Log-normal distribution, and the Gamma distribution [39, 45, 46]. Note that these models are approximations of the RL and NL models.

2.2 System Model of Spectrum Sensing

Primary users are in either idle state or active state. With the presence of the noise, the signal detection at the receiver can be viewed as a binary hypothesis testing problem in which Hypothesis 0 ($\mathcal{H}_0$) and Hypothesis 1 ($\mathcal{H}_1$) are the primary signal absence and the primary signal presence, respectively [25]. The nth, $n = 1, 2, \cdots$, sample of the received signal, $\mathbf{y}(n)$, can be given under the binary hypothesis as [25, 47]:

$$\mathbf{y}(n) = \begin{cases} \mathbf{w}(n) & : \mathcal{H}_0 \\ \mathbf{x}(n) + \mathbf{w}(n) & : \mathcal{H}_1 \end{cases} \tag{2.8}$$

where $\mathbf{x} = \mathbf{hs}$.

The complex signal, $\mathbf{s}$ has real component s_r and imaginary component s_i, i.e., $\mathbf{s} = s_r + js_i$.[1] The AWGN samples are assumed to be circularly symmetric complex Gaussian (CSCG) random variables with mean zero ($\mathbb{E}\{\mathbf{w}(n)\} = 0$) and variance $2\sigma_w^2$ ($\mathbb{V}\text{ar}\{\mathbf{w}(n)\} = 2\sigma_w^2$) where $\mathbb{E}\{\cdot\}$ and $\mathbb{V}\text{ar}\{\cdot\}$ stand for mean and variance, respectively, i.e., $\mathbf{w}(n) \sim \mathcal{CN}(0, 2\sigma_w^2)$. A noise sample is denoted as $\mathbf{w}(n) = w_r(n) + jw_i(n)$ where $w_r(n)$ and $w_i(n)$ are real-valued Gaussian random variables with mean zero and variance σ_w^2, i.e., $w_r(n), w_i(n) \sim \mathcal{N}(0, \sigma_w^2)$. The channel gain is denoted as $\mathbf{h} = h_r + jh_i$. The channel gain can be assumed as a constant within each spectrum sensing period. In general, (2.8) can be written as

$$\mathbf{y}(n) = \theta\mathbf{x}(n) + \mathbf{w}(n) \tag{2.9}$$

where $\theta = 0$ for $\mathcal{H}_0$ and $\theta = 1$ for $\mathcal{H}_1$.

[1] A complex number which has real and imaginary components z_r and z_i, respectively, is denoted as $\mathbf{z} = z_r + jz_i$.

2.3 Spectrum Sensing via Energy Detection

An energy detector is a device that may decide whether the transmitted signal is absent or present in the noisy environment. Energy detector does not require any prior knowledge of the transmitted signal (e.g., phase, shape, frequency). The conventional energy detector measures the energy of the received signal over specified time duration and bandwidth. The energy is then compared with an appropriately selected threshold to determine the presence or the absence of an unknown signal.

Two models of energy detector can be considered in time-domain implementations:

1. *Analog energy detector* which is illustrated in Fig. 2.1(a) is considered in [48]. It consists of a pre-filter followed by a square-law device and a finite time integrator. The pre-filter limits the noise bandwidth and normalizes the noise variance. The output of the integrator is proportional to the energy of the received signal of the square law device.

2. *Digital energy detector* is shown in Fig. 2.1(b). It consists of a low pass noise pre-filter which limits the noise and adjacent signal bandwidths, an analog-to-digital converter (ADC) which converts continuous signals to discrete digital signal samples, and a square law device followed by an integrator. The digital implementation is usually used at the experimental testbed.

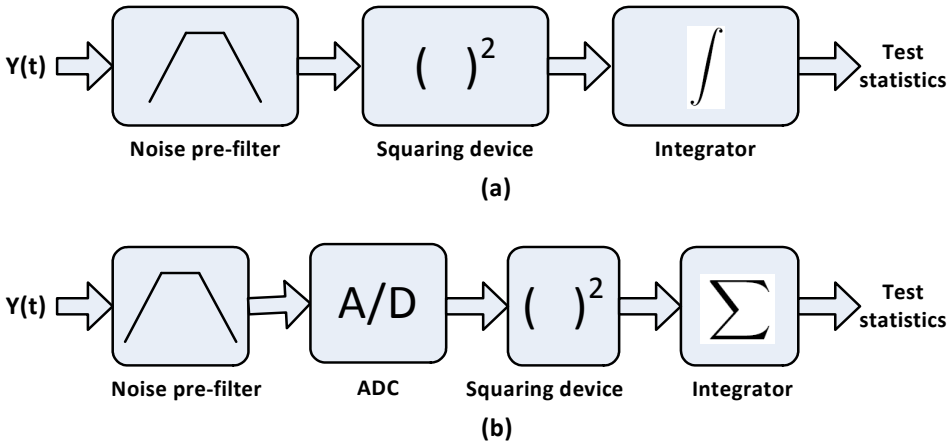

Figure 2.1: The conventional energy detectors: (a) analog and (b) digital .

The integrator output of any architecture is called decision statistic or test statistic. The test statistic is finally compared at the threshold device followed by decision device to make the final decision of the presence/absence of transmitted signal. The test statistic may not always be the integrator output, but it can be any function which is monotonic with the integrator output [48].

2.4 Test Statistic of Energy Detector

The test statistic of the analog energy detector is given as $\Lambda = \frac{1}{T}\int_{t-T}^{t}[\mathbf{y}(t)]^2\,\mathrm{d}t$ where T is the time duration [48]. A sample function with bandwidth W and time duration T can be described approximately by a set of samples $N \approx 2TW$. Therefore, the analog test statistic can be implemented by samples, where the test statistic is proportional to $\sum_{n=1}^{N}|\mathbf{y}(n)|^2$. In digital implementation, after proper filtering, sampling, squaring and integration, the test statistic is given by using (2.9) as

$$\Lambda = \sum_{n=1}^{N}|\mathbf{y}(n)|^2 = \sum_{n=1}^{N}\left(e_r(n)^2 + e_i(n)^2\right) \tag{2.10}$$

where $e_r(n) = \theta h_r s_r(n) - \theta h_i s_i(n) + w_r(n)$ and $e_i(n) = \theta h_r s_i(n) + \theta h_i s_r(n) + w_i(n)$. Since the test statistic only includes the received signal energy, energy detector is the optimal non-coherent detector for an unknown signal if the signal is Gaussian, uncorrelated and independent with the uncorrelated background noise [49].

The performance of energy detector (or of other detectors) is measured by using following metrics:

- False alarm probability (P_f): the probability of deciding the signal is present while $\mathcal{H}_0$ is true, i.e., $P_f = \mathcal{P}\left[\Lambda > \lambda|\mathcal{H}_0\right]$ where $\mathcal{P}\left[\cdot\right]$ stands for an event probability. P_f indicates the probability of undetected spectrum holes. A large P_f leads to poor spectral efficiency in cognitive radio.

- Missed-detection probability (P_{md}): the probability of deciding the signal is absent while $\mathcal{H}_1$ is true, i.e., $P_{md} = \mathcal{P}\left[\Lambda < \lambda|\mathcal{H}_1\right]$, which means a wrong decision on the unavailable spectrum. A large P_{md} means poor reliability, which introduces unexpected interference to primary users.

- Detection probability (P_d): the probability of deciding the signal is present when $\mathcal{H}_1$ is true , i.e., $P_d = \mathcal{P}\left[\Lambda > \lambda | \mathcal{H}_1\right]$, and thus, $P_d = 1 - P_{md}$.

Both reliability and efficiency are expected from the spectrum sensing technique built into the cognitive radio, i.e., a higher P_d (or lower P_{md}) and lower P_f are preferred.

The statistical properties of Λ are necessary to characterize the performance of energy detector. Based on the known properties of the received signal and noise, an accurate and analytically tractable model for Λ is thus vital for further discussion. While the noise components, $w_r(n)$ and $w_i(n)$, are zero-mean Gaussian, different models for the signal to be detected are possible. Therefore, several alternative models are discussed in the following. The PDFs of Λ under hypotheses $\mathcal{H}_0$ and $\mathcal{H}_1$ are denoted as $f_{\Lambda|\mathcal{H}_0}(x)$ and $f_{\Lambda|\mathcal{H}_1}(x)$, respectively.

2.4.1 Signal Models

Based on the available knowledge of $\mathbf{s}(n)$ at receiver, signal can be modeled differently, which helps to analyze the distribution of the test statistic under $\mathcal{H}_1$. For example, three different models, **S1, S2** and **S3**, are popularly used in the literature, and are given as follows.

S1: For given channel gain $\mathbf{h}$, the signal to be detected, $\mathbf{y}(n)$, can be assumed as Gaussian with mean $\mathbb{E}\{\mathbf{y}(n)\} = \mathbb{E}\{\mathbf{hs}(n) + \mathbf{w}(n)\} = \mathbf{hs}(n)$ and variance $\mathbb{V}\text{ar}\{\mathbf{y}(n)\} = 2\sigma_w^2$. For the signal transmitted over a flat band-limited Gaussian noise channel, a basic mathematical model of the test statistic of an energy detector is given in [48]. The receive SNR can thus be given as

$$\gamma_{\text{S1}} = \frac{|\mathbf{h}|^2 \frac{1}{N} \sum_{n=1}^{N} |\mathbf{s}(n)|^2}{2\sigma_w^2}. \tag{2.11}$$

S2: If the signal sample is considered as random variable which has a Gaussian distribution, i.e., $\mathbf{s}(n) \sim \mathcal{CN}(0, 2\sigma_s^2)$, then $\mathbf{y}(n) \sim \mathcal{CN}(0, 2(\sigma_w^2 + \sigma_s^2))$. The receive SNR can thus be given as

$$\gamma_{\text{S2}} = \frac{|\mathbf{h}|^2 2\sigma_s^2}{2\sigma_w^2}. \tag{2.12}$$

S3: If the signal sample is considered as random variable with mean zero and variance $2\sigma_s^2$, but with an unknown distribution, then $\mathbf{y}(n)$ has mean zero and $2(\sigma_w^2 + \sigma_s^2)$ variance. The receive SNR can also be given as

$$\gamma_{\text{S3}} = \frac{|\mathbf{h}|^2 2\sigma_s^2}{2\sigma_w^2}. \tag{2.13}$$

For sufficiently large number of samples, the signal variance can be written by using its sample variance as $2\sigma_s^2 \approx \frac{1}{N}\sum_{n=1}^{N} |\mathbf{s}(n)|^2 - \left(\frac{1}{N}\sum_{n=1}^{N} \mathbf{s}(n)\right)^2$. If the sample mean goes to zero, i.e., $\frac{1}{N}\sum_{n=1}^{N} \mathbf{s}(n) \to 0$, $2\sigma_s^2 \approx \frac{1}{N}\sum_{n=1}^{N} |\mathbf{s}(n)|^2$, and thus all the receive SNRs under different signal models which are given in (2.11)-(2.13) are equal. In general, the instantaneous SNR is denoted as γ.

2.4.2 Distribution of Test Statistics

The exact distributions of the test statistic (2.10) for different signal models are analyzed in the following under both hypotheses, $\mathcal{H}_0$ and $\mathcal{H}_1$.

Under $\mathcal{H}_0$

In this case, $e_r(n) = w_r(n)$ and $e_i(n) = w_i(n)$, and $e_r(n)$ and $e_i(n)$ follow $\mathcal{N}(0, \sigma_w^2)$. Thus, Λ is a sum of $2N$ squares of independent $\mathcal{N}(0, \sigma_w^2)$ random variables, and it follows central chi-square distribution which is given as [50]

$$f_{\Lambda|\mathcal{H}_0}(x) = \frac{x^{N-1} e^{-\frac{x}{2\sigma_w^2}}}{(2\sigma_w^2)^N \Gamma(N)}, \quad 0 \le x < \infty. \tag{2.14}$$

Thus, the false-alarm probability can be derived by using (2.14) as

$$P_f = \mathcal{P}\left[\Lambda > \lambda | \mathcal{H}_0\right] = \frac{\Gamma(N, \frac{\lambda}{2\sigma_w^2})}{\Gamma(N)} \tag{2.15}$$

where $\Gamma(\cdot, \cdot)$ is the upper incomplete Gamma function.

Under $\mathcal{H}_1$

In this case, the distribution of Λ, $f_{\Lambda|\mathcal{H}_1}(x)$, has two different distributions under two signal models, **S1** and **S2**, for a given channel. However, the distribution of Λ under **S3** cannot be derived.

For **S1**, $e_r(n)$ and $e_i(n)$ follow $\mathcal{N}(h_r s_r(n) - h_i s_i(n), \sigma_w^2)$ and $\mathcal{N}(h_r s_i(n) + h_i s_r(n), \sigma_w^2)$, respectively. Since Λ is a sum of $2N$ squares of independent and non-identically distributed Gaussian random variables with non-zero mean, Λ follows non-central chi-square distribution which is given as [50]

$$f_{\Lambda|\mathcal{H}_1}(x) = \frac{\left(\frac{x}{\sigma_w^2}\right)^{\frac{N-1}{2}} e^{-\frac{1}{2}\left(\frac{x}{\sigma_w^2}+\mu\right)}}{2\sigma_w^2 \mu^{\frac{N-1}{2}}} I_{N-1}\left(\sqrt{\frac{\mu x}{\sigma_w^2}}\right), \quad 0 \leq x < \infty, \tag{2.16}$$

where $I_\nu(\cdot)$ is the modified Bessel function of the first kind of order ν,

$$\mu = \sum_{n=1}^{N} \frac{(h_r s_r(n) - h_i s_i(n))^2}{\sigma_w^2} + \frac{(h_r s_i(n) + h_i s_r(n))^2}{\sigma_w^2} = 2N\gamma_{\text{S1}}$$

which is the non-centrality parameter, and γ_{S1} is given in (2.11). Thus, the detection probability can be derived for **S1** by using (2.16) as

$$P_{d,\mathbf{S1}} = \mathcal{P}\left[\Lambda > \lambda | \mathcal{H}_1\right] = Q_N\left(\sqrt{2N\gamma_{\text{S1}}}, \frac{\sqrt{\lambda}}{\sigma_w}\right) \tag{2.17}$$

where $Q_N(\cdot,\cdot)$ is the generalized Marcum-Q function. This signal model is widely used in the performance analysis of an energy detector in terms of the average detection probability [51–54].

For **S2**, $e_r(n)$ and $e_i(n)$ follow $\mathcal{N}(0, (1+\gamma_{\text{S2}})\sigma_w^2)$ where γ_{S2} is given in (2.12). Since Λ is a sum of $2N$ squares of independent and identically distributed (i.i.d.) Gaussian random variables with zero mean, Λ follows central chi-square distribution which is given as

$$f_{\Lambda|\mathcal{H}_1}(x) = \frac{x^{N-1} e^{-\frac{x}{2(1+\gamma_{\text{S2}})\sigma_w^2}}}{\left(2(1+\gamma_{\text{S2}})\sigma_w^2\right)^N \Gamma(N)},, \quad 0 \leq x < \infty. \tag{2.18}$$

The exact detection probability can be derived for **S2** by using (2.18) as

$$P_{d,\mathbf{S2}} = \frac{\Gamma(N, \frac{\lambda}{2\sigma_w^2(1+\gamma_{\text{S2}})})}{\Gamma(N)}. \tag{2.19}$$

This model is used in [55, 56].

For **S3**, $e_r(n)$ and $e_i(n)$ have unknown distributions, and the exact $f_{\Lambda|\mathcal{H}_1}(x)$ cannot be derived, and it may not be a central or non-central chi-square distribution as well. However, $f_{\Lambda|\mathcal{H}_1}(x)$ can be derived approximately by using the central limit theorem (CLT).

2.4.3 CLT Approach

According to the CLT, the sum of N i.i.d. random variables with finite mean and variance approaches to a normal distribution when N is large enough. Using the CLT, the distribution of the test statistic (2.10) can be accurately approximated with a normal distribution for sufficiently large number of samples as

$$\Lambda \sim \mathcal{N}\left(\sum_{n=1}^{N}\mathbb{E}\{|\mathbf{y}(n)|^2\}, \sum_{n=1}^{N}\mathbb{V}\text{ar}\{|\mathbf{y}(n)|^2\}\right).$$

When the distributions of test statistics under $\mathcal{H}_0$ and $\mathcal{H}_1$ are $\Lambda \sim \mathcal{N}(m_0, \sigma_0^2)$ and $\Lambda \sim \mathcal{N}(m_1, \sigma_1^2)$, respectively, the performance matrices can be derived as

$$P_f \approx Q\left(\frac{\lambda - m_0}{\sigma_0}\right) \text{ and } P_d \approx Q\left(\frac{\lambda - m_1}{\sigma_1}\right). \tag{2.20}$$

where $Q(\cdot)$ is the Gaussian-Q function.

If it is possible to evaluate $\mathbb{E}\{|\mathbf{y}(n)|^2\}$ and $\mathbb{V}\text{ar}\{|\mathbf{y}(n)|^2\}$, the CLT approach can be applied to $\mathcal{H}_0$ and $\mathcal{H}_1$ (with any signal model), and the performance matrices can also be derived as (2.20). The mean and variance for different cases are given as follows:

$$\mathbb{E}\{|\mathbf{y}(n)|^2\} = \begin{cases} 2\sigma_w^2 & : \mathcal{H}_0 \\ 2\sigma_w^2 + |\mathbf{h}|^2|\mathbf{s}(n)|^2 & : \textbf{S1} \\ 2\sigma_w^2 + |\mathbf{h}|^2(2\sigma_s^2) & : \textbf{S2},\ \textbf{S3}. \end{cases} \tag{2.21}$$

$$\mathbb{V}\text{ar}\{|\mathbf{y}(n)|^2\} = \begin{cases} (2\sigma_w^2)^2 & : \mathcal{H}_0 \\ 4\sigma_w^2(\sigma_w^2 + |\mathbf{h}|^2|\mathbf{s}(n)|^2) & : \textbf{S1} \\ 4(\sigma_w^2 + |\mathbf{h}|^2|\sigma_s^2)^2 & : \textbf{S2} \\ (2\sigma_w^2)^2 + 2|\mathbf{h}|^2(2\sigma_w^2)(2\sigma_s^2) + |\mathbf{h}|^4(\mathbb{E}\{|\mathbf{s}(n)|^4]\} - 4\sigma_s^4) & : \textbf{S3}. \end{cases} \tag{2.22}$$

If $\mathbf{s}(n)$ of **S3** is complex phase shift keying (PSK) signal, $\mathbb{E}\{|\mathbf{s}(n)|^4\} = 4\sigma_s^4$, and thus the variance can be evaluated as $\mathbb{V}\text{ar}\{|\mathbf{y}(n)|^2\} = (2\sigma_w^2)^2 + 2|\mathbf{h}|^2(2\sigma_w^2)(2\sigma_s^2)$. Therefore, the distribution of Λ can be given as

$$\Lambda \sim \mathcal{N}\begin{cases} \mathcal{N}\left(N(2\sigma_w^2), N(2\sigma_w^2)^2\right) & : \mathcal{H}_0 \\ \mathcal{N}\left(N(2\sigma_w^2)(1+\gamma), N(2\sigma_w^2)^2(1+2\gamma)\right) & : \textbf{S1}, \textbf{S3} \\ \mathcal{N}\left(N(2\sigma_w^2)(1+\gamma), N(2\sigma_w^2)^2(1+\gamma)^2\right) & : \textbf{S2}. \end{cases} \tag{2.23}$$

Approximated false-alarm probability and approximated detection probabilities can be derived by using (2.20) as

$$P_f \approx Q\left(\frac{\lambda - N(2\sigma_w^2)}{\sqrt{N}(2\sigma_w^2)}\right), \tag{2.24}$$

$$P_{d,\mathbf{S1}} \approx Q\left(\frac{\lambda - N(2\sigma_w^2)(1+\gamma)}{\sqrt{N(1+2\gamma)}(2\sigma_w^2)}\right), \tag{2.25}$$

$$P_{d,\mathbf{S2}} \approx Q\left(\frac{\lambda - N(2\sigma_w^2)(1+\gamma)}{\sqrt{N}(1+\gamma)(2\sigma_w^2)}\right). \tag{2.26}$$

Note that $P_{d,\mathbf{S3}}$ has the same expression as $P_{d,\mathbf{S1}}$.

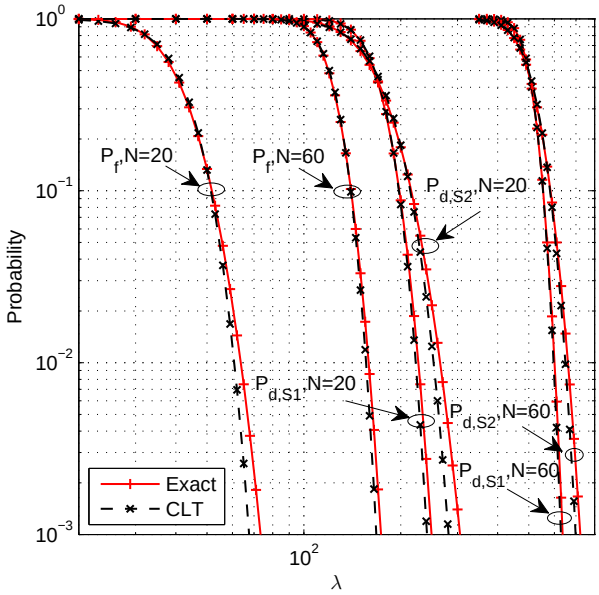

Figure 2.2: The exact and approximated (CLT) CDFs of the test statistic for **S1** and **S2** with $2\sigma_w^2 = 1$ and $\gamma = 5$dB.

Fig. 2.2 shows the exact P_f and P_d of the test statistic for **S1** and **S2**.[2] Both P_f and P_d increase significantly when the number of samples increases from $N = 20$ to $N = 60$. Fig. 2.2 also shows the CLT approximations of P_f and P_d. The exact curves (solid-line) match well with the CLT approximations (dashed-line) when $N = 60$, while they have a close match when $N = 20$. This confirms that the test statistic is approximately Gaussian for a sufficiently large number of samples.

Note that this thesis uses exact P_f and P_d expressions (2.15) (2.17) in Chapters 3–6, and uses approximated P_f and P_d expressions (2.24)-(2.26) (based on CLT) in Chapter 7.

[2] P_f and P_d are also the complementary cumulative distribution function (CDF)s of the test statistic.

2.5 Design Parameters

The main design parameters of the energy detector are the number of samples and threshold. However, the performance of the energy detector depends on SNR and noise variance as well, but the designer has very limited control over them because these parameters depend on the behavior of the mobile radio channel.

2.5.1 Threshold

A pre-defined threshold λ is required to decide whether the target signal is absent or present. The threshold determines all performance metrics, P_d, P_f and P_{md}, can vary from 0 to ∞, and selection of its operating threshold is important. The operating value can be chosen based on the target value of the performance metric of interest. Although having high P_d while keeping P_f low is preferable (e.g., as IEEE 802.22 WRAN), these two objectives are conflicting, and may not always be simultaneously achieved in practice.

When the threshold increases (or decreases), both P_f and P_d are decreased (or increased). For known N and σ_w, the common practice of setting the threshold is based on the constant false alarm probability P_f, e.g., $P_f \leq 0.1$. The selected threshold based on P_f can be given by using (2.24) as

$$\lambda_f^* = \left(Q^{-1}(P_f) + \sqrt{N}\right)\sqrt{N}2\sigma_w^2. \tag{2.27}$$

However this threshold may not guarantee that the energy detector achieves the target detection probability, e.g., the detection probability should be no less than 0.9 as specified in the IEEE 802.22 WRAN.

2.5.2 Number of Samples

The number of samples is also an important design parameter to achieve the requirements on detection and false alarm probabilities. For given false alarm probability P_f and average detection probability P_d, the minimum required number of samples can be given as a function of SNR. By eliminating λ from both P_f in (2.24) and P_d in (2.25) (here signal model **S1** is used as an example), N can be given as

$$N = [Q^{-1}(P_f) - Q^{-1}(P_d)\sqrt{2\gamma + 1}]^2\gamma^{-2} \tag{2.28}$$

which is not a function of the threshold. Due to the monotonically decreasing property of $Q^{-1}(x)$, it can be seen that the signal can be detected even in very low SNR region by increasing N when the noise power is perfectly known. Further, the approximately required number of samples to achieve a performance target on false alarm and detection probabilities is in the order of $\mathcal{O}(\gamma^{-2})$, i.e., energy detector requires more samples at very low SNR [57]. Since $N \approx \tau f_s$ where τ be the sensing time and f_s be the sampling frequency, the sensing time increases as N increases. This is a main drawback in spectrum sensing at low SNR because of the limitation on the maximal allowable sensing time (e.g., the IEEE 802.22 specifies that the sensing time should be less than 2 seconds).

2.6 IEEE 802.22 Standard

As mentioned in Section 1.2.1, FCC has permitted the TV white space spectrum to be used by broadband access systems. Several telecommunications standards have thus been developed to operate in the vacant TV bands based on cognitive radio technology. Among these standardization efforts [14–16], the IEEE 802.22 WRAN brings broadband access not only to the WiFi devices but also to general mobile networks (e.g., micro-, pico- or femto-cells), allowing the use of the cognitive radio technique on a non-interfering basis [11–13].

The IEEE 802.22 WRAN limits both false alarm (which indicates the level of undetected spectrum holes) and missed-detection (which indicates the level of unexpected interference to primary users) probabilities to 10%. While these two performance metrics reflect the overall efficiency and reliability of the cognitive network, the 10% requirement should be met even under very low SNR conditions, such as -20 dB SNR with a signal power of -116 dBm and a noise floor of -96 dBm [13].

The IEEE 802.22 WRAN does not prescribe a specific spectrum sensing technique, and designers are free to select any detection technique such as energy detection, matched filter detection, cyclostationary feature detection, covariance based detection, etc. [48, 53, 54, 58–65]. While the spectrum sensing techniques perform well at moderate and high SNRs, in which fine-sensing time can be in order of mil-

liseconds (e.g., 25 ms), they perform poorly at a low SNR. Although increasing the sensing time improves the performance, IEEE 802.22 limits the maximal detection latency to 2 seconds which may include sensing time and subsequent processing time. This maximal time limit is critical at low-SNR spectrum sensing.

2.7 Cooperative Spectrum Sensing

Achieving the IEEE 802.22 WRAN spectrum sensing specifications is a tough task because of shadowing, fading, and time variations of mobile radio channels. Moreover, the hidden terminal problem, which occurs when the link from a primary transmitter to a secondary user is shadowed (e.g., there is a tall building between them as shown in Fig. 2.3) while a primary receiver is operating in the vicinity of the secondary user, presents a tough challenge. Due to this, a secondary user may fail to notice the presence of the primary transmitter, and then accesses the licensed channel and causes interference to the primary receiver. To mitigate this problem, cooperative spectrum sensing has been introduced, in which single cooperative node or multiple cooperative nodes are introduced to the secondary network (Fig. 2.3). Cooperative nodes individually sense the spectrum, and send their collected data to a fusion center. The random spatial distribution of the cooperative nodes helps to reduce the impact of the hidden terminal problem.

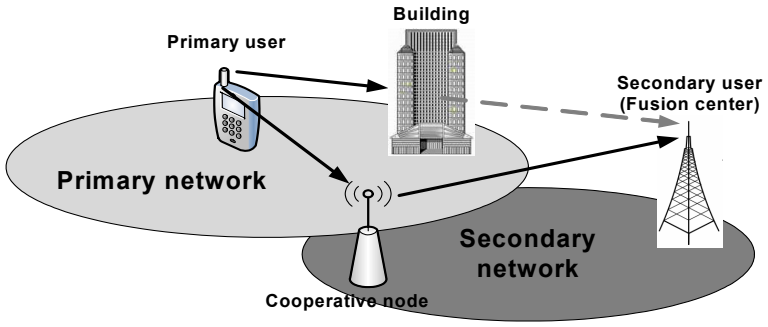

Figure 2.3: Cooperative spectrum sensing in a cognitive radio network.

In cooperative spectrum sensing, information from multiple cooperative nodes is combined at the fusion center to make a decision on the presence or absence of the primary user. When energy detection is utilized for cooperative spectrum

sensing, cooperative nodes report to a fusion center their sensing data, in either the data fusion or the decision fusion. In data fusion, each cooperative node simply amplifies the received signal from the primary user and forwards to the fusion center [66–68]. In decision fusion, each cooperative node makes its own hard decision on the primary user activity, and the individual decisions are reported to the fusion center. The performance of such system is analyzed in Chapter 6.

$\sim$

Chapter 3

Energy Detection over Composite Fading and Shadowing Channels

This chapter analyzes the performance of an energy detector over mobile radio channels with composite multipath fading and shadowing effects. These effects are modeled by using the K and K_G channel models. For these channels, the average detection probabilities of the energy detector are derived for the no-diversity reception case. A simple approximation of the average detection probability is also derived for large threshold values. The analysis is then extended to cases with diversity receptions including maximal ratio combining (MRC) and selection combining (SC).[1]

3.1 Introduction

The performance of energy detectors has been extensively analyzed by using different channel models assuming a flat, band-limited, Gaussian noise channel [48]. Subsequently, the average detection probability is analyzed over Rayleigh, Rice and Nakagami fading channels in [69]. Different analytical approaches are given in [53, 70] for the performance of an energy detector with no diversity for Rayleigh, Rice and Nakagami fading channels and with different diversity receptions such as MRC, SC and switch-and-stay combining. The performance with equal gain combining (EGC) under a Nakagami fading channel is analyzed in [54]. All these

[1] *A version of this chapter has been published in IEEE Trans. Wireless Commun., 9: 3662–3670 (2010).*

research papers have focused on multipath fading only.

Shadowing and multipath fading are the two main wireless propagation effects. While multipath fading can be modeled as a Rayleigh, Rice or Nakagami distribution, shadowing process is typically modeled as a lognormal distribution [39]. Practical communication channels can be modeled as multipath fading superimposed on lognormal shadowing, leading to composite channel models. Due to the analytical intractability of composite fading models, the shadowing effect is sometimes neglected in the literature.

The K and K_G channel models described in Section 2.1.2 have been well adopted for analysis of composite multipath fading and shadowing. Performance of different wireless communications networks has been analyzed over K or K_G channel model in [42,44,71–73]. The bit error rate (BER) is analyzed for the K channel model in [71] and for the K_G channel model in [73]. The outage probability with and without co-channel interference is presented based on the K_G channel model in [72]. The average BER with different diversity receptions is derived for the K_G channel model in [44]. Recently, performance of generalized selection combining receivers over the K channel model is presented in [42]. All these works show the impact of composite effect (multipath fading and shadowing) in the performance and design of wireless communications. However, the performance of an energy detector under composite fading is not available in the literature, and thus it is investigated in this chapter by using K and K_G channel models.

The chapter is organized as follows. The average detection probability of an energy detector is analyzed without and with diversity techniques in Section 3.2. Numerical and simulation results are presented in Section 3.3. The concluding remarks are made in Section 3.4.

3.2 Average Detection Probability

The performance of an energy detector for channels with both multipath fading and shadowing, by the adoption of the K and K_G channel models is analyzed based on **S1** signal model. When the threshold varies from 0 to ∞, the false alarm probability

can be easily calculated by using (2.15) for a given number of samples. On the other hand, the detection probability is determined by threshold, number of samples and also SNR. Since SNR depends on the channel fading/shadowing, it is essential to evaluate the average detection probability over the SNR distribution $f_\gamma(x)$ as

$$\overline{P_d} = \int_0^\infty P_d(x) f_\gamma(x)\, \mathrm{d}x. \tag{3.1}$$

The critical part of the analysis is the derivation of the average detection probability. This derivation requires the generalized Marcum-Q function be averaged over the K_G distribution. Since the K and K_G channel models contain modified Bessel functions, the direct integration appears intractable or does not seem to lead to simple solutions. In order to circumvent these difficulties, the following method is applied. Since K or K_G channel model actually is a result of averaging a conditional Rayleigh or Nakagami PDF by a gamma PDF, the existing results on the energy detector for Nakagami-m fading case can be averaged over the gamma PDF (which models the shadowing part) to get the avergae detection probability over K or K_G channel model. This simple trick allows us to avoid the averaging over the modified Bessel function of the second kind. Similar approach can be applied for the diversity combining techniques with each diversity branch having identical instantaneous shadowing effect.

3.2.1 With No-Diversity Reception

The average detection probability of the energy detector can be evaluated by averaging $P_d = Q_N\left(\sqrt{2N\gamma}, \sqrt{\lambda}\right)$, where $\sigma_w = 1$, in (2.17) over the SNR range, which can be expressed mathematically as

$$\begin{aligned}
\overline{P_d} &= \int_0^\infty Q_N(\sqrt{2N\gamma}, \sqrt{\lambda}) f_\gamma(\gamma)\, \mathrm{d}\gamma \\
&= \int_0^\infty \int_0^\infty Q_N(\sqrt{2N\gamma}, \sqrt{\lambda}) f_{\gamma|Y=y}(\gamma) d\gamma f_Y(y)\, \mathrm{d}y \\
&= \int_0^\infty P_d^{Fad}(y) f_Y(y)\, \mathrm{d}y,
\end{aligned} \tag{3.2}$$

where Y is the SNR with only shadowing effect (i.e., multipath fading is excluded), which follows a gamma distribution [39]

$$f_Y(y) = \frac{1}{\Gamma(k)\Omega^k} y^{k-1} e^{-\frac{y}{\Omega}}, \;\; y \geq 0 \tag{3.3}$$

and $P_d^{Fad}(y) = \int_0^\infty Q_N(\sqrt{2N\gamma}, \sqrt{\lambda}) f_{\gamma|Y=y}(\gamma)\, \mathrm{d}\gamma$ is the average[2] detection probability with a specific Y value. $P_d^{Fad}(y)$ for different applications under different multipath fading can be expressed using previous results in the literature [53] [69] [70], by replacing the $\bar{\gamma}$'s in previous results with y. The average detection probability can be derived after averaging $P_d^{Fad}(y)$ by $f_Y(y)$. This approach appears mathematically more tractable than the direct integration.

K Channel Model

The average detection probability over the K channel model, $\overline{P_d^K}$, can be evaluated by replacing each $\bar{\gamma}$ of the average detection probability over Rayleigh distribution in [53, eq. (9)] by y, and averaging over $f_Y(y)$ as given in Appendix A.1. Thus, $\overline{P_d^K}$ can be expressed as

$$\begin{aligned}
\overline{P_d^K} = {} & e^{-\frac{\lambda}{2}} \sum_{n=0}^{N-2} \frac{1}{n!} \left(\frac{\lambda}{2}\right)^n \\
& + \sum_{n=0}^{\infty} \frac{(-1)^n \left(\frac{\lambda}{2}\right)^n \Gamma(k-N+1)}{n!\Gamma(k)(N\Omega)^k} U\left(k-N+1; k-n+1; \frac{1}{N\Omega}\right) \\
& - \sum_{n=0}^{N-2} \frac{e^{-\frac{\lambda}{2}} \left(\frac{\lambda}{2}\right)^n \Gamma(n+k-N+1)}{n!\Gamma(k)(N\Omega)^k} U\left(n+k-N+1; k+1; \frac{1}{N\Omega}\right).
\end{aligned} \tag{3.4}$$

where $U(\cdot;\cdot;\cdot)$ is the confluent hypergeometric function of the second kind defined as [74, eq. (3.383.5)]

$$\int_0^\infty e^{-px} x^{q-1} (1+ax)^{-v}\, \mathrm{d}x = \frac{\Gamma(q)}{a^q} U\left(q; q+1-v; \frac{p}{a}\right) \tag{3.5}$$

with $q > 0$, $p > 0$, $a > 0$ and v a complex value.

[2]Here the "average" means the average with respect to multipath fading.

K_G Channel Model

The average detection probability over K_G channel model, $\overline{P_d^{K_G}}$, can be evaluated by replacing each $\bar{\gamma}$ of the average detection probability over Nakagami-m distribution in [53, eq. (7)] by y, and averaging over $f_Y(y)$ as given in Appendix A.2. Thus, $\overline{P_d^{K_G}}$ can be expressed as

$$\begin{aligned}\overline{P_d^{K_G}} &= \frac{1}{\Gamma(k)}\left(\frac{m}{N\Omega}\right)^k \\ &\times \Bigg[\sum_{s=0}^{\infty}\sum_{n=1}^{N-1}\frac{e^{-\frac{\lambda}{2}}\left(\frac{\lambda}{2}\right)^{n+s}(m)_s\Gamma(s+k)U\left(s+k;k-m+1;\frac{m}{N\Omega}\right)}{n!s!(n+1)_s} \\ &+\sum_{t=0}^{\infty}\sum_{v=0}^{m-1}\frac{(-1)^t(\frac{\lambda}{2})^{t+v}\Gamma(v+k)\binom{m-1}{m-v-1}U\left(v+k;k-t-m+2;\frac{m}{N\Omega}\right)}{t!v!} \\ &+\sum_{s=0}^{\infty}\sum_{n=0}^{m-2}\sum_{a=0}^{n}\frac{(-1)^s(\frac{\lambda}{2})^{a+s}\binom{n}{n-a}\Gamma(a+k+1)U\left(a+k+1;k-s-n+1;\frac{m}{N\Omega}\right)}{a!s!}\Bigg]\end{aligned} \tag{3.6}$$

where $\binom{n}{k}$ is the binomial coefficient defined as $\binom{n}{k}=\frac{n!}{k!(n-k)!}$, $(x)_s$ is the Pochhammer symbol defined as $(x)_s=\frac{\Gamma(x+s)}{\Gamma(x)}$. This is valid for integer m.

One challenge in calculating the expressions (3.4) and (3.6) is the infinite sums. As an example, the expression (3.4) is calculated as in the following. The expression (3.6) can be treated similarly. The expression (3.4) can be rewritten as

$$\overline{P_d^K}= e^{-\frac{\lambda}{2}}\sum_{n=0}^{N-2}\frac{1}{n!}\left(\frac{\lambda}{2}\right)^n+\sum_{n=0}^{\infty}(-1)^n a_n-\sum_{l=0}^{N-2}b_l \tag{3.7}$$

where

$$a_n=\frac{(\frac{\lambda}{2})^n\Gamma(k-N+1)U\left(k-N+1;k-n+1;\frac{1}{N\Omega}\right)}{n!\Gamma(k)(N\Omega)^k}$$

is the nth term of the auxiliary series $\sum_{n=0}^{\infty}(-1)^n a_n$, and

$$b_l=\frac{e^{-\frac{\lambda}{2}}\left(\frac{\lambda}{2}\right)^l\Gamma(l+k-N+1)U\left(l+k-N+1;k+1;\frac{1}{N\Omega}\right)}{l!\Gamma(k)(N\Omega)^k}$$

is the lth term of the finite series $\sum_{l=0}^{N-2}b_l$. Theoretically, the auxiliary series converges as $n\to\infty$. When λ is small, it is observed that the series converges for relatively small values of n, and thus, (3.4) can be accurately computed by using any mathematical software (e.g., MATHEMATICA [75]). When λ is large, the

sum requires the evaluation of a_n for large n, and therefore, accurate computation of (3.4) is difficult (e.g., numerical underflow and overflow errors degrade the accuracy). For higher λ values, the corresponding values of the average detection probability as well as the false alarm probability are very small (for instance, it can be less than 10^{-3}). Thus, an approximation is needed for large λ. Note that the first and the third terms in (3.7) are finite sums and therefore, can be calculated exactly. For accuracy of (3.7), it is essential to calculate the second term in (3.7), denoted as $I_K = \sum_{n=0}^{\infty}(-1)^n a_n$, accurately. In the following, convergence acceleration of I_K and an approximation method are given for I_K.

Convergence Acceleration

As $\lambda \to \infty$, a large number of terms in I_K need to be evaluated. This drawback can be avoided by using a convergence acceleration technique. The idea is to generate a new sequence by using $a_k|_{k=0}^{N}$. Consider the partial sums $s_n = \sum_{k=0}^{n}(-1)^k a_k$ for $n = 0, 1, \ldots, N-1$. The objective is to estimate the limit s_∞ by using as few as possible partial sums. The ϵ-algorithm [76] is a powerful convergence acceleration technique suitable for this purpose. The algorithm generates an array ϵ with $\epsilon_{-1}(s_n) = 0$, $\epsilon_0(s_n) = s_n$, and

$$\epsilon_{r+1}(s_n) = \epsilon_{r-1}(s_{n+1}) + \frac{1}{\epsilon_r(s_{n+1}) - \epsilon_r(s_n)} \tag{3.8}$$

where $r(\geq 0)$ is an integer. The acceleration method starts with a partial sum of I_K. It then estimates the converging point of n through (3.8) while keeping adding adequate terms in I_K to reach the required accuracy.

Approximation

After applying binomial expansion with some algebraic manipulations, I_K can be approximated for large λ as

$$\begin{aligned} I_K &\approx \frac{1}{\Gamma(k)\Omega^k} \sum_{s=0}^{N-1} \binom{N-1}{s} N^{s+1-N} \int_0^\infty y^{k-N+s} e^{-\left(\frac{\lambda}{2Ny} + \frac{y}{\Omega}\right)} \, \mathrm{d}y \\ &= \frac{2}{\Gamma(k)(N\Omega)^k} \sum_{s=0}^{N-1} \binom{N-1}{s} \left(\frac{\lambda\Omega}{2N}\right)^{\frac{p}{2}} K_p\left(\sqrt{\frac{2\lambda}{N\Omega}}\right) \end{aligned} \tag{3.9}$$

where the second equality comes from [74, eq. (3.478.4)] and $p = k - N + s + 1$. The expression (3.9) consists of a finite summation with $K_p(\cdot)$, which is available in most mathematical software. The accuracy of the average detection probability depends on the accuracy of this approximation. For instance, a four-decimal-point accuracy is achieved in the average detection probability when a four-decimal-point accuracy is achieved in I_K.

3.2.2 With Diversity Reception

In this section, the performance of an energy detector is considered with diversity combining methods. The L diversity branches are independent and modeled with the K distribution. The same analytical technique can be applied as in (3.2). Two diversity techniques such as MRC and SC are mainly focused here. Diversity combining techniques are used at the receiver to enhance the receive SNR. However, they may increase the implementation complexity because receiver may need additional knowledge of the network, e.g., knowledge of channel-state information (CSI).

Maximal Ratio Combining

The MRC is a coherent combining technique which needs CSI in non-coherent energy detection. Thus, it may increase the design complexity. The MRC receiver combines all the diversity branches weighted with their corresponding complex fading gains as shown in Fig. 3.1.

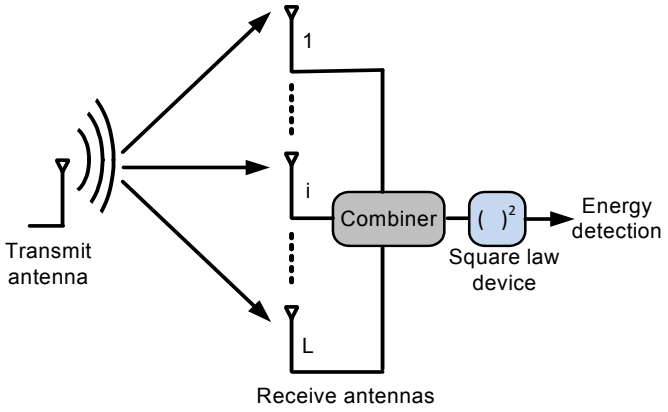

Figure 3.1: Energy detection with MRC.

The energy detector processes the samples of the combined signal of L diversity branches, $\mathbf{Y}(n)$, which can be given as

$$\mathbf{Y}(n) = \mathbf{H}\mathbf{s}(n) + \mathbf{W}(n) \tag{3.10}$$

where $\mathbf{H} = \sum_{l=1}^{L} |\mathbf{h}_l|^2$ and $\mathbf{W}(n) = \sum_{l=1}^{L} \mathbf{h}_l^* \mathbf{w}_l(n)$ are effective channel gain and noise sample, respectively, and $\mathbf{w}_l(n)$ and $\mathbf{h}_l$ are noise and channel coefficient of the lth branch, respectively. The output signal of the MRC can be written as (3.10). Thus the test statistic is given as

$$\Lambda = \sum_{n=1}^{N} |\mathbf{Y}(n)|^2 . \tag{3.11}$$

The effective number of samples for the test statistic is N. The instantaneous SNR of the combiner output is thus $\gamma^{\text{MRC}} = \gamma_1 + \gamma_2 + ... + \gamma_L$. Since energy detector compares the received energy after the L i.i.d. branches are combined, the expression of the false-alarm probability is same as (2.15) and the instantaneous detection probability for AWGN channels can be given as $P_d = Q_N\left(\sqrt{2N\gamma^{\text{MRC}}}, \sqrt{\lambda}\right)$. To derive the average detection probability, P_d should then be averaged over the Rayleigh fading first, and then averaged over the shadowing. The PDF of γ^{MRC} for i.i.d. Rayleigh fading channels is given by [39]

$$f_{\gamma^{\text{MRC}}}(x) = \frac{x^{L-1}\, e^{-\frac{x}{\bar{\gamma}}}}{\Gamma(L)\bar{\gamma}^L} \tag{3.12}$$

where $\bar{\gamma}$ is the average SNR in any branch (note that the "averaging" is on fading only, excluding shadowing). The $f_{\gamma^{\text{MRC}}}(x)$ in (3.12) is similar to the PDF of γ under Nakagami fading in no-diversity. Therefore, after averaging on Rayleigh fading, the P_d under MRC (P_d^{MRC}) can be obtained from the average detection probability for a Nakagami channel with no diversity (i.e. by replacing m by L and y by Ly in (A.1) in the Appendix). Therefore, the overall average detection probability for the K channel model with MRC, $\overline{P_d^{\text{MRC}}}$, can be obtained by averaging the "average detection probability for a Nakagami channel with no diversity" over a gamma distribution, which is exactly the expression $\overline{P_d^{K_G}}$ in (3.6), but with m replaced by L and Ω replaced by $L\Omega$.

Selection Combining

The combiner selects the branch having the strongest SNR among all diversity branches. The SNR at the output of the combiner is $\gamma^{\text{SC}} = \max\{\gamma_1, \gamma_2, ..., \gamma_L\}$. The PDF of γ^{SC}, without shadowing, is given in [70, eq. (29)]. Replacing each $\bar{\gamma}$ in [70, eq. (30)] by y and averaging it over $f_Y(y)$, the average detection probability for SC diversity scheme under the K channel model, $\overline{P_d^{\text{SC}}}$, can be evaluated as

$$\overline{P_d^{\text{SC}}} = L \sum_{p=0}^{L-1} \frac{(-1)^p}{p+1} \binom{L-1}{p} \overline{P_d^K} \left(\frac{\Omega}{p+1} \right)$$

where $\overline{P_d^K}\left(\frac{\Omega}{p+1}\right)$ is the $\overline{P_d^K}$ in (3.4) with the replacement of each Ω by $\left(\frac{\Omega}{p+1}\right)$.

3.3 Numerical and Simulation Results

Validation of the Analysis

Analytical results in (3.4) and (3.6) are verified by numerical methods[3] through the Gaussian-Legendre method and Monte Carlo simulations, as shown in Fig. 3.2a.

The expressions (3.4) and (3.6) are calculated by MATHEMATICA software package [75], as shown in Fig. 3.2a by legend "Equation (3.4)" and "Equation (3.6)". Since the number of terms to sum up to achieve the required accuracy (e.g., up to four decimal points) increases with the increase of λ, an acceleration method is used, in which an ϵ-algorithm [76] is applied to calculate the alternative series in (3.4) and (3.6). As an example, the converging points of n (which reaches the required accuracy) for different λ values are given in Table 3.1, for the equation (3.4), the ϵ-algorithm, and the Gaussian-Legendre method used in the numerical approximations.

Numerical integration is performed with the Gaussian-Legendre method, which is explained here briefly. If an integral is in the form $\int_{-1}^{1} f(x)\,\mathrm{d}x$, the Gaussian-Legendre rule can be applied as

$$\int_{-1}^{1} f(x)\,\mathrm{d}x \approx \sum_{i=1}^{n} w_i f(x_i)$$

[3]Note that the numerical methods are only for numerical calculation of the expression (3.4) and (3.6). On the other hand, the expression (3.9) is an approximation for (3.4).

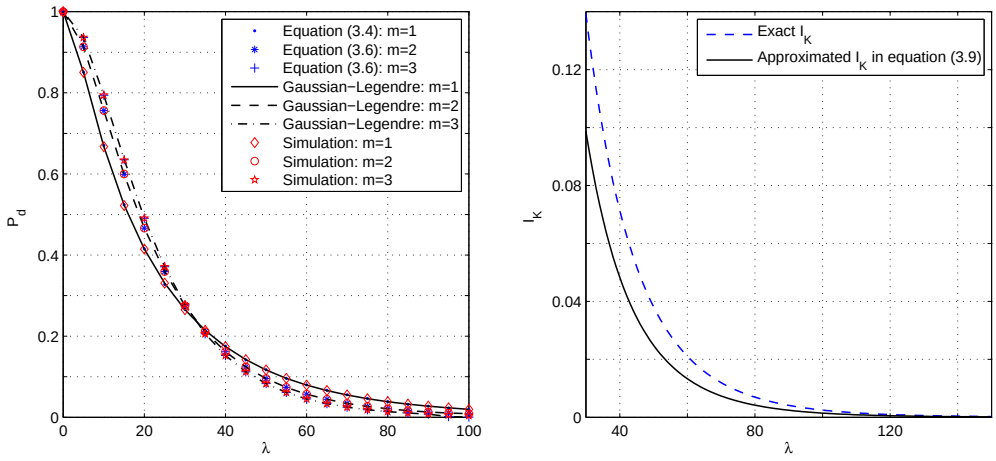

(a) (b)

Figure 3.2: (a) Comparison of analytical expressions (3.4) and (3.6) with numerical approximations by the Gaussian-Legendre method, and Monte Carlo simulations ($N = 2$, $k = 5.5$ and $\bar{\gamma} = 10$ dB); (b) Comparison of exact I_K with approximation in (3.9).

	Converging point of (n)			
	$\lambda = 25$	$\lambda = 50$	$\lambda = 75$	$\lambda = 100$
Equation (3.4)	20	50	84	114
$\epsilon-$Algorithm	11	15	19	23
Gaussian-Legendre	38	38	38	38

Table 3.1: Number of terms required to get the accuracy up to four decimal points.

by a suitable choice of the nodes (Legendre points) x_i's and weights w_i's ($i = 1, ..., n$), where n is the number of nodes. The integral of I_K in the form of $\int_0^\infty h(y)\,\mathrm{d}y$ can be transformed to the form $\int_0^{\frac{\pi}{2}} \phi(\theta)\,\mathrm{d}\theta$ by using the substitution $y = \tan\theta$. Further, it can be transformed to the form $\int_{-1}^{1} f(x)\,\mathrm{d}x$ using the substitution $\theta = \frac{\pi}{4}x + \frac{\pi}{4}$. With the help of the three-term recurrence relation, nodes x_i and weights w_i can be computed from the associated eigenvalues and eigenvectors [77, Table 25.4]. Therefore, the Gaussian-Legendre method is suitable for I_K to evaluate (3.4) numerically. A similar method can be applied to evaluate (3.6).

Fig. 3.2a shows that the analytical results in (3.4) and (3.6) match well with the simulations, and the Gaussian-Legendre method provides an accurate approximation.

Accuracy of the Approximation for I_K

In Fig. 3.2b, I_K (exact and approximation) vs λ is plotted. The approximation acts as a lower bound for all λ's and the bound gets tighter when λ increases from 0 to ∞ (i.e., for large λ's). As an example, accuracy of four decimal points can be achieved when $\lambda > 140$ with $N = 3$, $k = 5.5$ and $\Omega = 1$. However, it should be noted that for small λ's (practical threshold range), (3.4) and (3.6) can be used directly to evaluate the accurate detection probabilities without approximation. The approximation helps for asymptotic analysis.

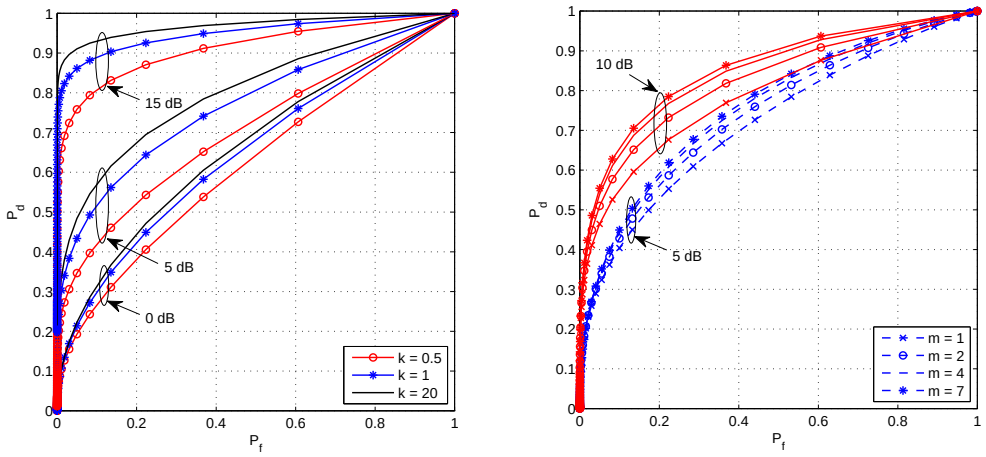

(a) (b)

Figure 3.3: (a) ROC curves for the K channel model with different k ($N = 1$, $\bar{\gamma} = 0$, 5, 15 dB); (b) ROC curves for K_G channel model with different fading parameters, m ($k = 5.5$, $N = 1$, $\bar{\gamma} = 5$, 10 dB).

Impact of the Shadowing and Fading

Fig. 3.3a shows the ROC curves (which are illustrated by P_d vs P_f [78]) for the K channel model with different k and average SNR $\bar{\gamma}$. With the increase of k, an improvement in the detection probability is observed. This is because increasing k diminishes the shadowing effect. When $k \to \infty$, the channel is a Rayleigh fading model. For K_G channel, Fig. 3.3b shows effect of multipath fading with fixed shadowing ($k = 5.5$). Different m values are taken, with $\bar{\gamma} = 5, 10$ dB. For larger m, the receiver has a higher detection probability with a lower false alarm probability, i.e.,

the channel fading conditions improve with the reduced fluctuations of the signal strength.

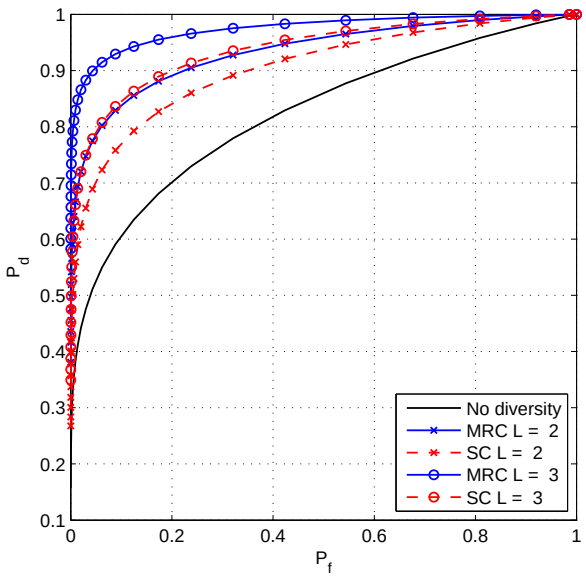

Figure 3.4: ROC curves for L-branch MRC and SC diversity receptions with K channel model ($N = 3$, $k = 6$, $\bar{\gamma} = 5$ dB).

Performance of Diversity Receptions

The performance of MRC and SC diversity schemes with different number L of diversity branches, which have the same instantaneous shadowing, is illustrated in Fig. 3.4. There is an obvious diversity gain in the case of diversity systems compared to no-diversity system (the case with $L = 1$). Further, MRC always outperforms SC.

Shadowing Effect

Further, it is important to notice the differences between Rayleigh-lognormal distribution and K distribution. In general, the performance of shadowing effect is compared with respect to shadow standard deviation σ_Ω and mean μ_Ω in lognormal distribution [39, eq. (2.200)]. The relationships between the parameters in Rayleigh-lognormal distribution (σ_Ω and μ_Ω) and parameters in K distribution (k

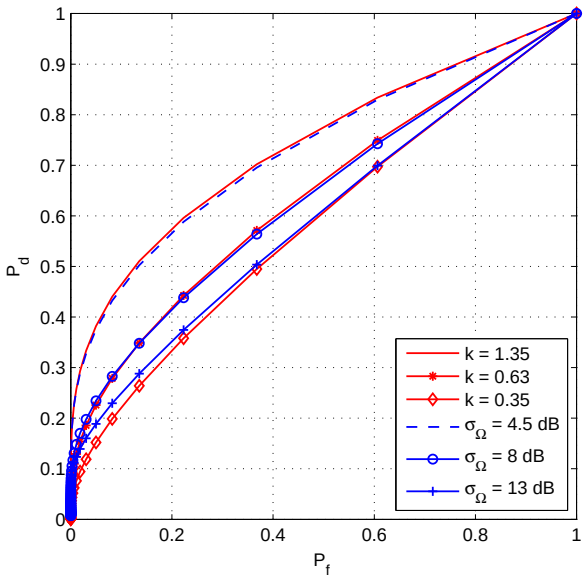

Figure 3.5: Comparison of K channel model with Rayleigh-lognormal channel.

and Ω) can be obtained as [41]

$$\xi\mu_\Omega = \ln\Omega + \Psi(k) \qquad \text{and} \qquad (\xi\sigma_\Omega)^2 = \Psi^{'}(k)$$

where $\xi = \frac{\ln 10}{10}$, $\Psi(\cdot)$ is the psi function [77], and $\Psi^{'}(\cdot)$ is the first derivative of $\Psi(\cdot)$. Fig. 3.5 shows the ROC curves of the energy detector for $\sigma_\Omega \approx 4.5$ dB, 8 dB and 13 dB to represent urban area, typical microcell and worst case of macrocell, respectively. The respective k and μ_Ω values for $\sigma_\Omega \approx 4.5$, 8.0, 13 dB are $k \approx$ 1.35, 0.63, 0.35 and $\mu_\Omega \approx 2.5155$, -3.2254, -9.893 dBm with Ω =2, respectively. Fig. 3.5 shows that the K distribution is a well-approximated model for the the Rayleigh-lognormal distribution.

3.4 Conclusion

The performance of an energy detector under both multipath fading and shadowing effects is studied by using K and K_G channel models. The average detection probabilities are derived along with the approximations for large λ values. Convergence acceleration based on the ϵ-algorithm is suggested to efficiently compute the infinite series representation. Moreover, the numerically efficient Gaussian-Legendre

quadrature is useful for numerical approximations. These results show that the detection probability increases with the fading parameter m and shadowing parameter k. The reason is that as $m \to \infty$ and $k \to \infty$, the channel approaches the AWGN channel. Furthermore, when diversity receptions such as MRC and SC are used to boost the performance of the energy detector, their performance is also analyzed under multipath faded and shadowed diversity branches. The ROC reveals the effect of diversity advantage, and, as expected, MRC improves the performance of the energy detector more than SC.

$\sim$

Chapter 4

A Mixture Gamma Distribution to Model the SNR of Wireless Channels

As discussed in Section 2.1.2, composite fading which includes multipath fading and shadowing has increasingly been analyzed by means of the K channel and related models. Nevertheless, these models do have computational and analytical difficulties when energy detection and other wireless network performance are analyzed. Motivated by this problem, this chapter develops a mixture gamma (MG) distribution which can represent several common wireless channels. The accuracy of the MG representation of composite fading channels and small-scale fading channels is also examined. Performance analysis and numerical results are given from the unified analytical framework.[1]

4.1 Introduction

Performance Analysis Based on K and K_G Models

The use of K and K_G models for performance analysis has greatly increased recently (see [44, 73, 79–86], among many others). For instance, the statistics of SNR, the average channel capacity and the BER are analyzed in [73, 79]. The outage performance, the average BER, and the channel capacity of several adaptive schemes are derived in [80]. The average output SNR, amount of fading and outage probability of different diversity receivers are derived in [44]. The closed-form BER

[1] *A version of this chapter has been published in IEEE Trans. Wireless Commun., 10: 4193–4203 (2011).*

is derived for (post-detection) EGC in [81]. The performance of dual-hop non-regenerative relays and multihop regenerative relays is analyzed in [82–84]. The average BER of orthogonal frequency division multiplexing (OFDM) systems is evaluated in [85]. The ergodic capacity of multiple-input multiple-output (MIMO) systems is investigated in [86]. The performance of an energy detector is analyzed in Chapter 3 of this thesis. These studies and others show the importance of K and K_G models.

Limitations of K and K_G Models

While Rayleigh-lognormal (RL) and Nakagami-lognormal (NL) do not have closed-form PDFs, the K, K_G and $\mathcal{G}$- models do. Nevertheless, their PDFs include special functions (e.g., modified Bessel functions). Consequently, mathematical complications arise in the evaluation of wireless performance metrics. For instance, the CDF of the K_G model is derived in [73] by using generalized hypergeometric functions. The computation of such functions can be difficult as their series expressions may give rise to numerical issues. Asymptotic expansions may hence be required for certain ranges of the parameters and the variables. Moreover, the PDF of a sum of SNRs (required in MRC) is intractable. As well, even numerical methods for MRC by using the characteristic function approach is quite difficult due to the Whittaker function [46]. To avoid these difficulties, a K_G random variable (RV) is approximated by a Gamma RV in [46], and the PDF of the sum of independent K_G RVs is further approximated by PDF of another K_G RV [87]. These approximations use moment matching.

While performance evaluation over composite channels is highly important, the use of K, K_G and $\mathcal{G}$ models has analytical and/or computational difficulties. Hence, an alternative approach is developed by using the MG distribution in this chapter.

The rest of the chapter is organized as follows. The MG distribution is described in Section 4.2. Several common mobile radio channels are represented by using the MG model in Section 4.3. In Section 4.4, the accuracy of the MG representation of composite fading channels and small-scale fading channels is examined. Performance analysis and the numerical results from the unified framework are shown in

Section 4.5 and Section 4.6. The concluding remarks are in Section 4.7.

4.2 Mixture Gamma Distribution

The MG distribution provides several advantages due to several reasons. First, since it is a linearly weighted sum of gamma distributions, it inherits several advantages of the gamma distribution. For example, the MGF and CDF, which are required in wireless system analysis, have mathematically tractable expressions. Second, this distribution can approximate not only composite fading channels, but also any small-scale fading channels. Third, high accuracy is possible by adjusting the parameters. Overall, by using the MG model, performance of any wireless systems over a variety of fading channels can be analyzed in a unified framework.

In [88], it is shown that any function $f(x)$, where $\lim_{x\to+\infty} f(x) \to 0$ and $x \in (0,\infty)$, can be given as $f(x) = \lim_{u\to+\infty} \mathcal{F}_u(x)$ where $\mathcal{F}_u(x) := e^{-ux}\sum_{k=0}^{\infty}\frac{(ux)^k}{k!}f\left(\frac{k}{u}\right)$, $u > 0$. Thus, an arbitrarily close approximation to $f(x)$ can be obtained by increasing the number of terms in the mixture [89]. Note that $\mathcal{F}_u(x)$ is a weighted sum of gamma PDFs. This result provides the motivation for using the MG distribution to represent any wireless SNR models. We start with the SNR distribution, which is required for analysis of wireless communication systems. The instantaneous received SNR and the average SNR are denoted by γ and $\bar{\gamma}$, respectively.

Probability Density Function (PDF)

The following MG distribution is proposed to approximate the PDF of γ as

$$f_\gamma(x) = \sum_{i=1}^{S} w_i f_i(x) = \sum_{i=1}^{S} \alpha_i x^{\beta_i - 1} e^{-\zeta_i x}, \quad x \geq 0 \tag{4.1}$$

where $f_i(x) = \frac{\zeta_i^{\beta_i} x^{\beta_i - 1} e^{-\zeta_i x}}{\Gamma(\beta_i)}$ is a standard Gamma distribution, $w_i = \frac{\alpha_i \Gamma(\beta_i)}{\zeta_i^{\beta_i}}$, S is the number of terms, and α_i, β_i and ζ_i are the parameters of the ith, $i = 1, \cdots, S$, Gamma component. Further, $\sum_{i=1}^{S} w_i = 1$ as $\int_0^\infty f_\gamma(x)\,\mathrm{d}x = 1$. The special case $S = 1$ reverts to SNR distributions of Rayleigh and Nakagami-m fadings. Discussion of how to choose S is provided in Section 4.4. Note that formula (4.1) can approximate the PDF of any positive random variable.

Cumulative Distribution Function (CDF)

The CDF of the MG distribution can be evaluated as $F_\gamma(x) = \int_0^x f_\gamma(t)\,\mathrm{d}t$ to yield

$$F_\gamma(x) = \sum_{i=1}^{S} \alpha_i \zeta_i^{-\beta_i} \gamma\left(\beta_i, \zeta_i x\right) \tag{4.2}$$

where $\gamma(\cdot,\cdot)$ is the lower incomplete gamma function [74, eq. (8.350.1)].

Moment Generating Function (MGF)

The MGF of MG distribution, $\mathcal{M}_\gamma(s)$, can be evaluated as $\mathcal{M}_\gamma(s) = \mathbb{E}\{e^{-s\gamma}\}$. Thus, $\mathcal{M}_\gamma(s) = \int_0^\infty e^{-sx} f_\gamma(x)\,\mathrm{d}x$ can be derived as

$$\mathcal{M}_\gamma(s) = \sum_{i=1}^{S} \frac{\alpha_i \Gamma(\beta_i)}{(s+\zeta_i)^{\beta_i}}. \tag{4.3}$$

Moments

The r-th ($r = 0, 1, \cdots, \infty$) moment associated with the MG distribution, $m_\gamma(r)$, can be calculated as $m_\gamma(r) = \mathbb{E}\{\gamma^r\}$, to yield

$$m_\gamma(r) = \sum_{i=1}^{S} \alpha_i \Gamma(\beta_i + r) \zeta_i^{-(\beta_i + r)}. \tag{4.4}$$

The mathematically tractable expressions (4.1)-(4.4) demonstrate the major benefit of the MG distribution. These performance metrics have convenient expressions without complicated special functions. This fact can facilitate the performance studies enormously. If a given mobile radio channel can be represented as an MG distribution, the common performance metrics such as error rates, outage and others are immediately derived, with details given in Section 4.5.

4.3 MG Distribution for Typical mobile radio channels

This section shows how to represent the SNR PDF of the NL, K, K_G, κ-μ, Hoyt, η-μ and Rician channel models in the form of an MG model, as in (4.1).

4.3.1 Nakagami-lognormal Channel

The SNR distribution of the NL channel is a gamma-lognormal (GL) distribution, given as [90]

$$f_\gamma(x) = \int_0^\infty \frac{x^{m-1} e^{-\frac{mx}{\rho y}}}{\Gamma(m)} \left(\frac{m}{\rho y}\right)^m \frac{e^{-\frac{(\ln y - \mu)^2}{2\lambda^2}}}{\sqrt{2\pi}\lambda y} \, \mathrm{d}y \tag{4.5}$$

where m is the fading parameter in Nakagami-m fading, ρ is the unfaded SNR, and μ and λ are the mean and the standard deviation of the lognormal distribution, respectively. When $m = 1$, expression (4.5) is the SNR distribution of the RL distribution. The fading and shadowing effects diminish for larger m and smaller λ, respectively. A closed-form expression of the composite GL SNR distribution is not available in the literature.

By using substitution $t = \frac{\ln y - \mu}{\sqrt{2}\lambda}$, expression (4.5) can be written as

$$f_\gamma(x) = \frac{x^{m-1}}{\sqrt{\pi}\,\Gamma(m)} \left(\frac{m}{\rho}\right)^m \int_{-\infty}^{\infty} e^{-t^2} g(t) \, \mathrm{d}t \tag{4.6}$$

where $g(t) = e^{-m(\sqrt{2}\lambda t + \mu)} e^{-\frac{m}{\rho} e^{-(\sqrt{2}\lambda t + \mu)} x}$. The integration, $I = \int_{-\infty}^{\infty} e^{-t^2} g(t) \, \mathrm{d}t$, in (4.6) is a Gaussian-Hermite integration which can be approximated as $I \approx \sum_{i=1}^{S} w_i g(t_i)$ where t_i and w_i are the abscissas and weight factors for the Gaussian-Hermite integration [77]. Therefore, $f_\gamma(x)$ in (4.6) can be expressed as the MG distribution given in (4.1). After normalization of $\int_0^\infty f_\gamma(x) \, \mathrm{d}x = 1$, parameters can be given as

$$\alpha_i = \psi(\theta_i, \beta_i, \zeta_i), \ \beta_i = m, \ \zeta_i = \frac{m}{\rho} e^{-(\sqrt{2}\lambda t_i + \mu)}, \ \theta_i = \left(\frac{m}{\rho}\right)^m \frac{w_i e^{-m(\sqrt{2}\lambda t_i + \mu)}}{\sqrt{\pi}\Gamma(m)} \tag{4.7}$$

where $\psi(\theta_i, \beta_i, \zeta_i) = \frac{\theta_i}{\sum_{i=1}^{S} \theta_i \Gamma(\beta_i) \zeta_i^{-\beta_i}}$. Function $\psi(\theta_i, \beta_i, \zeta_i)$ is also used for subsequent cases.

4.3.2 K and K_G Channels

The SNR distribution of the K_G channel has a closed-form expression with the nth-order modified Bessel function of the second kind [73]. With some mathematical

simplifications, the SNR distribution of the K_G channel, which is a gamma-gamma distribution, can be rewritten in an integral form as

$$f_\gamma(x) = \frac{\lambda^m x^{m-1}}{\Gamma(m)\Gamma(k)} \int_0^\infty e^{-t} g(t)\, \mathrm{d}t \tag{4.8}$$

where $g(t) = t^{\alpha-1} e^{-\frac{\lambda x}{t}}$, $\lambda = \frac{km}{\bar{\gamma}}$ and $\alpha = k - m$. Here k and m are the distribution shaping parameters, which represent the multipath fading and shadowing effects of the mobile radio channel, respectively. The integral in (4.8), $I = \int_0^\infty e^{-t} g(t)\, \mathrm{d}t$, can be approximated as a Gaussian-Laguerre quadrature sum as $I \approx \sum_{i=1}^{S} w_i g(t_i)$ where t_i and w_i are the abscissas and weight factors for the Gaussian- Laguerre integration [77]. Thus, (4.8) can be written as the MG distribution with parameters

$$\alpha_i = \psi(\theta_i, \beta_i, \zeta_i),\ \beta_i = m,\ \zeta_i = \frac{\lambda}{t_i},\ \theta_i = \frac{\lambda^m w_i t_i^{\alpha-1}}{\Gamma(m)\Gamma(k)} \tag{4.9}$$

for $i = 1, \cdots, S$.

4.3.3 η-μ Channel

The η-μ channel model is a generalized form to model the non-line of sight small-scale fading of a mobile radio channel [91]. The Rayleigh, Nakagami-m and Hoyt distributions are special cases of the η-μ channel model. The η-μ SNR distribution is given as [92]

$$f_\gamma(x) = \frac{2\sqrt{\pi}\mu^{\mu+\frac{1}{2}} h^\mu x^{\mu-\frac{1}{2}} e^{\frac{-2\mu h x}{\bar{\gamma}}}}{\Gamma(\mu) H^{\mu-\frac{1}{2}} \bar{\gamma}^{\mu+\frac{1}{2}}} I_{\mu-\frac{1}{2}}\left(\frac{2\mu H x}{\bar{\gamma}}\right) \tag{4.10}$$

where the parameter $\mu = \frac{\left(1+H^2/h^2\right)\mathbb{E}\{\gamma\}^2}{2\mathbb{V}\mathrm{ar}\{\gamma\}}$ ($\mu > 0$) represents the number of multipath clusters, and $I_v(\cdot)$ is the vth-order modified Bessel function of the first kind. Parameters h and H are to be explained in the following. The η-μ channel includes two fading formats, Format 1 and Format 2, for two different physical representations. In Format 1, the independent in-phase and quadrature components of the fading signal have different powers, and η ($0 < \eta < \infty$) is the power ratio of the in-phase component to the quadrature component. Two parameters h and H are defined as $h = \frac{2+\eta^{-1}+\eta}{4}$ and $H = \frac{\eta^{-1}-\eta}{4}$, respectively. In Format 2, the in-phase

and quadrature components of the fading signal are correlated and have identical powers. η ($-1 < \eta < 1$) is the correlation coefficient between the in-phase and quadrature components. Two parameters h and H are defined as $h = \frac{1}{1-\eta^2}$ and $H = \frac{\eta}{1-\eta^2}$, respectively [91].

Only a few performance studies for the η-μ channel have been published in the literature, probably because the modified Bessel function of the first kind in (4.10) leads to mathematical complexity [92–95]. In the following, the η-μ SNR distribution is approximated by using the MG distribution.

For a real number v, the function $I_v(z)$ can be computed using [74]

$$I_v(z) = \sum_{k=0}^{\infty} \frac{1}{k!\Gamma(v+k+1)} \left(\frac{z}{2}\right)^{2k+v}. \tag{4.11}$$

Therefore, the η-μ SNR distribution (4.10) can be given in an alternative form as

$$f_\gamma(x) = \frac{2\sqrt{\pi}\mu^{\mu+\frac{1}{2}}h^\mu e^{\frac{-2\mu h x}{\bar{\gamma}}}}{\Gamma(\mu)H^{\mu-\frac{1}{2}}\bar{\gamma}^{\mu+\frac{1}{2}}} \sum_{i=1}^{\infty} \frac{\left(\frac{\mu H}{\bar{\gamma}}\right)^{2i+\mu-\frac{5}{2}} x^{2\mu-3+2i}}{(i-1)!\Gamma(\mu+i-\frac{1}{2})}. \tag{4.12}$$

The required accuracy[2] to approximate the exact $f_\gamma(x)$ can be achieved by summing a finite number, S, of terms in (4.12). By matching the two PDFs given in (4.10) and (4.12), the parameters of the MG distribution can be evaluated as

$$\begin{aligned} \alpha_i =& \psi(\theta_i, \beta_i, \zeta_i),\ \beta_i = 2(\mu - 1 + i),\ \zeta_i = \frac{2\mu h}{\bar{\gamma}}, \\ \theta_i =& \frac{2\sqrt{\pi}\mu^{\mu+\frac{1}{2}}h^\mu}{\Gamma(\mu)H^{\mu-\frac{1}{2}}\bar{\gamma}^{\mu+\frac{1}{2}}} \frac{\left(\frac{\mu H}{\bar{\gamma}}\right)^{2i+\mu-\frac{5}{2}}}{(i-1)!\Gamma(\mu+i-\frac{1}{2})}. \end{aligned} \tag{4.13}$$

Alternatively, the vth-order modified Bessel function of the first kind, $I_v(z)$, can be approximated by using the integral representation [74, eq. (8.431.5)]

$$I_v(z) = \int_0^{\pi} \frac{e^{z\cos\vartheta}\cos(v\vartheta)\,\mathrm{d}\vartheta}{\pi} - \int_0^{\infty} \frac{\sin(v\pi)e^{-z\cosh t - vt}\,\mathrm{d}t}{\pi}. \tag{4.14}$$

With $\vartheta = \frac{u\pi}{2} + \frac{\pi}{2}$ and $vt = p$, $I_v(z)$ can be further written as $I_v(z) = I_1 - I_2$, where $I_1 = \int_{-1}^{1} g_1(u)\,\mathrm{d}u$ is a Gaussian-Legendre integration, and $I_2 = \int_0^{\infty} e^{-p} g_2(p)\,\mathrm{d}p$

[2]The required accuracy can be defined in terms of the mean square error (MSE) between the exact and approximated expressions or by matching the first r moments.

is a Gaussian-Laguerre integration where $g_1(u) = \frac{1}{2}e^{-z\sin(\frac{\pi u}{2})}\cos\left((u+1)\frac{\pi v}{2}\right)$ and $g_2(p) = \sin(\pi v)e^{-z\cosh(\frac{p}{v})}/(\pi v)$. Similar to Section 4.3.1 with Gaussian-Hermite integration, the SNR distribution of the η-μ channel can be approximated by the MG model.

4.3.4 Nakagami-q (Hoyt) Channel

Satellite links with strong ionospheric scintillation can be modeled with this distribution, and its SNR distribution is given as [90]

$$f_\gamma(x) = \frac{1+q^2}{2q\bar{\gamma}}e^{-\frac{(1+q^2)^2}{4q^2\bar{\gamma}}x}I_0\left(\frac{1-q^4}{4q^2\bar{\gamma}}x\right) \tag{4.15}$$

where $I_0(\cdot)$ is the zeroth-order modified Bessel function of the first kind. The fading parameter q varies from 0 to 1, where $q = 0$ and $q = 1$ represent the one-sided Gaussian and Rayleigh distributions, respectively. Further, this distribution is a special case of the η-μ distribution when $\mu = \frac{1}{2}$ and $\eta = q^2$. Using Format 1 of the η-μ distribution, the parameters of the MG distribution for the Nakagami-q channel can be derived from (4.13) to yield

$$\alpha_i = \psi(\theta_i, \beta_i, \zeta_i),\ \beta_i = 2i-1,\ \zeta_i = \frac{(1+q^2)^2}{4q^2\bar{\gamma}},\ \theta_i = \frac{(1+q^2)\left(\frac{1-q^4}{8q^2\bar{\gamma}}\right)^{2i-2}}{2q\bar{\gamma}\Gamma(i)(i-1)!}. \tag{4.16}$$

4.3.5 κ-μ Channel

The κ-μ distribution fits well with line-of-sight channels. Nakagami-n (Rician) and Nakagami-m channels are special cases of the κ-μ channel. The κ-μ SNR distribution is [92]

$$f_\gamma(x) = \frac{\mu(1+\kappa)^{\frac{\mu+1}{2}}}{\kappa^{\frac{\mu-1}{2}}e^{\mu\kappa}\bar{\gamma}^{\frac{\mu+1}{2}}}x^{\frac{\mu-1}{2}}e^{-\frac{\mu(1+\kappa)}{\bar{\gamma}}x}I_{\mu-1}\left(2\mu\sqrt{\frac{\kappa(1+\kappa)}{\bar{\gamma}}x}\right) \tag{4.17}$$

where κ ($\kappa > 0$) is the power ratio of the dominant components to the scattered components of the signal, and μ ($\mu > 0$) is defined as $\mu = \frac{(1+2\kappa)\mathbb{E}\{\gamma\}^2}{(1+\kappa)^2\mathbb{V}\text{ar}\{\gamma\}}$. Since $f_\gamma(x)$ includes the modified Bessel function of the first kind with the square root of the random parameter x, it is difficult to obtain the MG form with one of the Gaussian

integration methods, as discussed in previous subsections. To address this difficulty, the κ-μ SNR distribution given in (4.17) can be written using (4.11) as

$$f_\gamma(x) = \frac{\mu(1+\kappa)^{\frac{\mu+1}{2}}}{\kappa^{\frac{\mu-1}{2}} e^{\mu\kappa} \bar{\gamma}^{\frac{\mu+1}{2}}} \sum_{i=1}^{\infty} \left[\frac{\mu^{2i+\mu-3} \left(\frac{\kappa(1+\kappa)}{\bar{\gamma}} \right)^{\frac{2i+\mu-3}{2}}}{\Gamma(\mu-1+i)(i-1)!} x^{\mu+i-2} e^{-\frac{\mu(1+\kappa)}{\bar{\gamma}} x} \right]. \tag{4.18}$$

The required accuracy for approximating the exact $f_\gamma(x)$ can be achieved by summing a finite number, S, of terms in (4.18). By matching the two PDFs given in (4.17) and (4.18), the parameters of the MG distribution can be evaluated as

$$\begin{aligned} \alpha_i =& \psi(\theta_i, \beta_i, \zeta_i),\ \beta_i = \mu + i - 1,\ \zeta_i = \frac{\mu(1+\kappa)}{\bar{\gamma}}, \\ \theta_i =& \frac{\mu(1+\kappa)^{\frac{\mu+1}{2}}}{\kappa^{\frac{\mu-1}{2}} e^{\mu\kappa} \bar{\gamma}^{\frac{\mu+1}{2}}} \frac{\mu^{2i+\mu-3} \left(\frac{\kappa(1+\kappa)}{\bar{\gamma}} \right)^{\frac{2i+\mu-3}{2}}}{\Gamma(\mu-1+i)(i-1)!}. \end{aligned} \tag{4.19}$$

Alternatively, one can use a different approach in which the MGF of SNR under $\kappa - \mu$ distribution can be matched with the MGF of SNR under the MG distribution given in (4.3). Using the power series expansion of the exponential function $e^x = \sum_{n=0}^{\infty} \frac{x^n}{n!}$, the MGF of the κ-μ SNR distribution given in [93] can be re-written as an infinite form. By matching the two MGFs, the parameters of (4.1) can be evaluated.

4.3.6 Nakagami-n (Rician) Channel

The Nakagami-n or Rician channel model fits well with channels having a strong line-of-sight component. The corresponding SNR distribution is given as [90]

$$f_\gamma(x) = \frac{(1+n^2)e^{-n^2}}{\bar{\gamma}} e^{-\frac{(1+n^2)}{\bar{\gamma}} x} I_0 \left(2n \sqrt{\frac{(1+n^2)}{\bar{\gamma}} x} \right) \tag{4.20}$$

where n is the fading parameter ($0 \leq n < \infty$), and the Rician factor K is given as $K = n^2$. The Nakagami-n distribution is a special case of the κ-μ distribution when $\mu = 1$ and $\kappa = n^2$. Therefore, the parameters of the MG distribution given in (4.1) can be evaluated as

$$\alpha_i = \psi(\theta_i, \beta_i, \zeta_i),\ \beta_i = i,\ \zeta_i = \frac{(1+n^2)}{\bar{\gamma}},\ \theta_i = \frac{(1+n^2)}{e^{n^2}[(i-1)!]^2 \bar{\gamma}} \left(\frac{n^2(1+n^2)}{\bar{\gamma}} \right)^{i-1}. \tag{4.21}$$

4.3.7 Rayleigh and Nakagami-m Channels

The SNR distributions of the Rayleigh and Nakagami-m channels are exponential and gamma distributions, respectively [90, eq. (2.7) and (2.21)]. The two distributions are special cases of the MG distribution. When the Rayleigh distribution is written in the MG form given in (4.1), the corresponding parameters are $S = 1$, $\alpha_1 = \frac{1}{\bar{\gamma}}$, $\beta_1 = 1$ and $\zeta_1 = \frac{1}{\bar{\gamma}}$. For the Nakagami-$m$ distribution, the corresponding parameters are $S = 1$, $\alpha_1 = \frac{m^m}{\Gamma(m)\bar{\gamma}^m}$, $\beta_1 = m$ and $\zeta_1 = \frac{m}{\bar{\gamma}}$.

4.4 Determination of the Number S

For the MG distribution, the number of components S needs to be determined. This can be selected as the minimum value such that (i) the MSE or Kullback-Leibler (KL) divergence between the target distribution and the MG distribution is below a threshold; or (ii) the first r moments of the two distributions match.

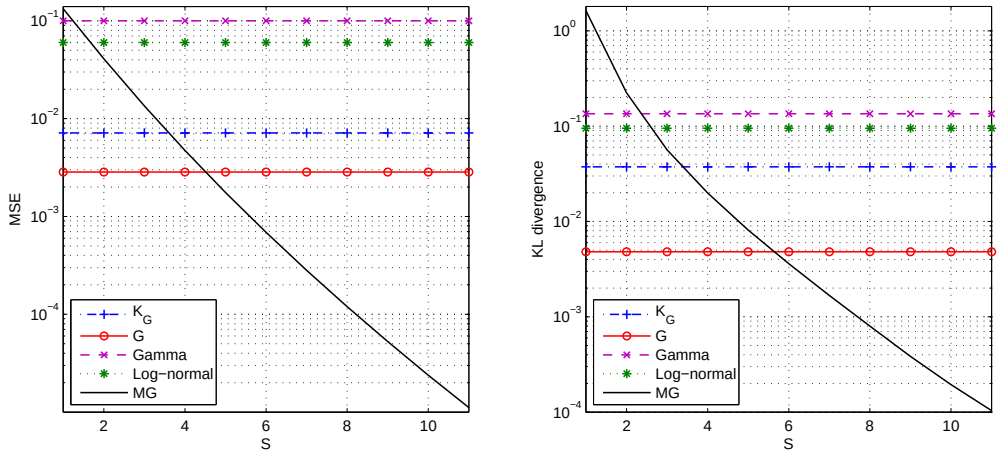

(a) (b)

Figure 4.1: (a) The MSE versus S when the GL distribution is approximated by K_G, $\mathcal{G}$, Gamma, Log-normal and MG for $m = 2.7$, $\lambda = 1$, $\mu = 0$, and the average SNR = 0 dB; (b) The KL divergence ($\mathcal{D}_{KL}$) versus S when the GL distribution is approximated by K_G, $\mathcal{G}$, Gamma, Log-normal and MG for $m = 2.7$, $\lambda = 1$, $\mu = 0$, and the average SNR = 0 dB.

4.4.1 Accuracy of MG Distribution to Approximate mobile radio channel SNR

In the literature, the composite GL model has been approximated by K_G [43], $\mathcal{G}$ [45], Log-normal [39], and Gamma models [46]. Here, the accuracy of the MG approximation is compared with that of those approximations. One of the possible measures of accuracy is the MSE between two PDFs: the approximate PDF, $f_{App}(x)$, and the exact PDF, $f_{Ext}(x)$, where MSE $= \mathbb{E}\{(f_{Ext}(x) - f_{App}(x))^2\}$. Another possible measure of accuracy is the KL divergence ($\mathcal{D}_{KL}$) between $f_{App}(x)$ and $f_{Ext}(x)$, where $\mathcal{D}_{KL} = \int_{-\infty}^{\infty} f_{Ext}(x) \log \frac{f_{Ext}(x)}{f_{App}(x)} \, \mathrm{d}x$.[3]

The K_G, $\mathcal{G}$, Log-normal and Gamma distributions are selected for the comparison. The Log-normal approximation and the Gamma approximation are obtained by approximating GL PDF by a Log-normal PDF [39], and K_G PDF by a Gamma PDF [46], respectively. The MSEs and $\mathcal{D}_{KL}$s between the GL and its MG approximation (eq. (4.7)), GL and K_G, GL and $\mathcal{G}$, GL and Log-normal, and GL and Gamma can be calculated numerically, as shown in Fig. 4.1a and Fig. 4.1b, respectively, for $m = 2.7$, $\lambda = 1$, $\mu = 0$, and the average SNR = 0 dB. The parameters of K_G, $\mathcal{G}$, Log-normal and Gamma distributions to match the target GL distribution are obtained from [39, 41, 45, 46]. The MSE and $\mathcal{D}_{KL}$ between GL and MG distributions are less than 10^{-3} when the number of components $S \geq 6$ and $S \geq 8$, respectively. Based on MSE, MG model is better than Gamma, Log-normal, K_G and $\mathcal{G}$ models when $S \geq 2, 2, 4$ and 5, respectively. Based on KL divergence, MG model is better than Gamma, Log-normal, K_G and $\mathcal{G}$ models when $S \geq 3, 3, 4$ and 6, respectively. It can be seen that MSE and KL divergence give similar results for the minimum value of S that makes the MG model more accurate than Gamma, Log-normal, K_G or $\mathcal{G}$ model. Further, these MSE and $\mathcal{D}_{KL}$ with MG model decrease significantly as S slightly increases.

This fact is also evidenced by Fig. 4.2a, which shows the CDFs of the GL and its approximations by K_G, $\mathcal{G}$, Log-normal, Gamma and MG models. These curves are plotted on a GL paper. The ordinate of the GL paper is obtained using

[3] Although both the MSE and the KL divergence are measures of the difference between two PDFs, they give different measurements. Nevertheless, they give similar results for the minimum value of S that makes the MG model more accurate than Gamma, K_G or $\mathcal{G}$ model, as shown subsequently.

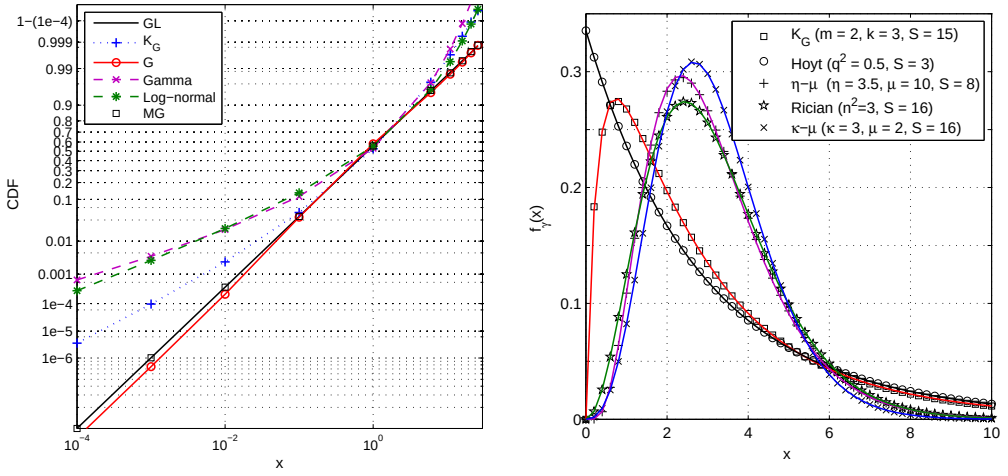

(a) (b)

Figure 4.2: (a) The exact CDF of GL distribution and the CDFs of the K_G, $\mathcal{G}$, Log-normal, Gamma and MG approximations. The parameter values are $m = 2.7$, $\lambda = 1$, $\mu = 0$, and the average SNR = 0 dB. The number of components in the MG model is $S = 5$; (b) Exact SNR distributions of K_G, Nakagami-q (Hoyt), η-μ (Format 1), Rician and κ-μ channel models and their MG approximations.

the transformation $F_{\text{GL}}^{-1}(t)$ where $F_{\text{GL}}(x)$ is the CDF of GL distribution. Thus the GL distribution is a straight line on the GL paper, and others are not. The inverse function is numerically calculated using MATLAB. The following observations are made:

1. The exact GL CDF (solid line) matches perfectly with the MG approximation (small squares) for all x. Just $S = 5$ terms have been used in this case. Even better accuracy is possible by slightly increasing S.

2. The K_G approximation [43] deviates significantly in the lower tail ($x < 0.09$) and also in the upper tail ($x > 5$).

3. The $\mathcal{G}$ approximation [45] deviates in the lower tail ($x < 0.1$).

4. The Gamma or Log-normal approximation [39, 46] deviates significantly in both lower tail ($x < 1$) and the upper tail ($x > 5$).

Clearly, the MG distribution is a more accurate representation of composite fading channels.

	$(\kappa,\ \mu)$					
	(3, 0.5)	(3, 1)	$(3, 2)$	(7, 0.5)	(7, 1)	(7, 2)
1st moment	3	3	3	3	3	3
2nd moment	19	14	12	15	12	11
3rd moment	154	83	55	87	57	43
S	8	11	16	12	20	26

Table 4.1: The selected value of S and the nearest integer values of the first three moments of both exact and approximated SNR distributions of κ-μ channel.

Similarly, Fig. 4.2b shows the SNR distributions of the K_G, Nakagami-q (Hoyt), η-μ (Format 1), Rician and κ-μ channel models and their corresponding approximations in the MG form, when the value of S in the MG distribution is selected as the minimum value that satisfies MSE $\leq 10^{-6}$. Excellent match is also observed in all curves. Note that in Fig. 4.2b and subsequent figures in this chapter, the continuous lines and discrete markers show the curves corresponding to the exact and MG distributions, respectively.

4.4.2 Moment Matching

The parameters of α_i, β_i and ζ_i in the MG distribution can be determined based on matching the MGFs of the exact distribution and the MG distribution. For brevity, the value of S is determined as the minimum value such that the first r moments of the two distributions have the same nearest integer values. Table 4.1 shows the selected S value when $r = 3$ for κ-μ distribution. The exact distribution and the approximated MG distribution have the same nearest integer values for the first 3 moments, which are also shown in Table 4.1. In Table 4.1, the (3, 1) and (7, 1) columns are corresponding to Nakagami-n distribution (Rician) with Rician factors $K = 3$ and $K = 7$, respectively.

To determine the parameters of the MG distribution to approximate other channel models, the exact SNR moment expressions ($m_\gamma(r) = \mathbb{E}\{\gamma^r\}$) for the NL, K_G, Nakagami-q and Nakagami-n are available in the literature [73, 90, 96], and the exact SNR moment expressions of η-μ and κ-μ distributions can be derived from their moments of the envelope distribution given in [91, eqs. (5), (43), and (46)].

4.4.3 Complexity of Determining S

The number of terms S in the MG model may be determined iteratively. S can be increased until the MSE or KL divergence requirements are met. In our numerical result shown in Figs. 1 and 2, approximately $S = 8$ can meet the accuracy requirement of 10^{-3}. To achieve 10^{-6} accuracy, approximately $S = 15$ is needed.

Each iteration (corresponding to a particular S) requires $3N$ parameters α_i, β_i and ζ_i ($i = 1, \cdots, S$). If Gaussian integration methods (Gaussian-Legendre, Gaussian- Laguerre, or Gaussian-Hermite) are used, their abscissas and weight factors are already tabulated (e.g., in [77]), or can be generated efficiently by using simple MATLAB codes. Note that special functions are not involved in the calculations of the parameters.

4.5 MG Channel Performance Analysis

Performance analysis of wireless technologies such as MIMO, cooperative communications, cognitive radio and ultra-wideband (UWB) radio has become important recently. The MG distribution helps to provide a unified performance analysis framework, because of the mathematical tractability of its CDF, MGF and moments (Section 4.2) and because of its versatility (Section 4.3). To this end, this section shows how the MG distribution allows the derivation of typical performance metrics such as error rate, outage, and others.

Diversity Order

The diversity order is the magnitude of the slope of the error probability versus SNR curve (log-log scale) in the high SNR region. The array gain measures the shift of the error probability curve to the left. The diversity order and the array gain relate to the asymptotic value of the MGF near the infinity, i.e., if the MGF, $\mathcal{M}_\gamma(t)$, can be written in the form

$$|\mathcal{M}_\gamma(t)| = b|t|^{-d} + \mathcal{O}(|t|^{-(d+1)}) \text{ as } t \to \infty$$

then b and d define the array gain and diversity order, respectively [97]. Clearly, using the binomial series expansion, (4.3) can be rewritten as

$$|\mathcal{M}_{\gamma}(s)| = \sum_{i=1}^{S} \alpha_i \Gamma(\beta_i) \left(s^{-\beta_i} + \sum_{k=1}^{\infty} \binom{-\beta_i}{k} \zeta_i^k s^{-(\beta_i+k)} \right). \tag{4.22}$$

Therefore, the array gain is $b \approx \alpha_n \Gamma(\beta_n)$ and the diversity order is $d = \beta_n$, where n is the index of the first nonzero α_i, i.e., $\alpha_i = 0 \; \forall i < n$, and $\alpha_n \neq 0$. Accordingly, the diversity orders of NL, K, K_G, η-μ, Hoyt, κ-μ, Rician, Rayleigh and Nakagami-m fading channels are m, 1, m, 2μ, 1, μ, 1, 1, and m , respectively.

Average Channel Capacity

By using Shannon's theorem, the average channel capacity of a single-input single-output (SISO) channel, C, can be calculated by averaging the instantaneous channel capacity over the SNR distribution as $C = \int_0^{\infty} B \log_2(1+x) f_{\gamma}(x) \, \mathrm{d}x$, where B is the signal transmission bandwidth. If β_i is an integer, the average channel capacity over the MG distribution, C, can be calculated by using results in [98], as

$$C = \frac{B}{\ln 2} \sum_{i=1}^{S} \alpha_i (\beta_i - 1)! e^{\zeta_i} \sum_{k=1}^{\beta_i} \frac{\Gamma(k-\beta_i, \zeta_i)}{\zeta_i^k} \tag{4.23}$$

where $\Gamma(\cdot,\cdot)$ is the upper incomplete gamma function [74, eq. (8.350.2)]. Next a method is provided to calculate C for any value of β_i. By replacing $\log_2(1+x)$ with the Meijer's G-function [75, eq. (01.04.26.0003.01)], C can be evaluated, which is valid for any β_i, as

$$C = \frac{B}{\ln 2} \sum_{i=1}^{S} \alpha_i \zeta_i^{-\beta_i} G_{3,2}^{1,3} \left[\zeta_i^{-1} \middle| \begin{matrix} 1-\beta_i, \, 1, \, 1 \\ 1, \, 0 \end{matrix} \right] \tag{4.24}$$

where $G_{m,n}^{p,q}[\cdot]$ is the Meijer-G function. For integer β_i, both expressions in (4.23) and (4.24) are equal numerically.

Average SER

Since there is a MGF without special functions in the MG channel model, it can be used to evaluate the average SER of M-PSK, M-QAM and M-amplitude modulation (AM), as follows.

M-PSK

The average SER for M-PSK, P_e^{psk}, is given in [90, eq. (9.15)] for some channel models. With the MGF given in (4.3), the average SER for M-PSK over the MG distribution P_e^{psk} can be evaluated as

$$P_e^{psk} = \sum_{i=1}^{S} \frac{\alpha_i \Gamma(\beta_i)}{\pi {\zeta_i}^{\beta_i}} \int_0^{\frac{(M-1)\pi}{M}} \left(\frac{\sin^2\theta}{\sin^2\theta + \frac{g_{psk}}{\zeta_i}} \right)^{\beta_i} \mathrm{d}\theta \tag{4.25}$$

where $g_{psk} = \sin^2(\frac{\pi}{M})$. Therefore, the average SER of the M-PSK modulation can be evaluated in closed-form for any value of β_i with the aid of [99, eq. (10)].

M-QAM

Square M-QAM signals with a constellation size $M = 2^k$ with even k values are considered. The average SER for M-QAM, P_e^{qam}, is given in [90, eq. (9.21)] for some channel models. When the MG distribution is used, P_e^{qam} can be evaluated as

$$\begin{aligned} P_e^{qam} = \sum_{i=1}^{S} \frac{K\alpha_i \Gamma(\beta_i)}{{\zeta_i}^{\beta_i}} \Bigg[& \int_0^{\frac{\pi}{2}} \left(\frac{\sin^2\theta}{\sin^2\theta + \frac{g_{qam}}{\zeta_i}} \right)^{\beta_i} \mathrm{d}\theta \\ & - \frac{\sqrt{M}-1}{\sqrt{M}} \int_0^{\frac{\pi}{4}} \left(\frac{\sin^2\theta}{\sin^2\theta + \frac{g_{qam}}{\zeta_i}} \right)^{\beta_i} \mathrm{d}\theta \Bigg] \end{aligned} \tag{4.26}$$

where $g_{qam} = \frac{3}{2(M-1)}$ and $K = \frac{4}{\pi}(1 - \frac{1}{\sqrt{M}})$. P_e^{qam} in (4.26) can be evaluated in closed-form for any value of β_i with the aid of [99, eq. (12)].

M-AM

Similarly, the average SER for M-AM, P_e^{am}, is given in [90, eq. (9.19)] for some channels. For the MG distribution, it can be evaluated as

$$P_e^{am} = \frac{2(M-1)}{\pi M} \sum_{i=1}^{S} \frac{\alpha_i \Gamma(\beta_i)}{\pi {\zeta_i}^{\beta_i}} \int_0^{\frac{\pi}{2}} \left(\frac{\sin^2\theta}{\sin^2\theta + \frac{g_{am}}{\zeta_i}} \right)^{\beta_i} \mathrm{d}\theta \tag{4.27}$$

where $g_{am} = \frac{3}{(M^2-1)}$. With the aid of [90, eq. (5A.1)] or [99, eq. (5)], P_e^{am} can be evaluated in closed-form for any value of β_i.

Similarly, the SER analysis for other modulation schemes over different digital communication systems, for example, as given in [100, 101], can be performed using the MG distribution.

Outage Probability

The outage probability, which is the probability that the received SNR is below a given threshold γ_{th}, can easily be calculated as $P_{out} = F_{\gamma}(\gamma_{th})$, where $F_{\gamma}(x)$ is given in (4.2).

Energy Detection Related Performance

The MG model can also be used when energy detection related performance metrics, such as AUC and average detection probability, are analyzed, as detailed in Chapters 6 and 7.

4.6 Numerical Results

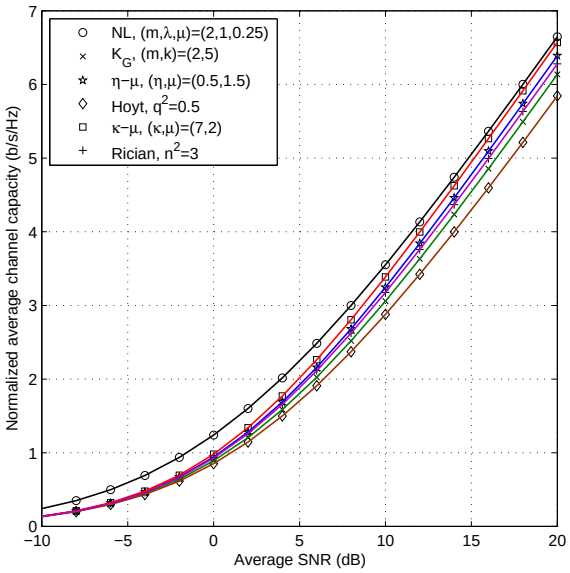

Figure 4.3: The average capacity of an SISO channel versus average SNR over different fading channels.

Two main focuses of this sub-section are (1) to show how the performance analysis based on the MG approximation matches with the exact results, and (2) to compare the performance of different fading channels. Typical distribution parameters are choosen. The value of S is selected as the minimum value to satisfy MSE $\leq 10^{-6}$. As an example, the parameters and S for the NL, K_G, η-μ (Format 1), Hoyt, κ-μ and Rician channels are chosen as (m, λ, μ, S)=$(2, 1, 0.25, 10)$, (m, k, S)=$(2, 5, 6)$, (η, μ, S)=$(0.5, 1.5, 5)$, (q^2, S)=$(0.5, 3)$, (κ, μ, S)= $(7, 2, 36)$ and (n^2, S)=$(3, 16)$, respectively.

The performance curves for the average channel capacity, the outage probability, and average SER for binary phase shift keying (BPSK) and QAM are plotted in Figs. 4.3-4.4b, respectively, based on both exact (continuous lines) and approximated (discrete points) MG distributions. All figures show an excellent match.

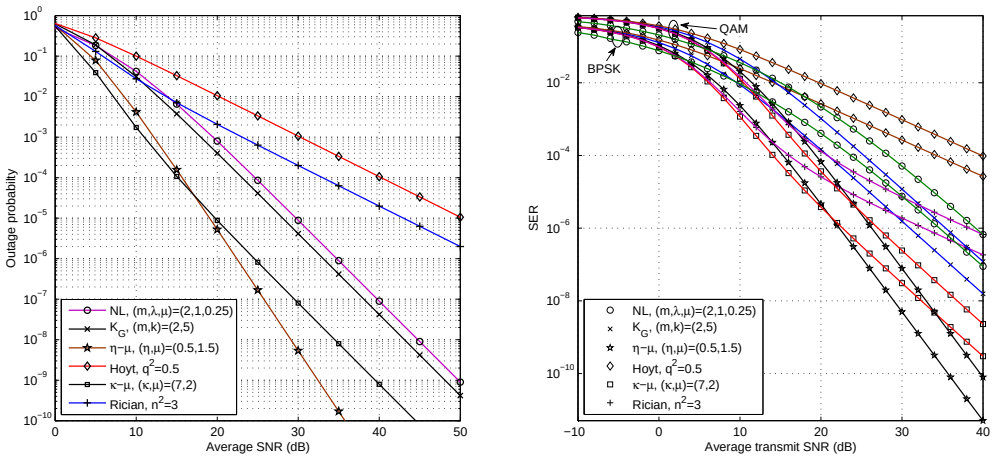

(a) (b)

Figure 4.4: (a) The outage probability of an SISO channel versus average SNR over different fading channels for $\gamma_{th} = 0$ dB; (b) The SER of an SISO channel versus average SNR over different fading channels for BPSK and QAM.

As discussed in Section 4.5, the achievable diversity orders of NL, K, K_G, η-μ, Hoyt, κ-μ, Rician, Rayleigh and Nakagami-m fading channels are m, 1, m, 2μ, 1, μ, 1, 1, and m, respectively. The diversity order can be illustrated by using outage probability (Fig. 4.4a) or SER (Fig. 4.4b) versus average SNR plots in the high SNR region. From the figures, NL and K_G models show diversity order 2 because their

fading parameters are $m = 2$. Hoyt and Rician models always have diversity order 1. Since η-μ and κ-μ models have $\mu = 1.5$ and $\mu = 2$, they have diversity order 3 and 2, respectively. All these confirm accuracy of our analysis in Section 4.5. Further, the performance of η-μ and Hoyt channels are compared. Although both channels have same power ratios in our numerical examples (i.e., η=q^2=0.5), the η-μ channel has higher effective multipath clusters, which help to achieve a diversity order of 3 (=2μ) while the Hoyt channel has diversity order of one. Therefore, performance of η-μ channel with (η, μ)=(0.5,1.5) is better than the performance of Hoyt channel with q^2=0.5 in terms of channel capacity, outage, and SER (Figs. 4.3-4.4b). Similarly, performance of κ-μ and Rician channels can be compared. For the two channels in our numerical examples, the power ratios of the dominant components to the scattered components of the signal are $\kappa = 7$ and $n^2 = 3$, respectively, and the diversity orders are 2 and 1, respectively. So performance of κ-μ channel with (κ, μ)=(7,2) is better than the performance of Rician channel with n^2=3 in terms of channel capacity, outage, and SER (Figs. 4.3-4.4b). Since NL, K_G, η-μ, and κ-μ channel models do not have straightforward relationships among each other, no clear-cut performance comparison can be done.

4.7 Conclusions

The MG distribution to model the SNR of the mobile radio channels has been proposed. Theoretical results [88] [102] show it converges to any PDF over $(0, \infty)$, a justification of this model. It is not only ideal for composite channels, but also effective for small-scale fading channels. The MG parameters to match a target distribution can be obtained by approximating with Gaussian quadrature formulas, by matching moments or by matching PDFs. The MG model offers a more accurate representation of composite fading channels than those provided by the K models and other alternatives, which have recently been used in wireless research.

$\sim$

Chapter 5

Area under the ROC Curve of Energy Detection

The Area Under the ROC Curve (AUC) has been identified as a metric which can represent different concepts of a hypothesis test. For instance, it is a compact and single-value quantity which is a measure for the overall detection capability of a detector. Thus, a comprehensive analysis of the AUC is given for an energy detector. The average AUCs are derived for the case of no-diversity reception and diversity reception cases. The detection diversity orders are also derived by using high SNR approximation of the complementary AUC (CAUC).[1]

5.1 Introduction

The performance of an energy detector is traditionally characterized through its ROC curves, (for example, as we discussed in Section 3.3). ROC curves are generated by plotting either detection probability versus false alarm probability or missed detection probability versus false alarm probability (called complementary ROC) [48]. Extensive ROC analysis of the energy detector is available in the wireless literature [53,54,69,70]. Looking further afield, it is found that ROC analysis is regularly used, for example, in the health care field for diagnostic tests, drug testing and others [103], and in machine learning algorithms [104].

Detection probability and false alarm probability depend on the threshold, num-

[1] *Versions of this chapter have been published in IEEE Trans. Wireless Commun., 9: 1216–1225 (2010) and IEEE Commun. Lett., 15: 1301–1303 (2011).*

ber of samples, fading parameters, number of diversity branches or number of relays, and average SNR. When threshold changes from $0 \to \infty$, the ROC curve starts at the upper-right point $(1, 1)$ and eventually moves to the lower-left point $(0, 0)$, or when the number of samples increases, ROC curves shift to the upper left-hand side of the ROC graph. Generally, ROC curves are plotted by varying only one parameter while keeping other parameters fixed, and a variety of curves can be generated for different combinations of parameters of interest.

Although the ROC curves fully characterize the performance of an energy detector, it is desirable to have a single figure of merit. Such a measure is the AUC, which varies between $\frac{1}{2}$ and 1. If the ROC curve can be given as $P_d = f\left(P_f\right)$ where P_d is a function of P_f, and as P_f varies from 0 to 1, the AUC can be evaluated as

$$\mathcal{A} = \int_0^1 P_d \, \mathrm{d}P_f. \tag{5.1}$$

If the detector performs no better than flipping a coin, then the AUC becomes $\frac{1}{2}$, and it increases to one as the detector performance improves. As well, the Area Theorem [105] has shown that the AUC is a measure of the detection capability. Actually, in [106], it has been pointed out that the area under the curve represents the probability that choosing the correct decision at the detector is more likely than choosing the incorrect decision. However, as indicated in [107, 108], the exact computation of AUC is difficult for realistic detection tasks. Therefore, the previous research efforts mainly focus on bounds of the AUC [107, 108] or the asymptotic expansion and limiting value of AUC [109]. Unlike [107–109], this chapter targets at deriving rigorous expressions for the AUC of an energy detector in several scenarios that are of interest to wireless researchers.

This chapter is organized as follows. The AUC of the energy detector is analyzed in Section 5.2. The average AUCs of the energy detector are analyzed for different scenarios in Section 5.3. The numerical and simulation results are presented in Section 5.4. The concluding remarks are made in Section 5.5.

5.2 AUC for Instantaneous SNR

For two energy detectors, it is difficult to compare their performance based on visual perception of their ROC curves, since the curves may cross. On the other hand, following the Area Theorem [105], the AUC is introduced, which is equal to the area covered by the ROC curve. As aforementioned, the AUC is a measure of the detection capability of the energy detector. Generally, as the threshold λ in the energy detection varies from ∞ to 0, the false alarm and the detection probabilities vary from value 0 to value 1, and accordingly, the AUC varies from $\frac{1}{2}$ to 1.

Consider the ROC curve of detection probability versus false-alarm probability (P_d versus P_f). Let $\mathcal{A}(\gamma)$ denotes the AUC which is a function of instantaneous SNR value γ. Therefore, $\mathcal{A}(\gamma)$ can be evaluated as

$$\mathcal{A}(\gamma) = \int_0^1 P_d(\gamma, \lambda)\, \mathrm{d}P_f(\lambda). \tag{5.2}$$

Since $P_f(\lambda)$ and $P_d(\gamma, \lambda)$ are functions of the threshold λ, the threshold averaging method can be applied for the AUC calculation [110]. When the value of $P_f(\lambda)$ varies from $0 \to 1$, it is equivalent to λ ranging from $\infty \to 0$. Therefore, (5.2) can be rewritten as

$$\mathcal{A}(\gamma) = -\int_0^\infty P_d(\gamma, \lambda) \frac{\partial P_f(\lambda)}{\partial \lambda}\, \mathrm{d}\lambda \tag{5.3}$$

where $\partial P_f(\lambda)/\partial\lambda$ is the partial derivative of P_f with respect to λ, which is given from (2.15) as

$$\frac{\partial P_f(\lambda)}{\partial \lambda} = -\frac{\lambda^{N-1} e^{-\frac{\lambda}{2}}}{2^N \Gamma(N)}. \tag{5.4}$$

After the substitution of (2.17) and (5.4) into (5.3), and the transformation $\sqrt{\lambda} = t$, (5.3) can be written as

$$\mathcal{A}(\gamma) = \frac{1}{2^{N-1}\Gamma(N)} \int_0^\infty t^{2N-1} e^{-\frac{t^2}{2}}\, Q_N(\sqrt{2N\gamma}, t)\, \mathrm{d}t. \tag{5.5}$$

Using the following identity of the Marcum-Q function

$$Q_N(\beta, \alpha) = 1 - Q_N(\alpha, \beta) + e^{-\frac{\alpha^2+\beta^2}{2}} \sum_{r=1-N}^{N-1} \left(\frac{\alpha}{\beta}\right)^r I_r(\alpha\beta)$$

where $I_r(\cdot)$ is the rth-order modified Bessel function of the first kind, (5.5) can be rewritten as

$$\mathcal{A}(\gamma) = \frac{1}{2^{N-1}\Gamma(N)} \int_0^\infty t^{2N-1} e^{-\frac{t^2}{2}} \Bigg[1 - Q_N(t, \sqrt{2N\gamma}) + e^{-\frac{2N\gamma+t^2}{2}} \sum_{k=1-N}^{N-1} \left(\frac{t}{\sqrt{2N\gamma}} \right)^k I_k(\sqrt{2N\gamma}t) \Bigg] \mathrm{d}t. \tag{5.6}$$

After some mathematical manipulations as provided in Appendix B.1, $\mathcal{A}(\gamma)$ can be evaluated as (see the Appendix B.2 for the detailed derivation)

$$\mathcal{A}(\gamma) = 1 - \sum_{k=0}^{N-1} \frac{N^k \gamma^k e^{-\frac{N\gamma}{2}}}{2^k\, k!} + \sum_{k=1-N}^{N-1} \frac{\Gamma(N+k) e^{-N\gamma} {}_1\tilde{F}_1\left(N+k; 1+k; \frac{N\gamma}{2}\right)}{2^{N+k}\Gamma(N)} \tag{5.7}$$

where ${}_1\tilde{F}_1(\cdot;\cdot;\cdot)$ is the regularized confluent hypergeometric function of the confluent hypergeometric function ${}_1F_1(\cdot;\cdot;\cdot)$ [75]. Note that (5.7) gives the AUC of an energy detector for a specific value of instantaneous SNR γ. Therefore, $\mathcal{A}(\gamma)$ is the unfaded AUC. The average AUC under the AWGN channel can be found from (5.7) after replacing γ by $\bar{\gamma}$, where $\bar{\gamma}$ is the average SNR.

5.2.1 Complementary AUC

The multipath fading environment, diversity combining schemes, and relay networks introduce detection diversity gain on energy detection. However, neither the ROC curve nor the AUC curve is able to show the order of improvement in detection capability clearly (in graphically) when the average SNR increases. Therefore, CAUC is introduced as a proxy for the overall detection capability, which can demonstrate the order of improvement based on a log-log scale of a CAUC versus average SNR plot when average SNR increases. The CAUC, $\mathcal{A}'$, which is the area under the complementary ROC curve (the curve of P_{md} versus P_f) is given as

$$\mathcal{A}' = \int_0^1 (1 - P_d)\, \mathrm{d}P_f = 1 - \mathcal{A}. \tag{5.8}$$

When the average SNR increases, while $\mathcal{A}$ goes from 0.5 to 1, $\mathcal{A}'$ goes from 0.5 to 0. Since $\mathcal{A}' \to 0$ as $\bar{\gamma} \to \infty$, CAUC is a better performance metric to discuss detection

diversity order, which shows how fast the CAUC decreases with the increase in the SNR in the high SNR range. Thus, detection diversity order can be defined as

$$d \triangleq -\lim_{\bar{\gamma}\to\infty} \frac{\log\left(\mathcal{A}'\right)}{\log\left(\bar{\gamma}\right)}. \tag{5.9}$$

In general, the average CAUC can be given as $\overline{\mathcal{A}'} = c\bar{\gamma}^{-d} + \mathcal{O}(\bar{\gamma}^{-(d+1)})$ where c is a constant which is independent of $\bar{\gamma}$, and d is the detection diversity order.

5.2.2 Partial AUC

Although AUC measures overall detection capability, it may not always unambiguously indicate when one detector is better than another. For example, when two ROC curves cross, it is possible that their AUC's are the same. This situation arises when the two associated detectors have different performance in different regions of detection threshold λ. The area of the ROC curve (for λ from 0 to ∞) only gives the overall detection performance, but cannot differentiate the two detectors in a small region of λ, say $\lambda_1 \leq \lambda \leq \lambda_2$. To remedy this drawback, the partial area under the ROC curve [111] in region (λ_1, λ_2) can be used to demonstrate the difference, as given by

$$\mathcal{A}_{Par}(\gamma) = -\int_{\lambda_1}^{\lambda_2} P_d(\gamma,\lambda)\frac{\partial P_f(\lambda)}{\partial\lambda}\,\mathrm{d}\lambda. \tag{5.10}$$

Nevertheless, the partial AUC measure appears intractable for closed-form analysis. It can however be readily evaluated via numerical integration methods that are available in the mathematical software packages.

5.3 Average AUC over Fading Channels

In this section, average AUC expressions are derived for no-diversity and diversity receptions, respectively, over Nakagami-m distribution[2] which is widely employed for characterizing mobile radio channel fading. If the signal amplitude follows a

[2]Actually the MG channel model in Chapter 4 can be used here to model most existing fading channels. Please refer to Chapter 7 for details of applying the MG channel model in deriving the average AUC over various fading cases.

Nakagami-m distribution, then the SNR has a PDF given by [90]

$$f_{\gamma^{Nak}}(x) = \frac{1}{\Gamma(m)} \left(\frac{m}{\bar{\gamma}}\right)^m x^{m-1} e^{-\frac{m}{\bar{\gamma}}x},\ x \geq 0 \tag{5.11}$$

where $\bar{\gamma}$ is the average SNR and m is Nakagami fading parameter. Subsequently, the detection diversity order is also derived by using the average CAUC at the high SNR.

5.3.1 No-Diversity Reception

Direct Integration

The average AUC, $\bar{\mathcal{A}}$, over fading channel channels can be evaluated by averaging (5.7) with the SNR distribution which can be written as

$$\bar{\mathcal{A}} = \int_0^\infty \mathcal{A}(x) f_\gamma(x)\, \mathrm{d}x. \tag{5.12}$$

The average AUC for Nakagami-m fading channel with no diversity, $\bar{\mathcal{A}}_{Nak}$, can be evaluated through averaging $\mathcal{A}(\gamma)$ in (5.7) by the SNR distribution $f_{\gamma^{Nak}}(x)$ given in (5.11). It can be derived for integer m as (see the Appendix B.3 for the detailed derivation)

$$\begin{aligned}\bar{\mathcal{A}}_{Nak} =& 1 - \frac{1}{\Gamma(m)} \left(\frac{2m}{2m+N\bar{\gamma}}\right)^m \sum_{k=0}^{N-1} \frac{\Gamma(k+m)}{k!} \left(\frac{N\bar{\gamma}}{2m+N\bar{\gamma}}\right)^k \\ &+ \left(\frac{m}{m+N\bar{\gamma}}\right)^m \sum_{k=1-N}^{N-1} \frac{\Gamma(N+k)\,{}_2\tilde{F}_1\left(m; N+k; 1+k; \frac{N\bar{\gamma}}{2(m+N\bar{\gamma})}\right)}{2^{N+k}\Gamma(N)}\end{aligned} \tag{5.13}$$

where ${}_2\tilde{F}_1(\cdot;\cdot;\cdot;\cdot)$ is the regularized confluent hypergeometric function of the confluent hypergeometric function ${}_2F_1(\cdot;\cdot;\cdot)$ [75]. When $m = 1$, the result in (5.13) means the average AUC over a Rayleigh fading channel. For higher $\bar{\gamma}$, the average CAUC, $\overline{\mathcal{A}'}_{Nak}$, can be approximated by using (5.13) as

$$\begin{aligned}\bar{\mathcal{A}'}_{Nak} \approx& \left[\frac{(2m)^m}{N^m\Gamma(m)} \sum_{k=0}^{N-1} \frac{\Gamma(k+m)}{k!} \right. \\ &\left. - \sum_{k=1-N}^{N-1} \frac{m^m\Gamma(N+k)\,{}_2\tilde{F}_1\left(m; N+k; 1+k; \frac{1}{2}\right)}{2^{N+k}N^m\Gamma(N)}\right]\bar{\gamma}^{-m} \\ =& g^{Nak}(m,N)\bar{\gamma}^{-m}\end{aligned} \tag{5.14}$$

where $g^{Nak}(m,N)$ is the term in the square brackets which depends on parameters m and N. When m increases, the average AUC converges to 1, and the convergence speed is with the order of m, which is the detection diversity order.

Moment Generating Function (MGF) Approach

By using the derivative of $P_f(\lambda)$ with respect to λ and an alternative representation of $P_d(\gamma,\lambda)$, $\mathcal{A}(\gamma)$ can be written as

$$\begin{aligned}\mathcal{A}(\gamma) =& \int_0^\infty \frac{e^{-\frac{\lambda}{2}}}{j2\pi} \oint_\Omega \frac{e^{(\frac{1}{z}-1)N\gamma+\frac{\lambda}{2}z}}{z^N(1-z)} dz \frac{\lambda^{N-1}e^{-\frac{\lambda}{2}}}{2^N\Gamma(N)}\,\mathrm{d}\lambda \\ =& \frac{1}{j2\pi}\oint_\Omega \frac{e^{(\frac{1}{z}-1)N\gamma}}{z^N(1-z)(2-z)^N}dz\end{aligned} \tag{5.15}$$

where Ω is a circular contour of radius $r \in [0,1)$, and the second equality of (5.15) results after changing integration orders. The average AUC, $\bar{\mathcal{A}} = \int_0^\infty \mathcal{A}(x) f_\gamma(x)\,\mathrm{d}x$, can be written as

$$\bar{\mathcal{A}} = \frac{1}{j2\pi}\oint_\Omega g(z)dz, \text{ where } g(z) = \frac{\mathcal{M}_\gamma\left(1-\frac{1}{z}\right)}{z^N(1-z)(2-z)^N}, \tag{5.16}$$

and $\mathcal{M}_\gamma(s) = \mathbb{E}\{e^{-s\gamma}\}$ is MGF of the received SNR γ. The Residue Theorem in complex analysis is one of the effective techniques to evaluate the contour integral in (5.16). If $g(z) = \sum_{i=-\infty}^{\infty} a_i(z-z_0)^i$, the integration of $g(z)$ in a closed contour Ω encircling z_0 is given by $\oint_\Omega g(z)dz = j2\pi a_{-1}$ where a_{-1} is the complex residue. If the contour encloses multiple poles, then the general result is

$$\oint_\Omega g(z)dz = j2\pi \sum_{a_i\in\ominus} \text{Res}\left(g(z,a_i)\right) \tag{5.17}$$

where $\ominus$ is the set of poles contained inside the contour, and $\text{Res}(g;t)$ denotes residues of function $g(z)$ at $z=t$ [112]. The MGF of Nakagami-m fading model is $\frac{1}{\left(1+\frac{\bar{\gamma}}{m}s\right)^m}$. Thus The average AUC over Nakagami-m fading, $\bar{\mathcal{A}}_{\text{Nak}}$, is derived based on (5.16) and (5.17), as

$$\bar{\mathcal{A}}_{\text{Nak}} = \frac{1}{\left(1+\frac{\bar{\gamma}}{m}\right)^m}\begin{cases}\left(\text{Res}\left(g;\frac{\bar{\gamma}}{m+\bar{\gamma}}\right)+\text{Res}\left(g;0\right)\right): & N>m \\ \text{Res}\left(g;\frac{\bar{\gamma}}{m+\bar{\gamma}}\right): & N\le m\end{cases} \tag{5.18}$$

where

$$\text{Res}\left(g; \frac{\bar{\gamma}}{m+\bar{\gamma}}\right) = \frac{1}{(m-1)!} D^{m-1}\left(\frac{1}{z^{N-m}(1-z)(2-z)^N}\right)\Big|_{z=\frac{\bar{\gamma}}{m+\bar{\gamma}}},$$

$$\text{Res}(g;0) = \frac{1}{(N-m-1)!} D^{N-m-1}\left(\frac{1}{\left(z-\frac{\bar{\gamma}}{m+\bar{\gamma}}\right)^m (1-z)(2-z)^N}\right)\Big|_{z=0}, \tag{5.19}$$

and $D^n(f(z))$ denotes the nth derivative of $f(z)$ with respect to z.

5.3.2 Diversity Reception

The average AUCs under MRC and square-law combining (SLC) diversity receptions are derived. The L diversity paths are i.i.d. over Nakagami-m fading channels, and γ_k is the SNR in the kth branch.

Maximal Ratio Combining

In MRC, all the diversity branches are coherently combined, and the instantaneous SNR at the output of the combiner is $\gamma^{MRC} = \sum_{k=1}^{L} \gamma_k$. The PDF of γ^{MRC} for i.i.d. Nakagami-m fading channels is given by [90]

$$f_{\gamma^{MRC}}(x) = \frac{1}{\Gamma(Lm)}\left(\frac{m}{\bar{\gamma}}\right)^{Lm} x^{Lm-1}\, e^{-\left(\frac{m}{\bar{\gamma}}\right)x},\ x \geq 0. \tag{5.20}$$

Similar to the derivation of (5.13), the average AUC under MRC, $\overline{\mathcal{A}}_{Nak}^{MRC}$, can be evaluated through averaging $\mathcal{A}(\gamma)$ in (5.7) by the SNR distribution in (5.20), as

$$\begin{aligned}\overline{\mathcal{A}}_{Nak}^{MRC} =& 1 - \frac{1}{\Gamma(Lm)}\left(\frac{2m}{2m+N\bar{\gamma}}\right)^{Lm}\sum_{k=0}^{N-1}\frac{\Gamma(k+m)}{k!}\left(\frac{N\bar{\gamma}}{2m+N\bar{\gamma}}\right)^k \\ &+ \left(\frac{m}{m+N\bar{\gamma}}\right)^{Lm}\sum_{k=1-N}^{N-1}\frac{\Gamma(N+k)\,{}_2\tilde{F}_1\left(Lm, N+k; 1+k; \frac{N\bar{\gamma}}{2(m+N\bar{\gamma})}\right)}{2^{N+k}\Gamma(N)}.\end{aligned} \tag{5.21}$$

For higher $\bar{\gamma}$, the average CAUC $\overline{\mathcal{A}}'^{MRC}_{Nak}$ can be approximated by using (5.21) as

$$\begin{aligned}\overline{\mathcal{A}}_{Nak}^{MRC} \approx& \left[\frac{(2m)^{Lm}}{N^{Lm}\Gamma(Lm)}\sum_{k=0}^{N-1}\frac{\Gamma(k+m)}{k!}\right. \\ &\left. - \sum_{k=1-N}^{N-1}\frac{m^{Lm}\Gamma(N+k)\,{}_2\tilde{F}_1\left(Lm; N+k; 1+k; \frac{1}{2}\right)}{2^{N+k}N^{Lm}\Gamma(N)}\right]\bar{\gamma}^{-Lm} \\ =& g^{MRC}(m, L, N)\bar{\gamma}^{-Lm}\end{aligned} \tag{5.22}$$

where $g^{MRC}(m, L, N)$ is the term in the square brackets which depends on parameters m, L and N. The detection diversity gain is equal to Lm.

Square-Law Combining

In the non-coherent energy detection, having CSI of all the diversity branches at the receiver is infeasible. Hence, the non-coherent combining schemes which exploit the diversity gain in the absence of CSI are more preferable. In contrast to the MRC, each diversity branch in SLC has a square-law device which performs the square-and-integrate operation, and the combiner is implemented following the square-law operation as shown in Fig. 5.1. The energy detector receives the sum of L decision

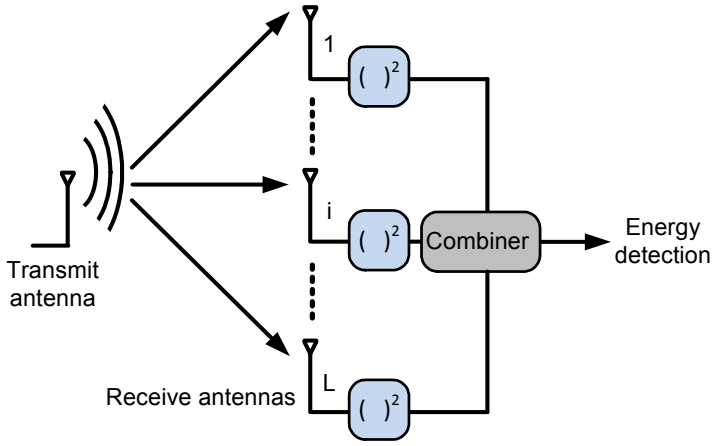

Figure 5.1: Energy Detection with SLC.

statistics. The outputs of the square-law devices of L branches are combined to yield a new decision statistic as

$$\Lambda_{\text{SLC}} = \sum_{i=1}^{L} \Lambda_i = \sum_{i=1}^{L} \sum_{n=1}^{N} |\mathbf{y}_i(n)|^2 \tag{5.23}$$

where Λ_i is the test statistic of the ith branch and $\mathbf{y}_i$ is the receive signal of the ith branch.

The resultant decision statistic under SLC follows a central chi-square distribution with $2LN$ degrees of freedom and a non-central chi-square distribution with $2LN$ degrees of freedom under hypothesis $\mathcal{H}_0$ and $\mathcal{H}_1$, respectively. Moreover, the false alarm and the detection probabilities under AWGN channel can be derived by

(2.15) and (2.17) with N and γ being replaced by LN and γ^{SLC}, respectively, where $\gamma^{SLC} = \sum_{k=1}^{L} \gamma_k$ [53]. Thus, it can be seen that the AUC under SLC for AWGN channel is equivalent to $\mathcal{A}(\gamma)$ in (5.7), after replacing N by LN. Since γ^{SLC} and γ^{MRC} have similar expression, the average AUC under SLC with Nakagami-m fading channels, $\overline{\mathcal{A}}_{Nak}^{SLC}$, can be evaluated as $\overline{\mathcal{A}}_{Nak}^{MRC}$ in (5.21) after replacing N by LN. Further, high average SNR approximation for CAUC can also be derived as

$$\overline{\mathcal{A}'}_{Nak}^{SLC} \approx g^{SLC}(m, L, N)\bar{\gamma}^{-Lm} \tag{5.24}$$

where $g^{SLC}(m, L, N)$ is equivalent to $g^{MRC}(m, L, N)$ after replacing N by LN. The detection diversity gain is equal to Lm.

5.4 Numerical and Simulation Results

In this section, numerical and Monte-Carlo simulation results are presented. Since the average AUC depends on parameters such as N, $\bar{\gamma}$, m and L (if diversity reception is used), several different cases are discussed here.

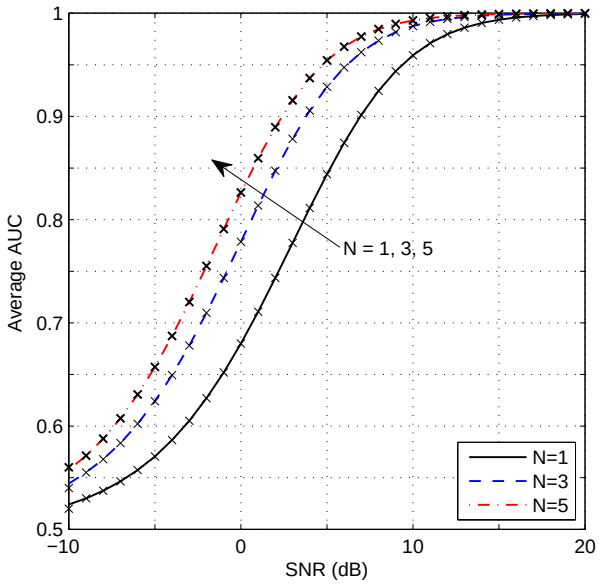

Figure 5.2: The average AUC versus the average SNR for different $N = 1, 3, 5$ with no diversity reception under Nakagami-2 fading channel.

Fig. 5.2 shows the average AUC versus the average SNR for different N with no diversity reception under Nakagami-2 fading channel. Analytical expressions for average AUCs are verified by numerical calculations and by Monte-Carlo simulations using MATHEMATICA and MATLAB software packages, respectively. Continuous and dashed lines in the figure represents numerical values, while discrete signs represent simulation values. Moreover, higher average SNR leads to larger average AUC and thus, higher overall detection capability. The influence of the number of samples N on the AUC performance is also illustrated in Fig. 5.2 which shows the average AUC versus the average SNR for different number of samples, N. A higher number of samples tends towards a higher detection capability. Although the detection and false alarm probabilities both increase when the value of N increases, the detection probability increases faster than the false-alarm probability, thus leading to a higher overall detection capability.

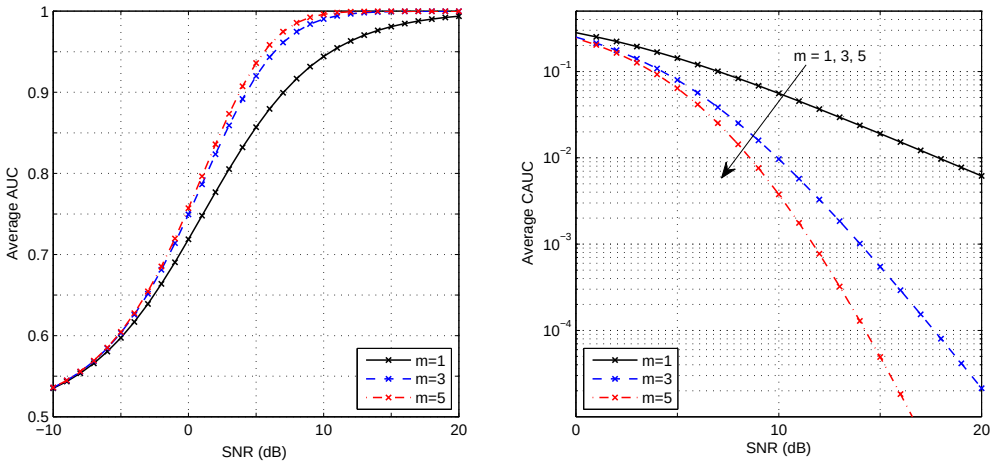

(a) (b)

Figure 5.3: (a) The average AUC versus the average SNR for different $m = 1, 3, 5$ with no diversity reception under Nakagami-m fading channel; (b) The average CAUC versus the average SNR for different $m = 1, 3, 5$ with no diversity reception under Nakagami-m fading channel.

Fig. 5.3a shows the average AUC versus the average SNR for different m values, which demonstrates the effect of fading parameter m on overall detection capability. When m increases, the average AUC increases, which means the

overall detection capability increases. However, Fig. 5.3a does not illustrate the order of increment clearly. Actually, for high SNRs, $\bar{\mathcal{A}}'_{Nak}$ is approximated as $\bar{\mathcal{A}}'_{Nak} \approx g^{Nak}(m, N)\bar{\gamma}^{-m}$ in (5.14). Thus the CAUC decreases according to order m which can be demonstrated clearly in Fig. 5.3b by plotting the average CAUC versus the average SNR for different m values. The detection diversity order is 1, 3 or 5.

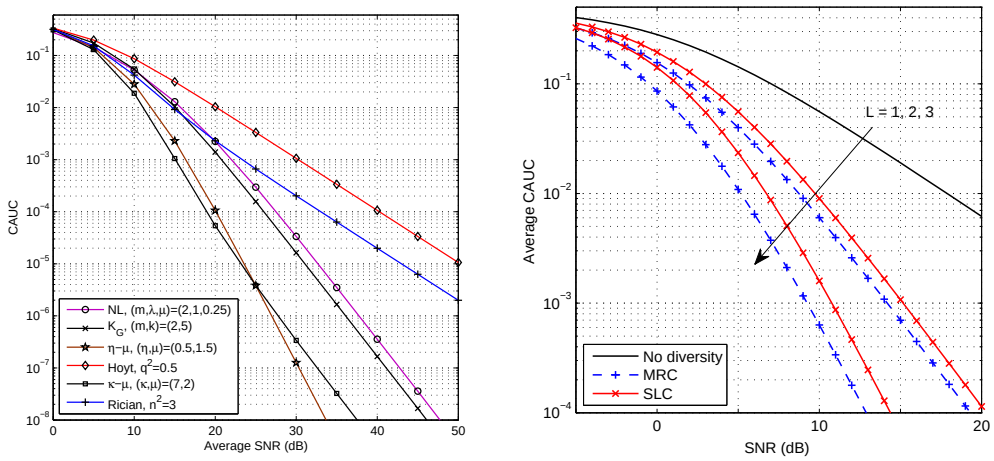

(a) (b)

Figure 5.4: (a) The average CAUC versus the average SNR for different fading channels based on the MG model; (b) The average CAUC versus the average SNR for different $L = 1, 2, 3$ with diversity reception under Rayleigh fading channel.

As discussed in Section 4.5, the achievable diversity orders of NL, K, K_G, η-μ, Hoyt, κ-μ, Rician, Rayleigh and Nakagami-m fading channels are m, 1, m, 2μ, 1, μ, 1, 1, and m, respectively. These diversity orders can also be illustrated by using the average CAUC versus average SNR plots in Fig. 5.4a in the high SNR region by using the mixture gamma (MG) channel model.

Fig. 5.4b shows the effect on the overall detection capability due to different combining techniques with different values of diversity branches L. It can be seen that, by increasing L, the average CAUC in all combining methods approaches to zero in the same order Lm in high SNR. For a particular L, although two curves corresponding to MRC and SLC are parallel to each other, MRC always outperforms SLC due to higher end-to-end SNR associated with MRC.

5.5 Conclusions

A simple figure of merit characterizing the performance of an energy detector is the AUC which is simply the area under the ROC curve. The average AUC of an energy detector is derived for Nakagami-m channels with no-diversity and with diversity reception (MRC and SLC). The detection diversity order is derived by using high SNR approximations of CAUC. It is anticipated that the AUC measure will also be useful for characterizing the performance of other numerous detection algorithms.

$\sim$

Chapter 6

Energy Detection based Cooperative Spectrum Sensing

Performance of an energy detector used for cooperative spectrum sensing is investigated. Single cooperative node, multiple cooperative nodes and multi-hop cooperative sensing networks are considered. Two fusion strategies, data fusion and decision fusion, are analyzed. For data fusion, upper bounds for average detection probabilities are derived. For decision fusion, the detection and false alarm probabilities are derived under the generalized "k-out-of-n" fusion rule at the fusion center by considering errors in the reporting channel.[1]

6.1 Introduction

The cooperative spectrum sensing by using data fusion and decision fusion is discussed in Section 2.7.

Data fusion

Data fusion has the similar function as the amplify-and-forward (AF) relaying in relaying networks, and thus a cooperative node does not need complex detection process. However, the bandwidth of the reporting channel (the channel between the cooperative node and the fusion center) may be no less than the bandwidth of the sensed channel. The complex-valued fading coefficients from the primary user to

[1] *A version of this chapter has been published in IEEE Trans. Wireless Commun., 10: 1232–1241 (2011).*

the cooperative node and from the cooperative node to the fusion center are denoted as $\mathbf{f}$ and $\mathbf{g}$, respectively. The AWGN at the cooperative node and the fusion center are $\mathbf{u}(n)$ and $\mathbf{v}(n)$, respectively, where $\mathbf{u}(n), \mathbf{v}(n) \sim \mathcal{CN}(0, 2\sigma_w^2)$.

In AF relaying, it can be assumed that the cooperative node has its own power budget P_r, and the amplification factor, α, is designed accordingly. First the received signal power is normalized, and then it is amplified to P_r. The CSI requirement depends on the AF relaying strategy, in which there are two types of relays [113, 114]:

- Non-coherent power coefficient: the cooperative node knows only the average fading power of the channel between the primary user and itself, i.e., $\mathbb{E}\{|\mathbf{f}|^2\}$, and uses it to constrain its average transmit power. Therefore, α is given as
$$\alpha = \frac{1}{2\sigma_w^2 + P_s\mathbb{E}\{|\mathbf{f}|^2\}} \tag{6.1}$$
where P_s is the power budget at the source.

- Coherent power coefficient: the cooperative node knows instantaneous CSI of the channel between the primary user and itself, i.e., $\mathbf{f}$, and uses it to constrain its average transmit power. Therefore, α is given as
$$\alpha = \frac{1}{2\sigma_w^2 + P_s|\mathbf{f}|^2}. \tag{6.2}$$

An advantage of the non-coherent power coefficient over the coherent one is in its less overhead, because the node does not need to estimate instantaneous CSI.

Decision Fusion

In decision fusion, each cooperative node makes one-bit hard decision on the primary user activity: '0' and '1' mean the absence and presence of primary activities, respectively. Then, each reporting channel is with a narrow bandwidth. Capability of complex signal processing is needed at each cooperative node. The fusion rule at the fusion center can be *OR*, *AND*, or *Majority* rule, which can be generalized as the "k*-out-of-*n*" rule*. The decision device of the fusion center with n cooperative nodes can be implemented with the k*-out-of-*n *rule* in which the fusion center

decides the presence of primary activity if there are k or more cooperative nodes that individually decide on the presence of primary activity. When $k = 1$, $k = n$ and $k = \lceil n/2 \rceil$, where $\lceil \cdot \rceil$ is the ceiling function, the k-out-of-n rule represents *OR rule*, *AND rule* and *Majority rule*, respectively.

A framework for two-user and multiple-user cooperative spectrum sensing with data fusion was introduced in [66, 115]. However, an analytical study for the detection capability of cooperative spectrum sensing has not been addressed. Decision fusion literature assumes for simplicity that the reporting channel is error-free [116, 117]. However, this assumption may not valid in practice. To fill these research gaps in this area, in this chapter, a rigorous analytical framework is provided for cooperative spectrum sensing with data fusion, and the detection performance with decision fusion in scenarios with reporting errors is also investigated.

The rest of the chapter is organized as follows. Section 6.2 gives the preliminaries for the analysis. Sections 6.3 and 6.4 are devoted to the analysis of cooperative spectrum sensing with data fusion and decision fusion, respectively. Section 6.5 presents our numerical and simulation results, followed by concluding remarks in Section 6.6.

6.2 Non-Cooperative Cases

For non-cooperative cases (i.e., there is only one secondary user that would make a decision on presence or absence of primary activities), the average detection probability can be calculated by direct averaging of the instantaneous detection probability over the respective SNR distribution as explained in Chapter 3. However, the direct integration is not possible with some cases. This is due to the detection probability being expressed by the generalized Marcum-Q function which has limited analytical results. Alternatively, the generalized Marcum-Q function can be written as a circular contour integral [118], which replaces the Marcum-Q function

in (2.17). Thus the average detection probability, $\bar{P}_d$, can be given as

$$\begin{aligned}\bar{P}_d &= \int_0^{\infty} \frac{e^{-\frac{\lambda}{2}}}{j2\pi} \oint_{\Gamma} \frac{e^{(\frac{1}{z}-1)Nx+\frac{\lambda}{2}z}}{z^N(1-z)} dz f_\gamma(x)\,\mathrm{d}x \\ &= \frac{e^{-\frac{\lambda}{2}}}{j2\pi} \oint_{\Gamma} \mathcal{M}_\gamma\left(N-\frac{N}{z}\right) \frac{e^{\frac{\lambda}{2}z}}{z^N(1-z)} dz\end{aligned} \tag{6.3}$$

where $f_\gamma(x)$ is the PDF of channel SNR γ, $\mathcal{M}_\gamma(\cdot)$ is the MGF of channel SNR γ, and Γ is a circular contour with radius $r \in [0, 1)$. Since the Residue Theorem [112] in complex analysis is a powerful tool to evaluate line integrals and/or real integrals of functions over closed curves, (6.3) may be solved in the closed form for mathematically tractable MGFs. If $\mathcal{M}_\gamma(s)$ is in a simple rational form (e.g., Nakagami-m and η-μ fading), MGF approach based on residue evaluation is effective. Unfortunately, MGFs of some fading models (e.g., K or K_G model) or some network scenarios do not give rise to a rational-form MGF. To circumvent the analytical difficulties, the mixture gamma (MG) model in Chapter 4 can be used as a generalized fading scenario. After substituting the MGF given in (4.3), $\bar{P}_d$ can be rewritten as

$$\overline{P_d} = e^{-\frac{\lambda}{2}} \sum_{i=1}^{S} \frac{\alpha_i \Gamma(\beta_i)}{(\zeta_i+N)^{\beta_i}} \frac{1}{j2\pi} \oint_{\Gamma} g(z) dz \tag{6.4}$$

where

$$g(z) = \frac{e^{\frac{\lambda}{2}z}}{z^{N-\beta_i}(1-z)\left(z-\frac{N}{N+\zeta_i}\right)^{\beta_i}}.$$

The contour integral can be solved by applying the Residue Theorem assuming integer values for β_i. Details are given in Section 5.3.1 and Appendix C.

There are two possible scenarios, $N > \beta_i$ and $N \leq \beta_i$. When $N > \beta_i$: There are $(N - \beta_i)$ poles at $z = 0$ and β_i poles at $z = \frac{N}{N+\zeta_i}$. Therefore, $\overline{P_d}$ can be calculated as

$$\overline{P_d} = e^{-\frac{\lambda}{2}} \sum_{i=1}^{S} \frac{\alpha_i \Gamma(\beta_i)}{(\zeta_i+N)^{\beta_i}} \left[\mathrm{Res}\,(g;0) + \mathrm{Res}\left(g;\frac{N}{N+\zeta_i}\right)\right] \tag{6.5}$$

where $\mathrm{Res}\,(g;0)$ and $\mathrm{Res}\left(g;\frac{N}{N+\zeta_i}\right)$ are the residues of $g(z)$ at $z = 0$ and $z = \frac{N}{N+\zeta_i}$, respectively. When $N \leq \beta_i$: There are β_i poles at $z = \frac{N}{N+\zeta_i}$. Therefore, $\overline{P_d}$ can be

calculated as

$$\overline{P_d} = e^{-\frac{\lambda}{2}} \sum_{i=1}^{S} \frac{\alpha_i \Gamma(\beta_i)}{(\zeta_i + N)^{\beta_i}} \text{Res}\left(g; \frac{N}{N + \zeta_i}\right). \tag{6.6}$$

In the following, we will derive average detection probability for cooperative spectrum sensing with one or multiple cooperative nodes, one or multiple hops.

6.3 Data Fusion

6.3.1 Cooperative Scheme

A cognitive radio network in Fig. 6.1 is considered with a number K of cooperative nodes (named r_1, r_2, ..., r_K). In the first phase, all cooperative nodes listen to the

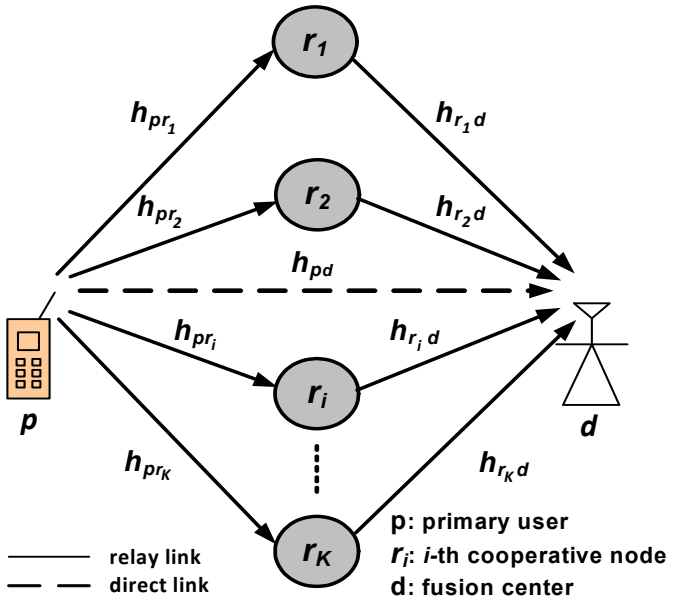

Figure 6.1: Illustration of a multiple-cooperative node network

.

primary user signal. Instead of making individual hard decision about the presence or absence of the primary user, each cooperative node amplifies and forwards the noisy version of its received signal to the fusion center in the second phase. These nodes will use orthogonal communication channels. The fusion center receives independent signals from cooperative nodes. The fusion center is equipped with

an energy detector which compares the received signal energy with a pre-defined threshold λ.

Single-Cooperative Node Networks

In a single-cooperative network, the node types are: primary user, cooperative node, and fusion center. The cooperative node continuously monitors the signal received from the primary user. The received signal at the cooperative node, denoted $\mathbf{y}_{pr}(n)$, is given by $\mathbf{y}_{pr}(n) = \theta \mathbf{h}_{pr}\mathbf{s}(n) + \mathbf{u}(n)$ where θ denotes the primary activity indicator, which is equal to 1 at the presence of primary activity, or equal to 0 otherwise, $\mathbf{h}_{pr}$ is the channel gain between the primary user and cooperative node, and $\mathbf{u}(n)$ is the AWGN at the cooperative node. The fusion center implements with an energy detector, which decides whether a signal is present or not by using the received signal. The decision is made from a binary hypothesis. In general, for hypothesis $\mathcal{H}_\theta$, $\theta \in \{0, 1\}$, the received signal at the decision maker (i.e., the fusion center) can be given as

$$\mathbf{y}(n) = \theta\sqrt{P_r\alpha}\mathbf{h}_{pr}\mathbf{h}_{rd}\mathbf{s}(n) + \sqrt{P_r\alpha}\mathbf{h}_{rd}\mathbf{u}(n) + \mathbf{v}(n) \tag{6.7}$$

where $\mathbf{h}_{rd}$ is the flat fading channel gain between the cooperative node and fusion center.

In this chapter, the non-coherent power coefficient is used which is given in (6.1). The same receiver structure as in reference [52] is used.[2] The effective noise in (6.7) can be modeled as $\mathbf{w}|_{\mathbf{h}_{rd}} \sim \mathcal{CN}\big(0, (P_r\alpha|\mathbf{h}_{rd}|^2+1)2\sigma_w^2\big)$. The received signal is first filtered by an ideal band-pass filter. The filter limits the average noise power and normalizes the noise variance. The output of the filter is then squared and integrated over time T to form decision statistic Λ. Therefore, the false alarm probability and detection probability can be written as (2.15) and (2.17), respectively, with the effective SNR $\gamma = \frac{\gamma_{pr}\gamma_{rd}}{C+\gamma_{rd}}$ where γ_{pr} and γ_{rd} are SNRs of the links from the primary user to the cooperative node and from the cooperative node to the fusion center, respectively, and $C = \frac{P_s\mathbb{E}\{|\mathbf{h}_{pr}|^2\}}{2\sigma_w^2} + 1$.

[2]Note that cooperative spectrum sensing is not considered in reference [52].

Multiple cooperative nodes Networks

A multiple-cooperative node network is shown in Fig. 6.1. There are K cooperative nodes between the primary user and the fusion center, and $\mathbf{h}_{pr_i}$, $\mathbf{h}_{pd}$ and $\mathbf{h}_{r_id}$ denote the channel gains from the primary user to the ith cooperative node r_i, from the primary user to the fusion center, and from the ith cooperative node r_i to the fusion center, respectively. All cooperative nodes receive primary user's signal through independent fading channels simultaneously. Each cooperative node (say cooperative node r_i) amplifies the received primary signal by an amplification factor α_{r_i}, and forwards to the fusion center over mutually orthogonal channels.

If the fusion center is implemented with MRC, the CSI of channels in the first hop (or primary network) should be forwarded to the fusion center. On the other hand, CSI may not be available for energy detection (which is non-coherent). In contrast to MRC, receiver with SLC (which is a non-coherent combiner) does not need instantaneous CSI of the channels in the first hop, and consequently results in a low complexity system. The number K of outputs from all the branches in the SLC, denoted $\{\Lambda_i\}_{i=1}^{K}$, are combined to form the decision statistic

$$\Lambda_{\text{SLC}} = \sum_{i=1}^{K} \Lambda_i = \sum_{i=1}^{K} \sum_{n=1}^{N} |\mathbf{y}_i(n)|^2$$

where $\mathbf{y}_i$ is received signal via the ith cooperative node. Under AWGN channels, Λ_{SLC} follows a central chi-square distribution with KN degrees of freedom (DoF) under $\mathcal{H}_0$, and a non-central chi-square distribution with KN DoF under $\mathcal{H}_1$. Further, effective SNR after the combiner is $\gamma_{SLC} = \sum_{i=1}^{K} \gamma_i$ where γ_i is the equivalent SNR of the ith relay path. The non-centrality parameter under $\mathcal{H}_1$ is $2\gamma_{SLC}$. The false alarm and detection probabilities can be calculated using (2.15) and (2.17) by replacing N by KN and γ by γ_{SLC}.

6.3.2 Analysis of Average Detection Probability

Multiple cooperative node network

The derivation of the average detection probability in (6.3) seems analytically difficult with the MGF of γ which is given in [114, eq. (12)]. Efficient numerical

algorithms are available to evaluate a circular contour integral. We can use MATHEMATICA or MATLAB software packages that provide adaptive algorithms to recursively partition the integration region. With a high precision level, the numerical method can provide an efficient and accurate solution for (6.4). In the following, we derive an upper bound of average detection probability.

The total SNR γ of a multiple-cooperative node network can be upper bounded by γ_{up} as $\gamma \leq \gamma_{\text{up}} = \sum_{i=1}^{K} \gamma_i^{\min}$, where $\gamma_i^{\min} = \min(\gamma_{pr_i}, \gamma_{r_i d})$, and γ_{pr_i} and $\gamma_{r_i d}$ are the SNRs of the links from the primary user to cooperative node r_i and from cooperative node r_i to the fusion center, respectively. Therefore, for independent channels, MGF of γ_{up} can be written as $\mathcal{M}_{\gamma_{\text{up}}}(s) = \prod_{i=1}^{K} \mathcal{M}_{\gamma_i^{\min}}(s)$ to yield

$$\mathcal{M}_{\gamma_{\text{up}}}(s) = \prod_{i=1}^{K} \frac{\overline{\gamma}_{pr_i} + \overline{\gamma}_{r_i d}}{\overline{\gamma}_{pr_i}\overline{\gamma}_{r_i d}} \frac{1}{\left(s + \frac{\overline{\gamma}_{pr_i} + \overline{\gamma}_{r_i d}}{\overline{\gamma}_{pr_i}\overline{\gamma}_{r_i d}}\right)}, \tag{6.8}$$

where $\overline{\gamma}_{pr_i}$ and $\overline{\gamma}_{r_i d}$ are the average SNRs for links from the primary user to cooperative node r_i and from cooperative node r_i to the fusion center, respectively. Substituting (6.8) into (6.3), an upper bound of $\overline{P_d}$, denoted $\overline{P_d^{\text{up}}}$, can be re-written as (6.3) with

$$g(z) = \frac{e^{\frac{\lambda}{2}z}}{z^{N-K}(1-z)} \prod_{i=1}^{K} \frac{1-\Delta_i}{z-\Delta_i},$$

and

$$\Delta_i = \frac{\gamma_{pr_i}\gamma_{r_i d}}{\gamma_{pr_i} + \gamma_{r_i d} + \gamma_{pr_i}\gamma_{r_i d}}.$$

Two scenarios need to be considered: 1) When $N > K$, there are $N - K$ poles at origin and K poles for Δ_i's ($i = 1, .., K$) in radius $r \in [0, 1)$, and 2) when $N \leq K$, there are K poles at Δ_i's ($i = 1, .., K$) in radius $r \in [0, 1)$. Therefore, $\overline{P_d^{\text{up}}}$ can be derived as

$$\overline{P_d^{\text{up}}} = \begin{cases} e^{-\frac{\lambda}{2}} \left(\text{Res}\,(g; 0) + \sum_{i=1}^{K} \text{Res}\big(g; \Delta_i\big) \right) & : N > K \\ e^{-\frac{\lambda}{2}} \sum_{i=1}^{K} \text{Res}\big(g; \Delta_i\big) & : N \leq K, \end{cases} \tag{6.9}$$

where $\text{Res}\,(g; 0)$ and $\text{Res}\big(g; \Delta_i\big)$ denote the residue of the function $g(z)$ at origin and Δ_i, respectively. Appendix C provides the details of the derivation of residue calculations $\text{Res}(g; \cdot)$.

Incorporation with the Direct Link

In preceding subsections, the fusion center receives only signals coming from cooperative nodes. If the primary user is close to the fusion center, the fusion center can however have a strong direct link from the primary user. The direct signal can also be combined at the SLC together with the relayed signals. Then the total SNR at the fusion center can be written as $\gamma^{\dagger} = \gamma_d + \sum_{i=1}^{K} \gamma_{r_i}$, where γ_d is the SNR of the direct path. Assuming independent fading channels, the MGF of $\gamma^{\dagger}$ can be written as

$$\mathcal{M}_{\gamma^{\dagger}}(s) = \mathcal{M}_{\gamma_d}(s) \prod_{i=1}^{K} \mathcal{M}_{\gamma_{r_i}}(s),$$

where $\mathcal{M}_{\gamma_d}(s)$ is given by $1/(1+\overline{\gamma}_d s)$ with $\overline{\gamma}_d = \mathbb{E}\{\gamma_d\}$, and $M_{\gamma_{r_i}}(s)$ is given in [114, eq. (12)]. As in preceding subsections, an accurate average detection probability can be found by using numerical integration. An upper bound is derived in the following. In this case, $g(z)$ in (6.3) can be written as

$$g(z) = \frac{(1-\Delta)e^{\frac{\lambda}{2}z}}{z^{N-K-1}(1-z)(z-\Delta)} \prod_{i=1}^{K} \frac{1-\Delta_i}{z-\Delta_i} \tag{6.10}$$

where $\Delta = \overline{\gamma}_d/(1+\overline{\gamma}_d)$. When $N > K+1$, there are $N-K-1$ poles at origin, one pole at Δ and K poles for Δ_i's ($i = 1, \cdots, K$) in radius $r \in [0,1)$. When $N \leq K+1$, there are one pole at Δ and K poles for Δ_i's ($i = 1, \cdots, K$) in radius $r \in [0,1)$. Therefore, a tight upper bound of the detection probability, denoted $\overline{P_d^{\dagger,\text{up}}}$, can be derived in closed-form as

$$\overline{P_d^{\dagger,\text{up}}} = \begin{cases} e^{-\frac{\lambda}{2}} \Big(\text{Res}\,(g;0) + \text{Res}\,(g;\Delta) + \sum_{i=1}^{K} \text{Res}\big(g;\Delta_i\big) \Big) : & N > K+1 \\ e^{-\frac{\lambda}{2}} \Big(\text{Res}\,(g;\Delta) + \sum_{i=1}^{K} \text{Res}\big(g;\Delta_i\big) \Big) : & N \leq K+1. \end{cases} \tag{6.11}$$

All residues, $\text{Res}\,(g;0)$, $\text{Res}\,(g;\Delta)$ and $\text{Res}\big(g;\Delta_i\big)$, are calculated in Appendix C.

6.3.3 Multi-hop cooperative Sensing

Multi-hop communication is introduced as a smart way of providing a broader coverage in wireless networks. The same idea is exploited in a cognitive radio network because the coverage area can be broadened with less power consumption. Channel coefficients of different hops can be non-identically distributed random variables.

Consider a cognitive radio network with M hops between the primary user and the fusion center. There are $M-1$ cooperative nodes $(r_1, \cdots, r_{M-1})$ between the primary user and the fusion center. The end-to-end SNR is given as $\gamma = \left(\sum_{i=1}^{M} \prod_{j=1}^{i} \frac{C_{j-1}}{\gamma_j}\right)^{-1}$ where γ_i is the instantaneous SNR of the ith hop and C_j is the constant in cooperative node r_j and $C_0 = 1$. Since γ can be upper bounded as $\gamma_{\text{up}} = \mathcal{Z}_M \prod_{i=1}^{M} \gamma_i^{\frac{M+1-i}{M}}$ where $\mathcal{Z}_M = \left(\prod_{i=1}^{M} C_i^{-(M-i)/M}\right)/M$ [119], the MGF of γ_{up} is expressed using the Padé approximation method as [120]

$$\mathcal{M}_{\gamma_{\text{up}}}(s) \cong \sum_{i=1}^{Q} \frac{\mu_i s^i}{i!} + \mathcal{O}(s^{Q+1}) \text{ where } \mu_i = \mathcal{Z}_M^i \prod_{j=1}^{M} \bar{\gamma_j}^{\frac{i(M-j+1)}{M}} \Gamma\left(\frac{i(M-j+1)}{M}\right),$$

Q is a finite number of terms of the truncated series, μ_i is ith moment of γ_{up} (here $\bar{\gamma_j}$ is the average SNR over the jth hop), and $\mathcal{O}(s^{Q+1})$ is the remainder of the truncated series. After applying the Padé approximation, $\mathcal{M}_{\gamma_{\text{up}}}(s)$ is given as

$$\mathcal{M}_{\gamma_{\text{up}}}(s) \cong \frac{\sum_{i=0}^{A} a_i s^i}{1 + \sum_{i=1}^{B} b_i s^i} = \sum_{i=1}^{B} \frac{q_i}{s + p_i} \tag{6.12}$$

where A and B are specified orders of the numerator and the denominator of the Padé approximation, a_i and b_i are approximated coefficients, and p_i and q_i can be obtained based on the second equality in (6.12), as detailed in [120, Sec. II-C], [121, Sec. IV]. Since $\mathcal{M}_{\gamma_{\text{up}}}(s)$ in (6.12) is a sum of rational functions, an upper bound of the average detection probability can be written using (6.3) to yield

$$\overline{P_d^{\text{up}}} = \frac{e^{-\frac{\lambda}{2}}}{j2\pi} \sum_{i=1}^{B} \frac{q_i}{1+p_i} \oint_{\Omega} g_i(z) dz, \tag{6.13}$$

where

$$g_i(z) = \frac{e^{\frac{\lambda}{2} z}}{\left(z - \frac{1}{1+p_i}\right) z^{N-1}(1-z)}.$$

When $N > 1$, there is a pole at $z = 1/(1+p_i)$ and $(N-1)$ poles at the origin, and when $N = 1$, there is only a pole at $z = 1/(1+p_i)$ of $g_i(z)$. Thus, $\overline{P_d^{\text{up}}}$ can be written as

$$\overline{P_d^{\text{up}}} = \begin{cases} e^{-\frac{\lambda}{2}} \sum_{i=1}^{B} \frac{q_i}{1+p_i} \left(\text{Res}\left(g_i; 0\right) + \text{Res}\left(g_i; \frac{1}{1+p_i}\right)\right) : & N > 1, \\ e^{-\frac{\lambda}{2}} \sum_{i=1}^{B} \frac{q_i}{1+p_i} \text{Res}\left(g_i; \frac{1}{1+p_i}\right) : & N = 1, \end{cases} \tag{6.14}$$

where $\text{Res}\left(g_i; 0\right)$ and $\text{Res}\left(g_i; 1/(1+p_i)\right)$ are given in Appendix C.

6.4 Decision Fusion

Each cooperative node makes its own one-bit hard decision: '0' and '1' mean the absence and presence of primary activities, respectively. The one-bit hard decision is forwarded independently to the fusion center, which makes the cooperative decision on the primary activity.

6.4.1 k-out-of-n Rule

It is assumed that the decision device of the fusion center is implemented with the *k-out-of-n rule* (i.e., the fusion center decides the presence of primary activity if there are k or more cooperative nodes that individually decide the presence of primary activity). When $k = 1$, $k = n$ and $k = \lceil n/2 \rceil$, the k-out-of-n rule represents *OR rule*, *AND rule* and *Majority rule*, respectively. In the following, for simplicity of presentation, p_f and p_d are used to represent false alarm and detection probabilities, respectively, for a cooperative node, and use P_f and P_d to represent false alarm and detection probabilities, respectively, in the fusion center.

Reporting Channels without Errors

If the sensing channels (the channels between the primary user and cooperative nodes) are identical and independent, then every cooperative node achieves identical false alarm probability p_f and detection probability p_d. If there are error free reporting channels (the channels between the cooperative nodes and the fusion center), P_f and P_d at the fusion center can be written as

$$P_\chi = \sum_{i=k}^{K} \binom{K}{i} (p_\chi)^i (1 - p_\chi)^{K-i} \tag{6.15}$$

where the notation 'χ' means 'f' or 'd' for false alarm or detection, respectively.

Reporting Channels with Errors

Because of the imperfect reporting channels, errors occur on the decision bits which are transmitted by the cooperative nodes. Assume bit-by-bit transmission from cooperative nodes. Thus, each identical reporting channel can be modeled as a binary

symmetric channel (BSC) with cross-over probability p_e which is equal to the BER of the channel.

Consider the ith cooperative node. When the primary activity is present (i.e., under $\mathcal{H}_1$), the fusion center receives bit '1' from the ith cooperative node when (1) the one-bit decision at the ith cooperative node is '1' and the fusion center receives bit '1' from the reporting channel of the ith cooperative node, with probability $p_d(1-p_e)$; or (2) the one-bit decision at the ith cooperative node is '0' and the fusion center receives bit '1' from the reporting channel of the ith cooperative node, with probability $(1-p_d)p_e$. On the other hand, when the primary activity is absent (i.e., under $\mathcal{H}_0$), the fusion center receives bit '1' from the ith cooperative node when (1) the one-bit decision at the ith cooperative node is '1' and the fusion center receives bit '1' from the reporting channel of the ith cooperative node, with probability $p_f(1-p_e)$; or (2) the one-bit decision at the ith cooperative node is '0' and the fusion center receives bit '1' from the reporting channel of the ith cooperative node, with probability $(1-p_f)p_e$. Therefore, the overall false alarm and detection probabilities with the reporting error can be evaluated as

$$P_\chi = \sum_{i=k}^{K} \binom{K}{i} (p_{\chi,e})^i (1-p_{\chi,e})^{K-i} \tag{6.16}$$

where $p_{\chi,e} = p_\chi(1-p_e) + (1-p_\chi)p_e$ is the equivalent false alarm ('χ' is 'f') or detection ('χ' is 'd') probabilities of the ith cooperative node.

Note that p_e is the cross-over probability of BSC. It is typically taken as a constant value (e.g., $p_e = 10^{-1}, 10^{-2}, 10^{-3}$) in a network with AWGN channels. In the system model, p_e can be calculated analytically as BER calculation of different modulation schemes under multipath fading and shadowing effects. For BPSK, BER can be calculated as $p_e = \frac{1}{\pi}\int_0^{\pi/2} \mathcal{M}_\gamma\left(1/\sin^2\theta\right) \mathrm{d}\theta$ to yield

$$p_e = \frac{1}{2}\left(1 - \sqrt{\frac{\overline{\gamma}}{1+\overline{\gamma}}}\right)$$

and

$$p_e = \frac{1}{2}\sum_{i=1}^{S} \frac{\alpha_i}{\zeta_i}\left(1 - \sqrt{\frac{1}{1+\zeta_i}}\right)$$

for Rayleigh fading and composite Rayleigh-lognormal fading, respectively. Here α_i and ζ_i are defined in (4.1).

6.4.2 Multi-hop Cooperative Sensing

Consider a multi-hop wireless network for both identical and non-identical channels. Each cooperative node makes a decision on the presence or absence of the primary activity and forwards the one-bit decision to the next hop. Each hop is modeled as BSC. It is assumed that there are M hops (i.e., $M-1$ cooperative nodes) between the primary user and the fusion center. A channel with $(M-1)$ non-identically cascaded BSCs, which is equivalent to a single BSC with 1) effective cross-over probability P_e given as (see Appendix C for the derivation)

$$P_e = \frac{1}{2}\left(1 - \prod_{i=1}^{M-1}(1-2p_{e,i})\right)$$

where $p_{e,i}$ is the cross-over probability of the ith BSC and 2) the approximately equivalent average SNR being the average SNR of the $M-1$ BSCs. A channel with $(M-1)$ identically cascaded BSCs, which is equivalent to a single BSC with effective cross-over probability $P_e = \frac{1}{2}[1-(1-2p_e)^{M-1}]$ and the average SNR being the average SNR of any BSC. Based on the channel gain of the equivalent single BSC, the detection and false alarm probabilities, p_d and p_f, of the BSC can be derived. The detection and false alarm probabilities under a multi-hop cooperative network can be given as $P_d = p_d(1-P_e) + (1-p_d)P_e$ and $P_f = p_f(1-P_e) + (1-p_f)P_e$, respectively.

6.5 Numerical and Simulation Results

This section provides analytical and simulation results to verify the analytical framework, and to compare the ROC curves [48] of different scenarios that are presented in the previous sections. Note that each of the following figures contains both analytical result and simulation result, which are represented by lines and discrete marks, respectively.

The performance of the energy detector in non-cooperative cases (as discussed in Section 6.2) is first shown, which is an important starting point of the investigation in the cooperative cases. Fig. 6.2 thus illustrates ROC curves for small scale fading with Rayleigh channel and composite fading (multipath and shadow-

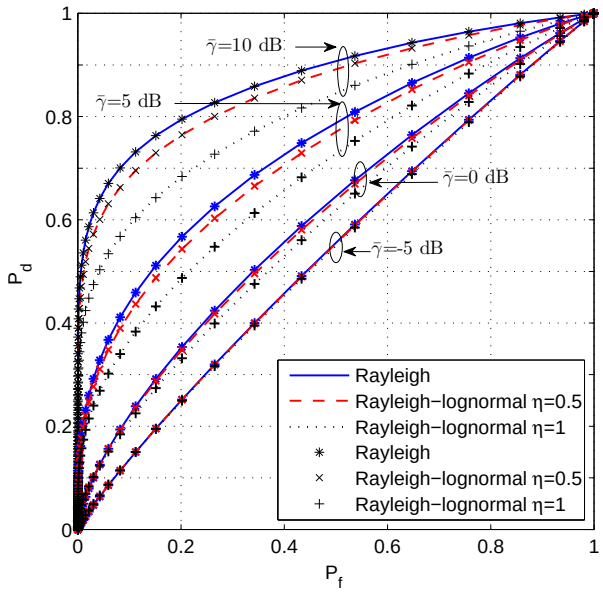

Figure 6.2: ROC curves of an energy detector over Rayleigh and Rayleigh-lognormal fading channels

.

ing) with Rayleigh-lognormal channel where $S = 10$ in (4.1), which makes the MSE between the exact gamma-lognormal channel model and the approximated MG channel model in (4.1) less than 10^{-4}. The numerical results match well with their simulation counterparts, confirming the accuracy of the analysis. The energy detector capabilities degrade rapidly when the average SNR of the channel decreases from 10 dB to -5 dB. Further, there is a significant performance degradation of the energy detector due to the shadowing effect η (η is the standard deviation of the lognormal distribution).

Second, cooperative cases (discussed in Sections 6.3 and 6.4) are evaluated, with focus on the impact of the number of cooperative nodes on detection capability. The upper bound of average detection probability, based on (6.9), and simulation results are shown in Fig. 6.3a. Note that the bound is tight for all the cases. Increasing the number of cooperative nodes improves the detection capability. Fig. 6.3b shows the impact of the direct path on the detection capability. The direct path has an average SNR value as -5 dB, -3 dB, 0 dB, 3dB or 5 dB, in network with $K = 1$ or $K = 3$ cooperative nodes. The average SNR for other channels (from

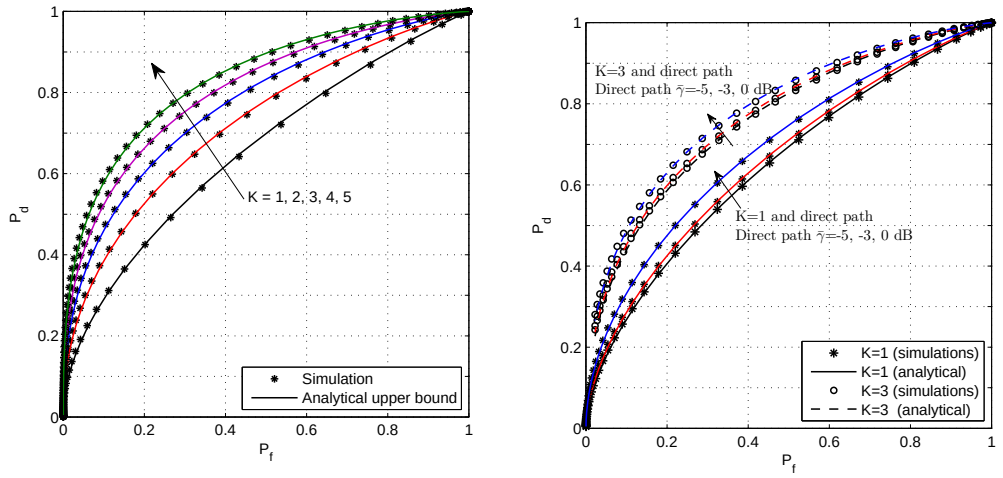

(a) (b)

Figure 6.3: (a) ROC curves for different number of cooperative nodes over Rayleigh fading channels $\overline{\gamma}$ = 5 dB; (b) ROC curves with the direct link over Rayleigh fading channels.

the primary user to each cooperative node and from each cooperative node to the fusion center) is 5 dB. When the average SNR of the direct link is improved from -5 dB to 5 dB, ROC curves move rapidly to the left-upper corner of the ROC plot, which means better detection capability. The presence of the direct path can significantly improve the detection performance. It is better to utilize the direct link for spectrum identification in the mobile wireless communication networks with data fusion strategy because there may be a possibility for the fusion center and the primary user to be close to each other.

Fig. 6.4a and Fig. 6.4b show the ROC curves for k-out-of-n rule in decision fusion strategy for error-free and erroneous reporting channels, respectively. Three fusion rules: OR, AND, and Majority rules, are considered. The average SNR in each link (from the primary user to each cooperative node, and from each cooperative node to the fusion center) is 5 dB. With error-free reporting channels, OR rule outperforms AND and Majority rules, and Majority rule has better detection capability than AND rule. With erroneous reporting channels, the comparative performances of the three fusion rules are not as clear-cut. However, OR rule outperforms AND and Majority rules in lower detection threshold (λ) values (i.e., higher

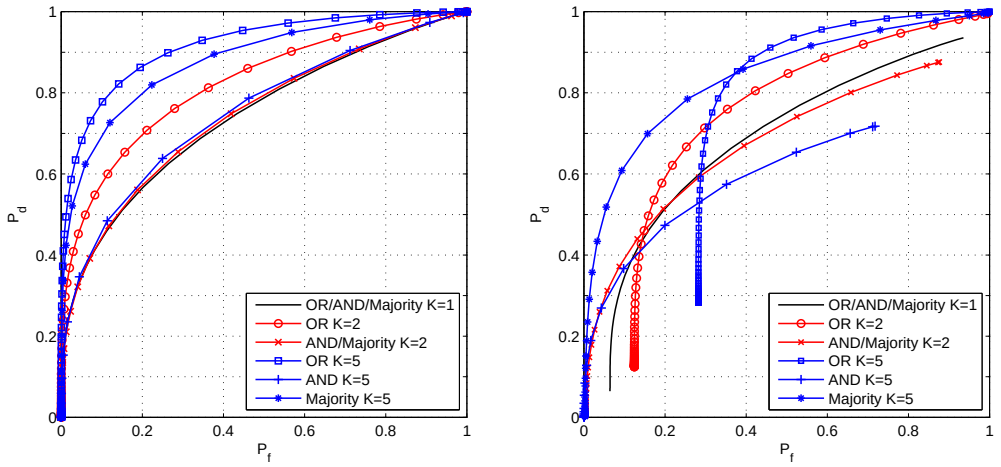

(a) (b)

Figure 6.4: (a) ROC curves for OR, AND and Majority fusion rules with error-free reporting channels; (b) ROC curves for OR, AND and the Majority fusion rules with Rayleigh faded reporting channels.

P_d and P_f). As shown in Fig. 6.4b, when $K = 5$, OR rule has better performance than Majority rule and AND rule when $\lambda < 12.3$ dB and $\lambda < 14.3$ dB, respectively. With the erroneous reporting channels, it cannot be expected $(P_f, P_d) = (1, 1)$ at $\lambda = 0$ and $(P_f, P_d) \to (0, 0)$ when $\lambda \to \infty$ on the ROC plot. When $\lambda = 0$, $P_f = P_d = \sum_{i=k}^{K} \binom{K}{i} (1 - p_e)^i p_e^{K-i}$; and when $\lambda \to \infty$, P_f and P_d approaches $\sum_{i=k}^{K} \binom{K}{i} {p_e}^i (1 - p_e)^{K-i}$. In both scenarios, the values of P_d and P_f depend only on the error probabilities of the reporting channels.

In Fig. 6.5, a multi-hop coopeative network and its detection capability over Rayleigh fading are considered. The average SNR in each hop is 5 dB. Note that for data fusion strategy, each ROC curve starts from (1, 1) when $\lambda = 0$ to (0, 0) when λ goes to infinity. On the other hand, for decision fusion strategy with erroneous reporting channels, when $\lambda = 0$, we have $P_d = P_f = 1 - P_e$, and when λ goes to infinity, P_d and P_f approaches P_e. Fig. 6.5 shows that the detection performance of both data fusion strategy (represented by continuous lines) and decision fusion strategy (represented by dashed lines) degrades rapidly as the number of hops increases.

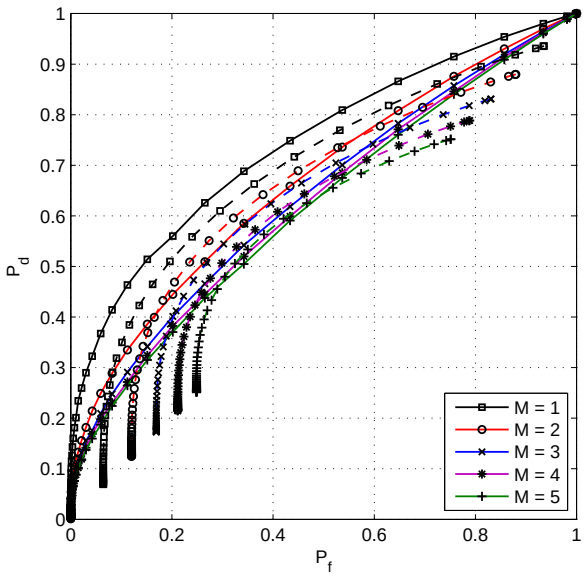

Figure 6.5: ROC curves for a multi-hop cooperative network

.

6.6 Conclusion

Detection performance of cooperative spectrum sensing is analyzed for data fusion and decision fusion strategies. A new set of results is derived for the average detection probability. For the data fusion strategy, the MGFs of received SNR of the primary user's signal at the fusion center are utilized to derive tight bounds of the average detection probability. For the decision fusion strategy in the cooperative spectrum sensing, the generalized k-out-of-n fusion rule is considered, with particular focus on the OR, AND, and Majority rules. OR rule always outperforms AND and Majority rules, and Majority rule has better detection capability than AND rule with error-free reporting channels. However, given a probability of reporting error, the performance is limited by the reporting error. The detection performance of both strategies degrades rapidly when the number of hops increases.

$\sim$

Chapter 7

Energy Detection in Low SNR

The IEEE 802.22 standard requires spectrum-sensing techniques to identify primary signals with a very low SNR. In this chapter, under such low-SNR levels, the detection performance of a conventional energy detector used for spectrum sensing in cognitive radio networks is investigated. The analysis focuses on deriving approximations for two performance metrics: (1) the average missed-detection probability, and (2) the average AUC, which measures the overall detection capability of an energy detector. The analysis develops a unified framework covering many existing fading channels, square-law diversity-combining technique and cooperative spectrum-sensing scenarios. The detection threshold is also optimized to minimize the total error rate subject to bounded false alarm and missed-detection probabilities.

7.1 Introduction

In Section 2.6, some of the specifications of the IEEE 802.22 standard are given, in which the requirements of false alarm and missed-detection probabilities (both are less than 0.1) should be met with a very low SNR, e.g., -20 dB SNR [13]. Thus, spectrum sensing at low SNR is vital. Research on various spectrum sensing techniques at moderate and high SNRs is frequently available in the literature [48, 53, 54]. However, research on spectrum sensing at low SNR is still very limited. The low SNR spectrum sensing is considered for a differential energy detection scheme of multi-carrier systems (e.g., OFDM) in [58], for multi-antenna

detectors (which improve the robustness to noise uncertainty) in [59, 60], and for a covariance matrix based detection algorithm in [61]. Moreover, low-SNR cooperative spectrum sensing techniques are considered for belief propagation in [62], for cyclostationary detection in [63], for optimal relaying scheme in [64], and for multi-antenna with a noise-uncertainty-free detector in [65]. These works consider generalized likelihood ratio detector, alternative energy detector, cyclostationary feature detector or covariance based detector, in which the operating SNR ranges generally from 0 to -30 dB.

Due to the mathematical complexity, none of the research in the literature provides a rigorous unified analytical framework (here 'unified' means the framework is valid with most existing fading channels) for the performance analysis (e.g., on average detection performance) and parameter optimization (e.g., on detection threshold or sensing time) for any spectrum sensing technique at low SNR. The reason is that although the average performance metrics (e.g., average detection probability) can be derived rigorously for some particular fading models, the same analytical framework may not work well for the parameter optimization [53, 54]. Therefore, a unified analytical framework is critically important to the cognitive radio industry and deserves full investigation, at least for the conventional energy detection as a benchmark because it is the simplest detection technique and its performance metrics can be an upper bound (e.g., on sensing time) or a lower bound (e.g., on detection probability) for other complex detection techniques. To achieve this, this chapter provides a basic rigorous unified analytical framework for conventional energy detection over various fading channels, analyzes the detection performance, derives the optimal detection threshold that minimizes the total error rate when both false alarm and missed-detection probabilities are bounded, and investigates detection performance in diversity combining and cooperative sensing scenarios.

The rest of this chapter is organized as follows. Section 7.2 discusses energy detection and its low-SNR model. Section 7.3 analyzes the low-SNR performance of an energy detector, in terms of the average missed-detection probability and the average AUC. Sections 7.4 is devoted to the analysis of the optimal detection thresh-

old. Section 7.5 presents numerical and simulation results, followed by concluding remarks in Section 7.6.

7.2 Low-SNR Model

Three signal models, **S1**, **S2** and **S3** which are given in Section 2.4.1, can be considered in the energy detection. For **S1** and **S2** signal models, the distribution of Λ is modeled exactly in Section 2.4.2. Under $\mathcal{H}_0$, the false-alarm probability is with the upper incomplete Gamma function. Under $\mathcal{H}_1$, the detection probabilities are with the Marcum-Q function and with the upper incomplete Gamma function for **S1** and **S2**, respectively. However, none of these functions have closed-form inverse functions, and thus there is no closed-form expression for the detection threshold λ when a false-alarm or detection probability is given even with AWGN channel. This problem becomes more complicated when the fading effect is considered. Although there are rigorous expressions for the average detection performance over some particular fading channels in the literature, such expressions may not help for the parameter optimization (e.g., optimizing detection threshold). Since **S1** and **S2** signal models have different set of expressions, results of one model cannot be derived from those of the other model. Moreover, the distribution of Λ cannot be modeled exactly for **S3**.

To solve all these problems, the CLT approach can be used as a unified approach of accurately approximating the distribution of Λ in the three signal models. Recalling (2.23), the distribution of Λ can be approximated as a normal distribution for sufficiently large N as

$$\Lambda \sim \begin{cases} \mathcal{N}\left(N(2\sigma_w^2), N(2\sigma_w^2)^2\right) & : \mathcal{H}_0 \\ \mathcal{N}\left(N(2\sigma_w^2)(1+\gamma), N(2\sigma_w^2)^2(1+2\gamma)\right) & : \mathcal{H}_1 \text{ with } \textbf{S1} \text{ or } \textbf{S3} \\ \mathcal{N}\left(N(2\sigma_w^2)(1+\gamma), N(2\sigma_w^2)^2(1+\gamma)^2\right) & : \mathcal{H}_1 \text{ with } \textbf{S2}. \end{cases} \tag{7.1}$$

Under the low-SNR assumption (i.e., $\gamma \ll 1$), the signal has little impact on the variance of the test statistic under $\mathcal{H}_1$, as used in the Edell model, Berkeley model and Torrieri model which are well-known Gaussian approximations for the test statistic under $\mathcal{H}_1$ [122, 123]. Thus, (7.1) can be accurately approximated for

any of the three signal models as

$$\Lambda_{\text{low}} \sim \begin{cases} \mathcal{N}\left(N\sigma^2, N\sigma^4\right) & : \mathcal{H}_0 \\ \mathcal{N}\left(N\sigma^2(1+\gamma), N\sigma^4\right) & : \mathcal{H}_1 \end{cases} \tag{7.2}$$

where $\sigma = \sqrt{2}\sigma_w$. The false alarm probability P_f and the missed-detection probability $P_{md}(\gamma)$ can be evaluated as

$$P_f = \frac{1}{2}\text{Erfc}\left(\frac{\lambda - N\sigma^2}{\sqrt{2N}\sigma^2}\right) \tag{7.3}$$

and

$$P_{md}(\gamma) \approx 1 - \frac{1}{2}\text{Erfc}\left(\frac{\lambda - N\sigma^2(1+\gamma)}{\sqrt{2N}\sigma^2}\right), \tag{7.4}$$

respectively, where where $Q(z) = \frac{1}{2}\text{Erfc}\left(\frac{z}{\sqrt{2}}\right)$ and $\text{Erfc}(\cdot)$ is the complementary error function defined as $\text{Erfc}(z) = \frac{2}{\sqrt{\pi}}\int_z^\infty e^{-t^2}\,\mathrm{d}t$ [74]. Since the detection probability, $P_d(\gamma) = 1 - P_{md}(\gamma)$, relates to the cumulative distribution function (CDF) of the test statistic, Fig. 7.1 shows the exact CDF of the test statistic Λ, denoted $F_{\Lambda|\mathcal{H}_1,|\mathbf{h}|}(x)$, with **S1** signal model and its low-SNR approximation for γ=-10 dB, -15 dB, or -20 dB when $\sigma = 1$ and $N = 2 \times 10^3$. The exact CDF (solid line) matches tightly with the approximation (discrete marks) for the simulated x range at γ =-20 dB, while the other two cases also show close matches, confirming the validity of the low-SNR approximation. The accuracy of the approximation is also shown by the ROC curves in Fig. 7.2 (see discussion in Section 7.5).

7.3 Performance Analysis at a Low SNR

The MG channel model introduced in Chapter 4 is considered as a generalized SNR distribution for the derivation of analytical results. The ROC curve, AUC, and the total error rate are used as the performance measures. The ROC curve is a measurement for the sensitivity of a detector used in a binary classifier system [124]. In signal-detection theory, the ROC (or the complementary ROC) curve is a graphical plot of $P_d(\gamma)$ (or $P_{md}(\gamma)$) versus P_f as the discrimination threshold λ varies. The ROC curves of spectrum-sensing detectors have highly non-linear behavior, and they are, in general, convex. In wireless communications, $P_d(\gamma)$ depends on the received instantaneous SNR, which is a function of the mobile radio channel

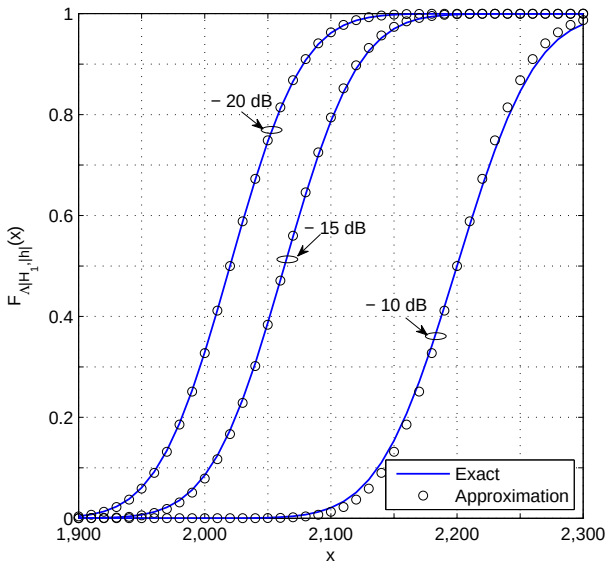

Figure 7.1: The exact and approximated (low-SNR) CDFs of the test statistic which is modeled using the CLT, with $\sigma = 1$ and $N = 2 \times 10^3$. **S1** is considered as an example. The exact CDF is based on (7.1) and approximated CDF is based on (7.2).

gain. Therefore, the average detection probability (or average missed-detection probability) over fading channels is important for plotting the ROC curve, which is discussed in Section 7.3.1. The AUC is the area under the ROC curve, which varies between $\frac{1}{2}$ and 1. It represents the probability that the detector is more likely to choose the correct decision than the incorrect decision. It is a single-valued measure for the overall detection capability of a detector. The average AUC can be derived by averaging instantaneous AUC over the SNR distribution which is discussed in Section 7.3.2. The total error rate, denoted P_e, is the sum of the false alarm and missed-detection probabilities, $P_{md}(\gamma) + P_f$, which both depend on the threshold λ. The total error rate is used in [125] (which is based on the **S1** signal model) as a possible metric for selecting λ. In this chapter, the total error rate is also adopted to select λ, as will be discussed in Section 7.4.

In this section, a unified approach will be developed to evaluate average detection probability and average AUC at the low-SNR region. Diversity combining and cooperative spectrum sensing are also investigated subsequently.

7.3.1 Average Missed-Detection Probability

Over Fading Channels

For fading channels, the average missed-detection probability, $\overline{P_{md}}$, can be calculated by directly averaging $P_{md}(\gamma)$ over the SNR distribution to yield $\overline{P_{md}} = \int_0^\infty P_{md}(x) f_\gamma(x)\,\mathrm{d}x$. Next the MG channel model (4.1) will be used for SNR distributions of many existing fading channels, diversity-combining techniques, and cooperative sensing.

With the aid of (7.4), (4.1), $\mathrm{Erfc}(-x) = 2 - \mathrm{Erfc}(x)$, and some straightforward algebraic manipulations, the average missed-detection probability over the generalized channel model (4.1), $\overline{P_{md}^{\text{Gen}}}$, can be given as

$$\overline{P_{md}^{\text{Gen}}} \approx \frac{1}{2}\sum_{i=1}^{S} \alpha_i \int_0^\infty x^{\beta_i - 1} e^{-\zeta_i x} \mathrm{Erfc}\left(\sqrt{\frac{N}{2}}x + \frac{N\sigma^2 - \lambda}{\sqrt{2N}\sigma^2}\right)\mathrm{d}x.$$

An integral expression, $\mathcal{I}(n, p, a, b)$, which will be used in the later analysis, is defined as [126, eq. (2.8.9.1)]

$$\begin{aligned}\mathcal{I}(n, p, a, b) &\triangleq \int_0^\infty x^n e^{-px} \mathrm{Erfc}(ax + b)\,\mathrm{d}x \\ &= (-1)^n \frac{\partial^n}{\partial p^n}\left[\frac{\mathrm{Erfc}(b) - e^{\frac{p^2 + 4pab}{4a^2}}\mathrm{Erfc}\left(b + \frac{p}{2a}\right)}{p}\right],\end{aligned} \tag{7.5}$$

where n is a positive integer, Re[p]> 0, $a > 0, b > 0$, and $\frac{\partial^n}{\partial p^n}[\cdot]$ is the nth-order partial derivative with respect to p. Therefore, $\overline{P_{md}^{\text{Gen}}}$ can be derived for integer β_i as

$$\overline{P_{md}^{\text{Gen}}} \approx \frac{1}{2}\sum_{i=1}^{S} \alpha_i \mathcal{I}\left(\beta_i - 1, \zeta_i, \sqrt{\frac{N}{2}}, \frac{N\sigma^2 - \lambda}{\sqrt{2N}\sigma^2}\right). \tag{7.6}$$

For example, for a Rayleigh fading channel, the corresponding parameters are $S = 1$, $\alpha_1 = \frac{1}{\bar{\gamma}}$, $\beta_1 = 1$ and $\zeta_1 = \frac{1}{\bar{\gamma}}$. Thus, the average missed-detection probability over the Rayleigh fading channel, $\overline{P_{md}^{\text{Ray}}}$, is

$$\overline{P_{md}^{\text{Ray}}} \approx \frac{1}{2}\left[\mathrm{Erfc}\left(\frac{N\sigma^2 - \lambda}{\sqrt{2N}\sigma^2}\right) - e^{\frac{\frac{1}{\bar{\gamma}^2} + \frac{4}{\bar{\gamma}}\left(\frac{N\sigma^2 - \lambda}{\sqrt{2N}\sigma^2}\right)\sqrt{\frac{N}{2}}}{2N}}\mathrm{Erfc}\left(\frac{N\sigma^2 - \lambda}{\sqrt{2N}\sigma^2} + \frac{1}{\bar{\gamma}\sqrt{2N}}\right)\right]. \tag{7.7}$$

For a Nakagami-m fading channel, the corresponding parameters are $S = 1$, $\alpha_1 = \frac{m^m}{\Gamma(m)\bar{\gamma}^m}$, $\beta_1 = m$ and $\zeta_1 = \frac{m}{\bar{\gamma}}$. Thus, for integer m, the average missed-detection probability over the Nakagami-m fading channel, $\overline{P_{md}^{\text{Nak}}}$, is

$$\overline{P_{md}^{\text{Nak}}} \approx \frac{1}{2\Gamma(m)} \left(\frac{m}{\bar{\gamma}}\right)^m \mathcal{I}\left(m-1, \frac{m}{\bar{\gamma}}, \sqrt{\frac{N}{2}}, \frac{N\sigma^2 - \lambda}{\sqrt{2N}\sigma^2}\right). \tag{7.8}$$

Similarly, the average missed-detection probabilities over many other existing fading channels such as Nakagami-lognormal, K, K_G, η-μ, Nakagami-q (Hoyt), κ-μ, or Nakagami-n (Rician) can be derived easily after properly selecting the parameters S, α_i, β_i, ζ_i ($i = 1, 2, ..., S$) in (4.1).

Diversity Reception

Since the traditional diversity techniques (e.g., MRC) may not work with energy detection because coherent MRC needs channel state information, which increases the system complexity, the SLC technique is considered. The outputs of the square-law devices of L branches are combined to yield a new decision statistic as in (5.23). Note that, if Λ_i is a normal distribution as $\Lambda_i \sim \mathcal{N}(\mu_i, \sigma_i^2)$, Λ_{SLC} is also a normal distribution as $\Lambda_{\text{SLC}} \sim \mathcal{N}\left(\sum_{i=1}^{L} \mu_i, \sum_{i=1}^{L} \sigma_i^2\right)$. Under $\mathcal{H}_0$ and $\mathcal{H}_1$, Λ_i is a normal distribution as in (7.1) with γ replaced by γ_i (the SNR of the ith branch). For SLC with a low SNR, the false alarm probability and the missed-detection probability under AWGN channels can be evaluated as (7.3) and (7.4), respectively, with N replaced by LN. For fading channels, if the PDF of $\gamma = \frac{1}{L}\sum_{i=1}^{L} \gamma_i$ is modeled by using the generalized channel (4.1),[1] with the aid of (7.6), the average missed-detection probability can be derived as

$$\overline{P_{md}^{\text{Gen,SLC}}} \approx \frac{1}{2} \sum_{i=1}^{S} \alpha_i \mathcal{I}\left(\beta_i - 1, \zeta_i, \sqrt{\frac{LN}{2}}, \frac{LN\sigma^2 - \lambda}{\sqrt{2LN}\sigma^2}\right). \tag{7.9}$$

Thus, the average missed-detection probability over a Rayleigh fading channel can be derived by using (7.9) with $S = 1$, $\alpha_1 = \frac{1}{\Gamma(L)}\left(\frac{L}{\bar{\gamma}}\right)^L$, $\beta_1 = L$ and $\zeta_1 = \frac{L}{\bar{\gamma}}$. Similarly, the average missed-detection probability over a Nakagami-m fading channel

[1] As special cases, the PDF of $\gamma = \frac{1}{L}\sum_{i=1}^{L} \gamma_i$ when signals of the branches follow i.i.d. Rayleigh and Nakagami-m fading is $f_\gamma(x) = \frac{1}{\Gamma(L)}\left(\frac{L}{\bar{\gamma}}\right)^L x^{L-1} e^{-\frac{L}{\bar{\gamma}}x}$ and $f_\gamma(x) = \frac{1}{\Gamma(mL)}\left(\frac{mL}{\bar{\gamma}}\right)^{mL} x^{mL-1} e^{-\frac{mL}{\bar{\gamma}}x}$, respectively.

can be derived by using (7.9) with $S = 1$, $\alpha_1 = \frac{1}{\Gamma(mL)} \left(\frac{mL}{\bar{\gamma}}\right)^{mL}$, $\beta_1 = mL$ and $\zeta_1 = \frac{mL}{\bar{\gamma}}$.

If the square-law selection combining technique is applied, the average missed-detection probability can be derived by using the results in [53] and the general expression given in eq. (7.6).

Cooperative Spectrum Sensing

Cooperative spectrum sensing can improve signal detection capability by sharing and combining the information from intermediate cognitive nodes (called cooperative nodes). Because the existing research in the literature focuses on the medium- or high-SNR region [116], the impact of cooperative spectrum sensing at a low SNR has not been clarified. To investigate this case, the decision fusion strategy, in which each cooperative node makes a decision on the primary user activity, is considered and individual 1-bit decisions are reported to a fusion center. If there are K cooperative nodes, and the fusion center uses the k-out-of-K fusion rule (i.e., the fusion center decides on the presence of primary activity if there are k or more cooperative nodes that individually decide on the presence of primary activity), the false alarm probability P_f^{Coop} and detection probability P_d^{Coop} at the fusion center can be written as $P_\chi^{\text{Coop}} = \sum_{i=k}^{K} \binom{K}{i} (p_\chi)^i (1-p_\chi)^{K-i}$, where the notation '$\chi$' means '$f$' or '$d$' for false alarm or detection, respectively. It is assumed that all cooperative nodes have i.i.d. channels from the primary user, and thus, achieve identical false alarm probability p_f and detection probability p_d. Thus, the average missed-detection probability of cooperative spectrum sensing over the generalized channel model is

$$\overline{P_{md}^{\text{Gen,Coop}}} \approx 1 - \sum_{i=k}^{K} \binom{K}{i} \left(\overline{P_{md}^{\text{Gen}}}\right)^i \left(1 - \overline{P_{md}^{\text{Gen}}}\right)^{K-i}, \tag{7.10}$$

with $\overline{P_{md}^{\text{Gen}}}$ given in (7.6). For example, for a Nakagami-m channel, the average missed-detection probability is equal to (7.10) with $\overline{P_{md}^{\text{Gen}}}$ replaced by $\overline{P_{md}^{\text{Nak}}}$ given in (7.8).

7.3.2 Average AUC

A general expression for the area under the curve is derived in the following Theorem 7.1 for the AWGN case.

Theorem 7.1 Two functions which depend on λ $(-\infty < \lambda < \infty)$[2] are defined as $P_f(\lambda) = \frac{1}{2}\text{Erfc}\left(\frac{\lambda - m_0}{\sqrt{2}\sigma_0}\right)$ and $P_d(\lambda) = \frac{1}{2}\text{Erfc}\left(\frac{\lambda - m_1}{\sqrt{2}\sigma_1}\right)$, where m_0, m_1, σ_0, and σ_1 are real positive values such that $m_0 \leq m_1$ and $\sigma_0 \leq \sigma_1$. By eliminating term λ, the two functions can be combined as $P_d = \frac{1}{2}\text{Erfc}\left(\frac{\sigma_0}{\sigma_1}\text{Erfc}^{-1}(2P_f) - \frac{m_1 - m_0}{\sqrt{2}\sigma_1}\right)$, which represents the P_d versus P_f curve. Thus, the area under the P_d versus P_f curve, $\mathcal{A}$, is given as

$$\mathcal{A} = 1 - \frac{1}{2}\text{Erfc}\left(\frac{m_1 - m_0}{\sqrt{2(\sigma_0^2 + \sigma_1^2)}}\right). \tag{7.11}$$

Proof: See Appendix D.1. ■

The instantaneous AUC of an energy detector at a low SNR can be derived from (7.11) by replacing $m_0 = N\sigma^2$, $m_1 = N\sigma^2(1+\gamma)$, $\sigma_0^2 = N\sigma^4$, and $\sigma_1^2 = N\sigma^4$, as $\mathcal{A}(\gamma) \approx 1 - \frac{1}{2}\text{Erfc}\left(\frac{\sqrt{N}}{2}\gamma\right)$. Then the average AUC over the generalized SNR distribution (4.1) is derived as $\overline{\mathcal{A}^{\text{Gen}}} = \int_0^\infty \mathcal{A}(x) f_\gamma(x)\,\mathrm{d}x$, to yield

$$\begin{aligned}\overline{\mathcal{A}^{\text{Gen}}} &\approx 1 - \frac{1}{2}\sum_{i=1}^{S}\alpha_i \int x^{\beta_i - 1} e^{-\zeta_i x}\text{Erfc}\left(\frac{\sqrt{N}}{2}x\right)\mathrm{d}x \\ &= 1 + \frac{1}{2}\sum_{i=1}^{S}(-1)^{\beta_i - 1}\alpha_i \frac{\partial^{\beta_i - 1}}{\partial p^{\beta_i - 1}}\left(\frac{1}{p}e^{\frac{p^2}{N}}\text{Erfc}\left(\frac{p}{\sqrt{N}}\right) - \frac{1}{p}\right)\Bigg|_{p=\zeta_i},\end{aligned} \tag{7.12}$$

where β_i is a positive integer, and the second equality comes after applying [126, eq. (2.8.5.4)]. This approximation can be used for many mobile radio channel models. For example, the average AUC over a Rayleigh fading channel, $\overline{\mathcal{A}^{\text{Ray}}}$, is

$$\overline{\mathcal{A}^{\text{Ray}}} \approx \frac{1}{2} + \frac{e^{\frac{1}{N\bar{\gamma}^2}}}{2}\text{Erfc}\left(\frac{1}{\bar{\gamma}}\sqrt{\frac{1}{N}}\right), \tag{7.13}$$

and the average AUC over a Nakagami-m fading channel, $\overline{\mathcal{A}^{\text{Nak}}}$, is

$$\overline{\mathcal{A}^{\text{Nak}}} \approx 1 + \frac{(-1)^{m-1}m^m}{2\Gamma(m)\bar{\gamma}^m}\frac{\partial^{m-1}}{\partial p^{m-1}}\left(\frac{1}{p}e^{\frac{p^2}{N}}\text{Erfc}\left(\frac{p}{\sqrt{N}}\right) - \frac{1}{p}\right)\Bigg|_{p=\frac{m}{\bar{\gamma}}}, \tag{7.14}$$

[2]This is the theoretical limit of λ, but negative values of threshold are not considered in practice.

where m is an integer.

For the SLC technique, , the average AUC over the generalized channel model is given in (7.12) with N replaced by LN if the PDF of $\gamma = \frac{1}{L}\sum_{i=1}^{L}\gamma_i$ is modeled by using the generalized channel. For example, the average AUC over Rayleigh fading channels can be derived by using (7.12) with $S = 1$, $\alpha_1 = \frac{1}{\Gamma(L)}\left(\frac{L}{\bar{\gamma}}\right)^L$, $\beta_1 = L$, $\zeta_1 = \frac{L}{\bar{\gamma}}$ and with N replaced by LN. Similarly, the average AUC over Nakagami-m fading channels can be derived by using (7.12) with $S = 1$, $\alpha_1 = \frac{1}{\Gamma(mL)}\left(\frac{mL}{\bar{\gamma}}\right)^{mL}$, $\beta_1 = mL$, $\zeta_1 = \frac{mL}{\bar{\gamma}}$ and with N replaced by LN.

For cooperative spectrum sensing, because P_d^{Coop} is difficult to be expressed in terms of P_f^{Coop}, the AUC may not be able to be evaluated even with some numerical methods. Alternatively, a threshold averaging approach which gives the AUC as $\mathcal{A} = -\int_{-\infty}^{\infty} P_d(\lambda)\frac{\partial P_f(\lambda)}{\partial\lambda}\,\mathrm{d}\lambda$ may be used, because the threshold, λ, affects the false alarm, the detection and the missed-detection probabilities, which are hence denoted as $P_f(\lambda)$, $P_d(\lambda)$ and $P_{md}(\lambda)$, respectively. By using the binomial expansion and the fact that $\frac{\partial}{\partial x}\left[\text{Erfc}\left(\frac{x-a}{b}\right)\right] = -\frac{2}{b\sqrt{\pi}}e^{-\frac{(x-a)^2}{b^2}}$, the AUC of cooperative spectrum sensing can be expressed in an integral, which can be evaluated by numerical methods. However, a closed-form expression appears difficult. Note that our analytical approach for the average missed-detection probability and the average AUC can also be applied to other alternative energy detection methods in which the energy detector test statistic is modeled as Gaussian via the CLT.

7.4 Threshold Selection

The traditional way of threshold selection is based on the false alarm probability only. For a given number of samples (N), estimated noise variance (σ^2), and the allowable false alarm probability (P_f), the threshold can thus be obtained by using (7.3) as $\lambda = \left(\sqrt{2}\text{Erfc}^{-1}(2P_f) + \sqrt{N}\right)\sqrt{N}\sigma^2$. Unfortunately, this threshold selection method is not suitable for cognitive radio networks where it is essential to keep a low missed-detection probability such that primary users are protected from interference. While threshold selection with different objective functions (by relaxing some constraints) has been performed in [67, 127] and among others, these

papers focus on non-fading scenarios because the optimal threshold is analytically intractable over fading channels. Moreover, the average missed-detection probability over fading channels has not been available for the low SNR model in (7.2). Therefore, threshold selection that takes missed-detection probability into account for the low SNR model over fading channels has not been studied previously, and is the focus of this section.

For a cognitive radio network, $P_{md}(\lambda)$ is required to be no more than a threshold denoted P_{md}^{th} (e.g., $P_{md}(\lambda) \leq 0.1$ is required in the IEEE 802.22). This requirement is equivalent to $\lambda \leq \lambda_{md}^*$ where $P_{md}(\lambda_{md}^*) = P_{md}^{\text{th}}$, since $P_{md}(\lambda)$ increases with threshold λ. In addition, it may be required that $P_f(\lambda)$ is no more than a threshold P_f^{th} (e.g., $P_f(\lambda) \leq 0.1$ is required in the IEEE 802.22) such that the spectrum opportunities are efficiently utilized. This requirement is equivalent to $\lambda \geq \lambda_f^*$ where $P_f(\lambda_f^*) = P_f^{\text{th}}$, since $P_f(\lambda)$ decreases with threshold λ.[3]

If $\lambda_f^* > \lambda_{md}^*$, then there is no feasible λ that satisfies both requirements on false alarm and missed-detection probabilities, which means other actions need to be taken, such as increasing the sampling rate of the received signal. If $\lambda_f^* \leq \lambda_{md}^*$, this means any λ value within range $[\lambda_f^*, \lambda_{md}^*]$ can satisfy both requirements on false alarm and missed-detection probabilities. To select a value in the range $[\lambda_f^*, \lambda_{md}^*]$, a combination metric of both $P_f(\lambda)$ and $P_{md}(\lambda)$ can be considered. For this purpose, the Bayesian cost [128], which is a popular metric to select the detection threshold in the literature [125, 129–131], can be used. If no cost is associated with correct decisions on $\mathcal{H}_0$ and $\mathcal{H}_1$, the Bayesian cost function can be given as

$$\mathcal{R}(\lambda) = C_{01} P_0 P_f(\lambda) + C_{10} P_1 P_{md}(\lambda),$$

where C_{01} and C_{10} are cost associated with false alarm and missed-detection, respectively, and P_0 and P_1 are probabilities of $\mathcal{H}_0$ and $\mathcal{H}_1$, respectively. Since it may not be reasonable for secondary users to know P_0 and P_1 in advance, it can be set $P_0 = P_1$, and also set $C_{01} = C_{10}$. Then minimizing the Bayesian cost is equivalent to minimizing the total error rate $P_e(\lambda) \stackrel{\triangle}{=} P_f(\lambda) + P_{md}(\lambda)$.[4] Therefore, the

[3]Note that if $P_f^{\text{th}} = 1$, it is equivalent to the case with no requirement on false alarm probability, which means $\lambda_f^* = 0$.

[4]Please note that, if the secondary users know P_0 and P_1, and/or $C_{01} \neq C_{10}$, our method for the

threshold selection problem is formulated as

$$\begin{aligned} \underset{\lambda}{\text{minimize}} \quad & P_e(\lambda) = P_f(\lambda) + P_{md}(\lambda) \\ \text{subject to} \quad & P_f(\lambda) \leq P_f^{\text{th}} \\ & P_{md}(\lambda) \leq P_{md}^{\text{th}}. \end{aligned} \tag{7.15}$$

In the optimization problem in (7.15), if the two constraints are relaxed, denote the optimal solution as λ_e^*. Then the optimal solution for problem (7.15), denoted λ^*, is given as

- $\lambda^* = \lambda_e^*$ if $\lambda_f^* \leq \lambda_{md}^*$ and $\lambda_e^* \in [\lambda_f^*, \lambda_{md}^*]$;
- $\lambda^* = \lambda_f^*$ or λ_{md}^*, whichever is closer to λ_e^*, if $\lambda_f^* \leq \lambda_{md}^*$ and $\lambda_e^* \notin [\lambda_f^*, \lambda_{md}^*]$;
- λ^* has no solution if $\lambda_f^* > \lambda_{md}^*$.

Since $P_f(\lambda)$ does not depend on fading effect, λ_f^* can be derived for any fading scenario by using (7.3) as

$$\lambda_f^* = \left(\sqrt{\frac{2}{N}} \text{Erfc}^{-1}\left(2P_f^{\text{th}}\right) + 1 \right) N\sigma^2. \tag{7.16}$$

In the following, exact λ_{md}^* and λ_e^* for AWGN channels and approximated λ_{md}^* and λ_e^* are derived for Rayleigh fading channels.

AWGN Channel

For an AWGN channel, the general case for test statistic Λ in (2.23) is considered. For **S1** or **S3** signal model with any SNR value γ, λ_{md}^* can be derived by using (2.23) as

$$\lambda_{md}^* = \left(\sqrt{\frac{2(1+2\gamma)}{N}} \text{Erfc}^{-1}\left(2(1-P_{md}^{\text{th}})\right) + (1+\gamma) \right) N\sigma^2, \tag{7.17}$$

and λ_e^* is given by using (2.23) as

$$\begin{aligned} \lambda_e^* &= \arg\min_{\lambda} \left(1 + \frac{1}{2}\text{Erfc}\left(\frac{\lambda - N\sigma^2}{\sqrt{2N}\sigma^2} \right) - \frac{1}{2}\text{Erfc}\left(\frac{\lambda - N\sigma^2(1+\gamma)}{\sqrt{2N(1+2\gamma)}\sigma^2} \right) \right) \\ &= \frac{N\sigma^2}{2} \left(1 + \sqrt{1 + 2\gamma \left(1 + \frac{(1+2\gamma)\ln(1+2\gamma)}{N\gamma^2} \right)} \right) \end{aligned} \tag{7.18}$$

optimal threshold selection also works, which minimizes the corresponding Bayesian cost subject to bounded false alarm and missed-detection probabilities.

where the second equality comes as explained in Appendix D.2. Similarly, λ_{md}^* and λ_e^* for **S2** signal model can be derived as

$$\begin{aligned}\lambda_{md}^* &= \left(\sqrt{\frac{2}{N}}(1+\gamma)\text{Erfc}^{-1}\left(2(1-P_{md}^{\text{th}})\right)+(1+\gamma)\right)N\sigma^2,\\ \lambda_e^* &= \frac{N\sigma^2}{2}\left(1+\sqrt{1+\frac{2(2+\gamma)\ln(1+\gamma)}{N\gamma}}\right)\left(\frac{1+\gamma}{1+\frac{\gamma}{2}}\right).\end{aligned} \tag{7.19}$$

Rayleigh Fading Channel

For a Rayleigh fading channel with low-SNR value, the exact λ_{md}^* and λ_e^* are difficult to be derived due to the non-linearity of $P_{md}(\lambda) = \overline{P_{md}^{\text{Ray}}}(\lambda)$ and $P_e(\lambda) = P_f(\lambda) + \overline{P_{md}^{\text{Ray}}}(\lambda)$, respectively, where $\overline{P_{md}^{\text{Ray}}}(\lambda)$ is given in (7.7). They can be calculated numerically by using mathematical software packages (e.g., MATHEMATICA and MATLAB). Here approximations for λ_{md}^* and λ_e^* are derived.

Defining $\alpha \stackrel{\triangle}{=} \frac{N\sigma^2-\lambda}{N\sigma^2\gamma}$ and $a \stackrel{\triangle}{=} \frac{1}{\sqrt{2N\gamma}}$, (7.7) can be written as

$$\overline{P_{md}^{\text{Ray}}}(\lambda) \approx \frac{1}{2}\Big[\text{Erfc}\,(\alpha) - e^{a^2}e^{2a\alpha}\text{Erfc}\,(a+\alpha)\Big]. \tag{7.20}$$

Over an AWGN channel at low SNR, it can be observed from (7.18) that, at a low SNR (i.e., $\gamma \ll 1, 1+2\gamma \approx 1$) and a large N (note that reliable detection is possible at a large N), λ_e^* can roughly be approximated as $\lambda_e^* \approx \frac{N\sigma^2}{2}\left(1+\sqrt{1+2\gamma}\,\right)$.[5] This rough information is used to find approximated λ_{md}^* and λ_e^* for Rayleigh fading. By using the Taylor series expansions of the $\text{Erfc}(x)$ and $e^{2ax}\text{Erfc}(a+x)$ at zero where

$$\text{Erfc}(x) = 1 - \frac{2x}{\sqrt{\pi}} + \frac{2x^3}{3\sqrt{\pi}} + \mathcal{O}(x^4)$$

and

$$\begin{aligned}e^{2ax}\text{Erfc}(a+x) =& \text{Erfc}(a) + \left(2a\text{Erfc}(a) - \frac{2e^{-a^2}}{\sqrt{\pi}}\right)x\\ &+ \left(2a^2\text{Erfc}(a) - \frac{2ae^{-a^2}}{\sqrt{\pi}}\right)x^2 + \mathcal{O}(x^3),\end{aligned}$$

[5]Here we consider **S1** or **S3** signal model, as **S2** signal model can be treated similarly.

$\overline{P_{md}^{\text{Ray}}}(\lambda)$ can be expanded when $\alpha \to 0$ as

$$\begin{aligned}\overline{P_{md}^{\text{Ray}}}(\lambda) \approx & \frac{1}{2}\left(1 - e^{a^2}\text{Erfc}(a)\right) - ae^{a^2}\text{Erfc}(a)\alpha \\ & + \left(\frac{a}{\sqrt{\pi}} - a^2 e^{a^2}\text{Erfc}(a)\right)\alpha^2 + \mathcal{O}(\alpha^3).\end{aligned} \tag{7.21}$$

Setting $\overline{P_{md}^{\text{Ray}}}(\lambda_{md}^*) = P_{md}^{\text{th}}$, λ_{md}^* can be calculated as

$$\lambda_{md}^* \approx \left(1 - \sqrt{\frac{2}{N}}\alpha^*\right) N\sigma^2 \tag{7.22}$$

where $\alpha^* = \frac{\left(A - \pi^{1/4}\sqrt{\left(4P_{md}^{\text{th}}a - 2a - \frac{A}{\sqrt{\pi}}\left(2a(2P_{md}^{\text{th}} - 1)\sqrt{\pi} + A - 2\right)\right)}\right)}{2a(1-A)}$ and $A = \sqrt{\pi}ae^{a^2}\text{Erfc}(a)$.

The total error rate is $P_e(\lambda) = P_f(\lambda) + \overline{P_{md}^{\text{Ray}}}(\lambda)$. For $\frac{\partial P_e(\lambda)}{\partial \lambda} = 0$, with the aid of (7.3) and (7.7), it can be written

$$\begin{aligned}\frac{\partial P_e(\lambda)}{\partial \lambda} &= \frac{e^{\frac{1}{2N\bar{\gamma}^2} - \frac{\lambda - N\sigma^2}{N\sigma^2\bar{\gamma}}}\text{Erfc}\left(\frac{1}{\sqrt{2N}\bar{\gamma}} - \frac{\lambda - N\sigma^2}{\sqrt{2N}\sigma^2}\right)}{2N\sigma^2\bar{\gamma}} - \frac{e^{-\frac{(\lambda - N\sigma^2)^2}{2N\sigma^4}}}{\sqrt{2\pi N}\sigma^2} = 0 \\ &\iff e^{\left(\frac{1}{\sqrt{2N}\bar{\gamma}} - \frac{\lambda - N\sigma^2}{\sqrt{2N}\sigma^2}\right)^2}\text{Erfc}\left(\frac{1}{\sqrt{2N}\bar{\gamma}} - \frac{\lambda - N\sigma^2}{\sqrt{2N}\sigma^2}\right) = \sqrt{\frac{2N}{\pi}}\bar{\gamma}.\end{aligned} \tag{7.23}$$

The argument of the exponential function and the complementary error function $\text{Erfc}(\cdot)$ in the second line of (7.23), denoted as $x = \left(\frac{1}{\sqrt{2N}\bar{\gamma}} - \frac{\lambda - N\sigma^2}{\sqrt{2N}\sigma^2}\right)$, becomes very small when N is large.[6] Therefore, the Taylor series expansions of these two functions are considered at zero, which are $e^{x^2} = 1 + x^2 + \frac{x^4}{2} + \mathcal{O}(x^6)$ and $\text{Erfc}(x) = 1 - \frac{2x}{\sqrt{\pi}} + \frac{2x^3}{3\sqrt{\pi}} + \mathcal{O}(x^5)$ when $x \to 0$. Define function

$$g(x) \triangleq e^{x^2}\text{Erfc}(x) = 1 - \frac{2x}{\sqrt{\pi}} + x^2 - \frac{4x^3}{3\sqrt{\pi}} + \frac{x^4}{2} - \frac{8x^5}{15\sqrt{\pi}} + \mathcal{O}(x^6). \tag{7.24}$$

Now $g(x) = c$ is to be solved where $c = \sqrt{\frac{2N}{\pi}}\bar{\gamma}$ as in (7.23). If the first two terms of (7.24) are considered, we have $x \approx \frac{\sqrt{\pi}}{2}(1 - c)$, which leads to

$$\lambda_e^* \approx \frac{2}{\sqrt{\pi}}\left(1 + \bar{\gamma} + \frac{1}{N\bar{\gamma}} - \sqrt{\frac{\pi}{2N}}\right) N\sigma^2.$$

[6] On the other hand, if N is small, the argument of the exponential function and the complementary error function $\text{Erfc}(\cdot)$ in the second line of (7.23) may approach to a large value. Therefore, the Taylor series expansion of $\text{Erfc}(x)$ around infinity can be considered, given as $\text{Erfc}(x) = e^{-x^2}\left(\frac{1}{\sqrt{\pi}x} - \frac{1}{2\sqrt{\pi}x^3} + \frac{3}{4\sqrt{\pi}x^5} + \mathcal{O}\left(\frac{1}{x^6}\right)\right)$ when $x \to \infty$. Thus it can be written $g(x) = e^{x^2}\text{Erfc}(x) = \frac{1}{\sqrt{\pi}x} - \frac{1}{2\sqrt{\pi}x^3} + \frac{3}{4\sqrt{\pi}x^5} + \mathcal{O}\left(\frac{1}{x^6}\right)$. Similar to the case with large N, a more accurate approximation for λ_e^* can be found by keeping increasing the number of terms of $g(x)$.

If the first three terms of (7.24) are considered, we have $x \approx \frac{1\pm\sqrt{1+(c-1)\pi}}{\sqrt{\pi}}$. Since $\lambda_e^* \geq 0$ and $\frac{\partial^2 P_e(\lambda)}{\partial \lambda^2}|_{\lambda_e^*} > 0$, P_e has a minimum at λ_e^*, and thus λ_e^* can be selected as

$$\lambda_e^* \approx \left(1 + \frac{1}{N\bar{\gamma}} - \sqrt{\frac{2}{N\pi}} + \sqrt{\frac{2}{N}\left(\frac{1}{\pi} + \sqrt{\frac{2N}{\pi}}\bar{\gamma} - 1\right)}\right) N\sigma^2. \tag{7.25}$$

Similarly, if the first four terms of (7.24) are considered, an analytical approximation for λ_e^* can be found by solving a quadratic equation. By keeping increasing the number of terms of (7.24), a more accurate approximation for λ_e^* can be found. λ_e^* in (7.25) is used in the subsequent discussion.

Nakagami-m Fading Channel

Derivation of λ_{md}^* and λ_e^* for a Nakagami-m fading channel is also analytically complicated as $\overline{P_{md}^{\text{Nak}}}(\lambda)$ and $P_e(\lambda) = P_f(\lambda) + \overline{P_{md}^{\text{Nak}}}(\lambda)$ have highly non-linear behavior. However, λ_{md}^* and λ_e^* can be calculated numerically. Some examples are given in Table 7.2 in Section 7.5. Since the Nakagami-m fading channel (when $1 < m < \infty$) varies between the Rayleigh fading channel ($m = 1$) and the Gaussian channel (no fading), it can also be claimed that, for Nakagami-m fading, λ_{md}^* is in between values given in (7.17) and (7.22), and λ_e^* is in between values given in (7.18) and (7.25).

Diversity or Cooperative Spectrum Sensing

If SLC is used, the results in (7.16)-(7.19) can be applied with N replaced by LN for SLC over AWGN in which $\gamma = \frac{1}{L}\sum_{i=1}^{L}\gamma_i$, and numerical methods can be used for other fading channels by using (7.9). Similarly, if cooperative sensing is used, the optimal threshold can be determined by numerical methods by using (7.10).

As shown in [66], the high-diversity advantage of cooperative systems results in improved detection capability and communication reliability. Cooperative sensing systems need mutually orthogonal reporting channels to avoid the inter-channel interference and data collision at the fusion center. Orthogonal channels are realized either by using frequency division or time division multiple access techniques. As frequency division requires a larger frequency bandwidth, it is not an effective solution for the spectrum scarcity problem. In time division, each reporting channel

requires a time slot with duration τ_r. By neglecting other processing delays at the cooperative nodes and the fusion center, the number of cooperative nodes that can participate in the cooperation is $K \leq \left(\tau - \frac{N}{f_s}\right) \frac{1}{\tau_r}$, where τ is the allowable sensing time and f_s is the sampling rate. Therefore, K is limited by the sensing time.

7.5 Numerical/Simulation Results and Discussion

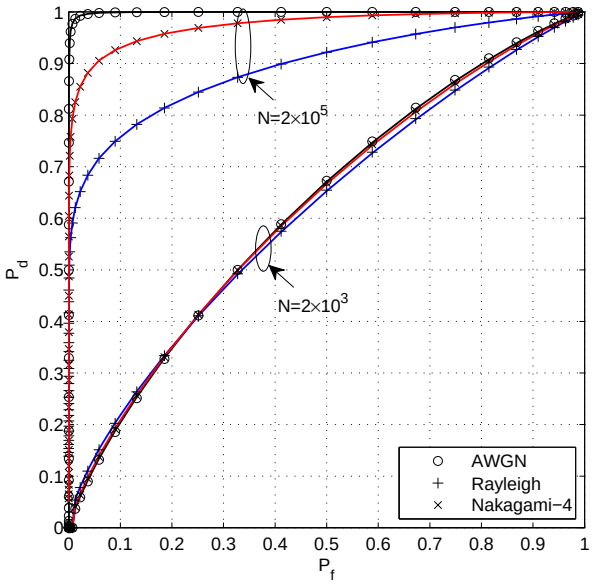

Figure 7.2: Approximated (low-SNR analysis) ROC curves (represented by solid lines) and simulated ROC curves (represented by discrete marks) of AWGN, Rayleigh and Nakagami-4 fading channels for $N = 2 \times 10^3$ and $N = 2 \times 10^5$ at -20 dB average SNR.

This section provides numerical results based on our analysis in Sections 7.3 and 7.4, and semi-analytical Monte-Carlo simulation results based on the system model in Section 7.2. Recalling that the receive SNR under the three signal models **S1**, **S2**, and **S3**are approximately equal, only the **S1** signal model is used for numerical and simulation results in this section.

The *normalized threshold* is defined as $\hat{\lambda} \triangleq \frac{\lambda}{N}$.[7] The noise variance is set to $\sigma^2 = 1$. For SLC diversity technique and cooperative spectrum-sensing, only Ray-

[7]This is the threshold if the decision statistic is selected as $\Lambda = \frac{1}{N} \sum_{n=1}^{N} |\mathbf{y}(n)|^2$.

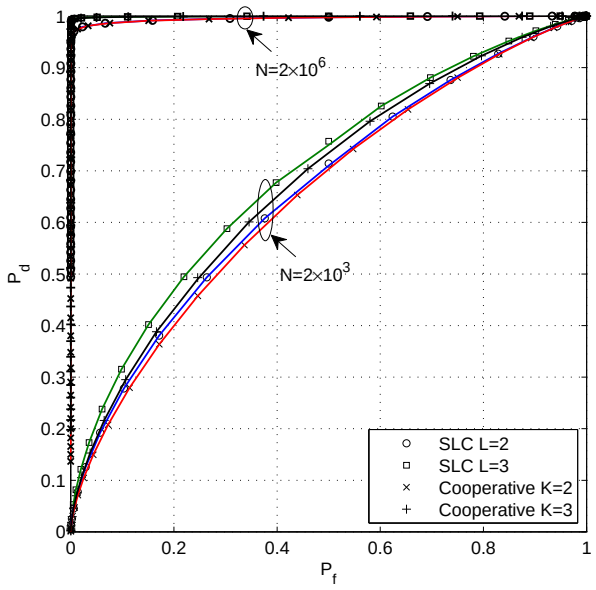

Figure 7.3: Approximated (low-SNR analysis) ROC curves (represented by solid lines) and simulated ROC curves (represented by discrete marks) of SLC when $L = 2, 3$ and cooperative spectrum sensing when $K = 2, 3$ for $N = 2 \times 10^3$ and $N = 2 \times 10^6$ over Rayleigh fading at -20 dB average SNR.

leigh fading channels are considered. The Rayleigh fading case provides a worst-case benchmark because performance loss in Rayleigh fading channel is much higher than those of AWGN and Nakagami-m ($m > 1$) fading channels.

One of the main contributions of this research is to derive analytical approximations for the average missed-detection probability in a low-SNR region. The analytical results can be used to plot ROC curves. Fig. 7.2 and Fig. 7.3 show the ROC curves calculated based on the analytically derived approximations given in (7.4), (7.7)-(7.10), and the simulated ROC curves. Specifically, Fig. 7.2 shows the ROC curves for three fading scenarios: the AWGN, Rayleigh and Nakagami-4 fading channels with -20 dB average SNR. The ROC curves are plotted in the range $\hat{\lambda} \in [0.95, 1.05]$ and $\hat{\lambda} \in [0.995, 1.02]$ for $N = 2 \times 10^3$ and $N = 2 \times 10^5$, respectively. Fig. 7.3 shows the ROC curves of the SLC diversity technique with $L = 2, 3$ and cooperative spectrum-sensing network (with *OR* decision fusion rule) with $K = 2, 3$ over Rayleigh fading at $\bar{\gamma}$= -20 dB when N takes two values: when $N = 2 \times 10^3$, the ROC curves are plotted in the range $\hat{\lambda} \in [1.92, 2.10]$

and $\hat{\lambda} \in [2.94, 3.10]$ for SLC with $L = 2$ and 3, respectively, and in the range $\hat{\lambda} \in [0.95, 1.1]$ for cooperative spectrum sensing; when $N = 2 \times 10^6$, the ROC curves are plotted in the range $\hat{\lambda} \in [2.00, 2.02]$ and $\hat{\lambda} \in [3.00, 3.03]$ for SLC with $L = 2$ and 3, respectively, and in the range $\hat{\lambda} \in [0.99, 1.03]$ for cooperative spectrum sensing. The analytical results perfectly match the simulation results for a high and low number of samples, and also for high and low P_d and P_f, confirming the accuracy of our low-SNR approximations in (7.4), (7.7)-(7.10). From the two figures, it can be seen that, when $N = 2 \times 10^3$, the IEEE 802.22 requirements on false alarm and missed-detection probabilities cannot be satisfied simultaneously in any case in the two figures; when $N = 2 \times 10^5$, the requirements can be satisfied simultaneously for all cases in Fig. 7.2 except Rayleigh fading case; when $N = 2 \times 10^6$, the requirements can be satisfied simultaneously for all cases in Fig. 7.3. The two figures clearly show that a larger N improves detection performance. Moreover, the detection capability is significantly increased with L and K due to the effect of diversity advantage.

Another contribution of this research is to derive approximations for the average low-SNR AUC. For example, in Fig. 7.2, the three ROC curves with $N = 2 \times 10^3$ intersect each other, making it difficult to compare the overall detection performance among the three fading scenarios. In such a case, the AUC, a single-valued measurement, is a better comparative performance metric. By using the approximations given in Section 7.3.2, the average AUCs with different fading channels and with SLC diversity combining are calculated and included in Table 7.1. In this table, the numbers in brackets are area under the simulated curves in Fig. 7.2 and Fig. 7.3. It can be seen that our approximations for AUC are accurate. As expected, AUC of energy detection over AWGN channel and that over Rayleigh fading channel vary from the largest to the smallest. With SLC, a larger number of branches leads to a higher AUC and provides better overall detection capability. Obviously, a larger number of samples also leads to a higher AUC confirming a better overall detection capability.

The next contribution of this research is that the optimal threshold, λ^*, is determined by minimizing the total error rate, $P_e(\lambda) = P_f(\lambda) + \overline{P_{\text{md}}}(\lambda)$ under con-

Fig. 7.2	$N = 2 \times 10^3$	$N = 2 \times 10^5$	Fig. 7.3	$N = 2 \times 10^3$	$N = 2 \times 10^6$
AWGN	0.624085 (0.623489)	0.999217 (0.999174)	SLC $L = 2$	0.663636 (0.662751)	0.995683 (0.995679)
Nakagami-4	0.622408 (0.62172)	0.974777 (0.97462)	SLC $L = 3$	0.698242 (0.697292)	0.999455 (0.999455)
Rayleigh	0.616163 (0.615361)	0.895188 (0.895034)			

Table 7.1: AUC approximations (the numbers in front of the brackets) versus the area under the simulated curves (the numbers in the brackets) for AWGN, Rayleigh, Nakagami-4 channels in Fig. 7.2 and SLC ($L = 2, 3$) in Fig. 7.3.

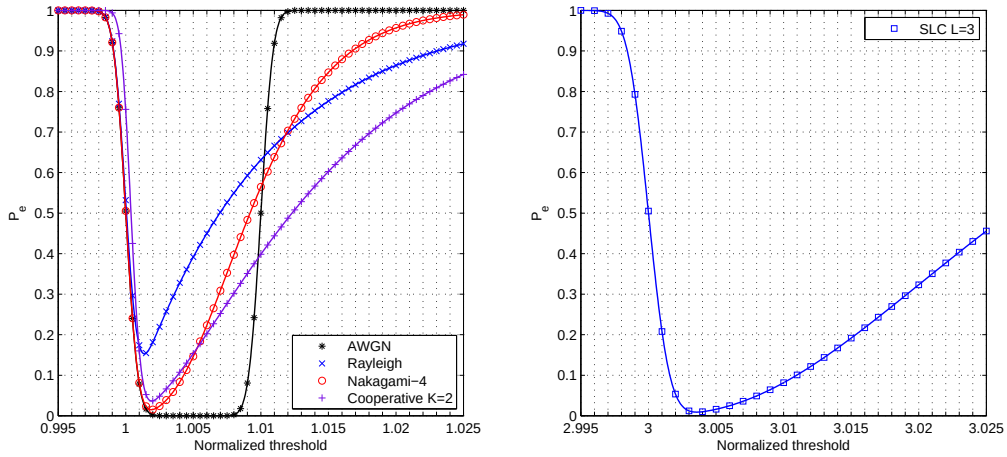

(a) (b)

Figure 7.4: Approximated total error rate (represented by solid lines) and simulated total error rate (represented by discrete marks) versus normalized threshold of (a) AWGN, Rayleigh and Nakagami-4 channels and cooperative spectrum sensing ($K = 2$) over Rayleigh fading; (b) SLC ($L = 3$) over Rayleigh fading, for $N = 2 \times 10^6$ at -20 dB average SNR.

straints $P_f(\lambda) \leq P_f^{\text{th}}, \overline{P_{\text{md}}(\lambda)} \leq P_{\text{md}}^{\text{th}}$. We denote $P_e^* = P_e(\lambda^*)$, $P_f^* = P_f(\lambda^*)$, and $P_{\text{md}}^* = \overline{P_{\text{md}}}(\lambda^*)$. When $\bar{\gamma}$= -20 dB and $N = 2 \times 10^6$, Fig. 7.4a and Fig. 7.4b show low-SNR approximated total error rates (analytical results represented by solid lines, where the average missed-detection probability is calculated based on our analysis in Section 7.3.1) and simulated total error rates (represented by discrete marks) versus the normalized threshold for the AWGN, Rayleigh, Nakagami-4 fading channels, cooperative spectrum sensing ($K = 2$), and SLC diversity combining ($L = 3$). Since the analytical results perfectly match the simulation results in Fig. 7.4, Table 7.2 shows only the numerically calculated normalized threshold values ($\hat{\lambda}_f^*$, $\hat{\lambda}_{\text{md}}^*$, $\hat{\lambda}_e^*$, $\hat{\lambda}^*$), and numerically calculated false alarm probability, missed-detection probability, and total error rate at $\hat{\lambda}_e^*$. In Table 7.2, the numbers

	AWGN	Rayleigh	Nakagami-4	SLC $L=3$ over Rayleigh	Cooperative $K=2$ over Rayleigh
$\hat{\lambda}_f^*$	1.00091	1.00091	1.00091	3.00157	1.00116
$\hat{\lambda}_{md}^*$	1.00908	1.00106 (1.0010)	1.00429	3.01096	1.00383
$\hat{\lambda}_e^*$	1.00498	1.00138 (1.0027)	1.00190	3.00357	1.00192
$P_f(\hat{\lambda}_e^*)$	9.90×10^{-13}	0.02	0.004	0.002	0.007
$P_{md}(\hat{\lambda}_e^*)$	9.90×10^{-13}	0.13	0.011	0.007	0.030
$P_e(\hat{\lambda}_e^*)$	1.98×10^{-12}	0.15	0.015	0.009	0.037
$\hat{\lambda}^*$	$\hat{\lambda}_e^*$	$\hat{\lambda}_{md}^*$	$\hat{\lambda}_e^*$	$\hat{\lambda}_e^*$	$\hat{\lambda}_e^*$

Table 7.2: Numerically calculated normalized threshold values ($\hat{\lambda}_f^*$, $\hat{\lambda}_{md}^*$, $\hat{\lambda}_e^*$, $\hat{\lambda}^*$) and numerically calculated error probabilities (P_f, P_{md}, P_e) at $\hat{\lambda}_e^*$ for AWGN, Rayleigh and Nakagami-4 channels, SLC, and cooperative spectrum sensing when $N = 2 \times 10^6$ and $\bar{\gamma} = -20$ dB. The numbers in brackets are approximated $\hat{\lambda}_{\text{md}}^*$ and $\hat{\lambda}_e^*$ for Rayleigh fading channels based on (7.22) and (7.25).

in brackets are approximated $\hat{\lambda}_{\text{md}}^*$ and $\hat{\lambda}_e^*$ for Rayleigh fading channels based on (7.22) and (7.25).[8] From Table 7.2, we have $\hat{\lambda}_f^* < \hat{\lambda}_e^* < \hat{\lambda}_{\text{md}}^*$ for AWGN channel, Nakagami-4 channel, SLC diversity combining, and cooperative sensing, and thus, $\hat{\lambda}^* = \hat{\lambda}_e^*$. However, for Rayleigh channel, $\hat{\lambda}_f^* < \hat{\lambda}_{\text{md}}^* < \hat{\lambda}_e^*$, and thus, $\hat{\lambda}^* = \hat{\lambda}_{\text{md}}^*$.

In the rest of this section, the IEEE 802.22 requirements for spectrum sensing are focused on by using standard parameter values. The IEEE 802.22 requirements specify that $P_f \leq 0.1$ and $\overline{P_{md}} \leq 0.1$, and that the channel sensing time $\tau \leq 2$ seconds for any detection technique. Since $N \approx \tau f_s$ where f_s is the sampling rate, which may depend on the sampling frequency of the ADC and the fast Fourier transform bin resolution, N cannot be increased beyond τf_s. In an experimental energy detection implementation [57], f_s is selected as $f_s = 62.5$ kHz which may be a typical test-bed bin resolution for moderate or high SNR. However, f_s can take several mega-hertz in other typical system implementations, e.g., some advanced ADCs can operate at $f_s = 20$ MHz [132], 500 MHz [133], which may benefit low-SNR sensing. In this chapter, we limit $f_s = 1$ MHz, and thus the maximal value of N is 2×10^6 for 2 seconds of sensing time.[9]

Fig. 7.5 and Fig. 7.6 show analytical error rates (represented by lines) and sim-

[8] For AWGN channels, there is exact analytical solution for $\hat{\lambda}_{\text{md}}^*$ and $\hat{\lambda}_e^*$ as given in (7.17) and (7.18). For Nakagami-m channels and for SLC or cooperative sensing over fading channels, there are no analytical results for $\hat{\lambda}_{\text{md}}^*$ and $\hat{\lambda}_e^*$.

[9] As only sensing but not the subsequent processing is considered, 2 seconds is used as a reference sensing time. For a fixed N, sensing time can be proportionally reduced by using a higher sampling rate, e.g., there are 2×10^6 samples within 10 milliseconds at $f_s = 200$ MHz as in [134].

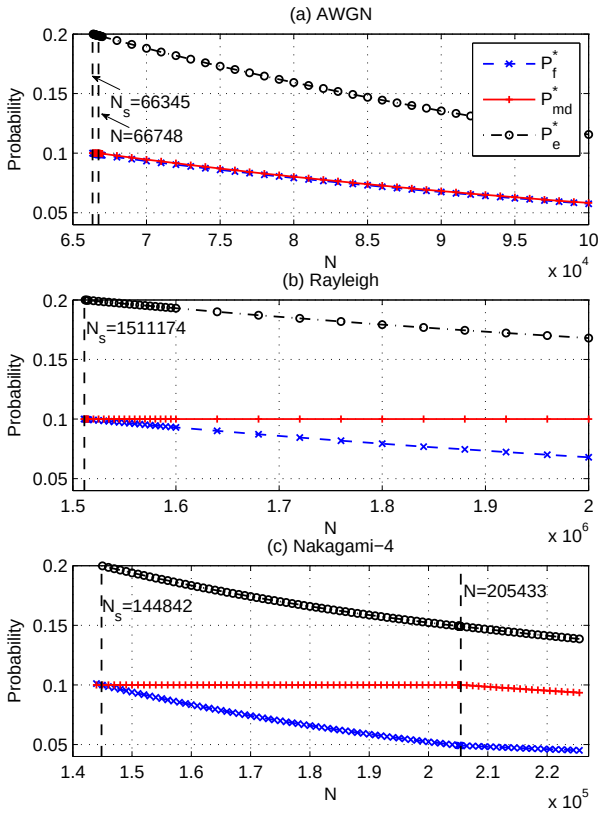

Figure 7.5: Analytical error rates (represented by lines) and simulated error rates (represented by discrete marks) at the optimal threshold value (total error: P_e^*; false alarm: P_f^*; and missed-detection: P_{md}^*) versus the number, N, of samples at -20 dB average SNR for (a) AWGN; (b) Rayleigh; (c) Nakagami-4 fading channels.

ulated error rates (represented by discrete marks) at the optimal threshold ($P_f^* = P_f(\lambda^*)$, $P_{md}^* = P_{md}(\lambda^*)$, and $P_e^* = P_e(\lambda^*)$) versus N for fading channels (AWGN, Rayleigh and Nakagami-4), diversity technique (SLC) and cooperative spectrum sensing with -20 dB average SNR. The optimal threshold, λ^*, is calculated based on low-SNR analysis in Section 7.4. Recall that an optimal threshold can be found only when $\lambda_f^* \leq \lambda_{md}^*$, which is equivalent to $N \geq N_s$ where N_s is the minimum number of samples to have a feasible detection threshold that satisfies both requirements on false alarm and missed-detection probabilities. Under this condition, there may be three possible cases such as (i) $\lambda_f^* \leq \lambda_{md}^* \leq \lambda_e^*$; (ii) $\lambda_f^* \leq \lambda_e^* \leq \lambda_{md}^*$; or (iii) $\lambda_e^* \leq \lambda_f^* \leq \lambda_{md}^*$. As examples given in Fig. 7.5 and Fig. 7.6, we do not have the third case.

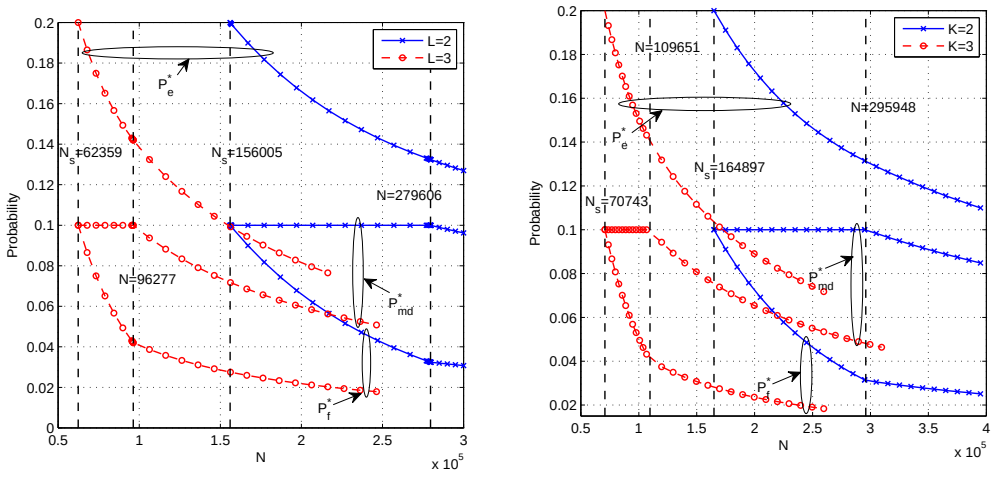

(a) (b)

Figure 7.6: Analytical error rates (represented by lines) and simulated error rates (represented by discrete marks) at the optimal threshold value (total error: P_e^*; false alarm: P_f^*; and missed-detection: P_{md}^*) versus the number, N, of samples at -20 dB average SNR for (a) SLC when $L = 2, 3$; (b) cooperative spectrum sensing when $K = 2, 3$, over Rayleigh fading.

Based on our analytical results in Fig. 7.5 and Fig. 7.6,[10] the regions of N for different possible cases are shown in Table 7.3. Table 7.3 also includes the minimal sensing time to have a feasible detection threshold when $f_s = 1$ MHz, given as $\tau_{\min} = \frac{N_s}{1 \text{ MHz}}$, and the minimal sampling rate to have a feasible detection threshold when the sensing time is 2 seconds, given as $f_{s,\min} = \frac{N_s}{2 \text{ sec}}$. Two cases are used in Fig. 7.5: AWGN and Rayleigh fading cases, as examples. For the AWGN channel, there is no feasible detection threshold when $N < N_s = 66345$. When $N \in [66345, 66747]$, we have $\lambda_f^* \leq \lambda_{md}^* \leq \lambda_e^*$, the optimal threshold is determined by the missed-detection probability requirement, and thus, in this region of N, P_{md}^* keeps at 0.1. When $N \geq 66748$, we have $\lambda_f^* \leq \lambda_e^* \leq \lambda_{md}^*$, and the optimal threshold is determined by minimizing the total error rate. For Rayleigh fading channel, there is no feasible detection threshold when $N < N_s = 1511174$. When N varies from N_s to 2×10^6 (the maximal number of samples when $f_s = 1$ MHz and sensing time $\tau = 2$ seconds), we have $\lambda_f^* \leq \lambda_{md}^* \leq \lambda_e^*$, and the optimal threshold is determined

[10] Since analytical and simulation results in Fig. 7.5 and Fig. 7.6 perfectly match, only the analytical results are used to generate Table 7.3.

by the missed-detection probability requirement, and thus, P^*_{md} keeps at 0.1 in this region of N.

	N				$\tau_{\min}$ (sec)	$f_{s,\min}$ (kHz)
	$\lambda^*_f > \lambda^*_{md}$	$\lambda^*_f \le \lambda^*_{md} \le \lambda^*_e$	$\lambda^*_f \le \lambda^*_e \le \lambda^*_{md}$	$\lambda^*_e \le \lambda^*_f \le \lambda^*_{md}$	at $f_s = 1$ MHz	at $\tau = 2$ sec
AWGN	≤ 66344	$[66345, 66747]$	≥ 66748	–	0.07	33.2
Rayleigh	≤ 1511173	$[1511174, 3871892]$	≥ 3871893	–	1.51	755.6
Nakagami-4	≤ 144841	$[144842, 205432]$	≥ 205433	–	0.14	72.4
SLC $L = 2$	≤ 156004	$[156005, 279605]$	≥ 279606	–	0.16	78.0
SLC $L = 3$	≤ 62358	$[62359, 96276]$	≥ 96277	–	0.06	31.2
Cooperative $K = 2$	≤ 164896	$[164897, 295947]$	≥ 295948	–	0.16	82.4
Cooperative $K = 3$	≤ 70742	$[70743, 109650]$	≥ 109651	–	0.07	35.4

Table 7.3: The regions of N for different cases of λ^*_f, λ^*_{md}, λ^*_e, the minimal sensing time $\tau_{\min}$ at $f_s = 1$ MHz, and the minimal sampling rate $f_{s,\min}$ at $\tau = 2$ seconds.

In the following, diversity-combining technique (SLC with $L = 2, 3$) and cooperative spectrum sensing ($K = 2, 3$) are evaluated, which can be used to increase the effective number of samples in the decision statistic while maintaining a small value of the sampling rate. The Rayleigh fading channel is considered to establish worse case scenario (than AWGN and Nakagami-m channels). From Table 7.3, for two or three diversity branches in SLC, N_s is reduced from N_s =1511174 (no diversity) to N_s =156005 or 62359, respectively, which results in the minimum sensing time at $f_s = 1$ MHz as $\tau_{\min} \approx 0.16$ or 0.06 seconds, and the minimal sampling rate at $\tau = 2$ seconds as $f_{s,\min} \approx 78.0$ kHz or 31.2 kHz, respectively. Similarly, for two or three cooperative nodes in a cooperative spectrum sensing network with OR fusion rule, the minimum sensing time is $\tau_{\min} \approx 0.16$ or 0.07 seconds, and the minimal sampling rate is $f_{s,\min} \approx 82.4$ kHz or 35.4 kHz, respectively. Thus, to satisfy both IEEE 802.22 requirements on false alarm and missed-detection probabilities, diversity combining and cooperative spectrum sensing can significantly reduce the required sensing time and/or the required sampling rate. Note that, for diversity combining and cooperative spectrum sensing, different processing delays may be needed in different networks, which is not accounted in this research.

7.6 Conclusion

In this chapter, low-SNR energy detection in cognitive radio networks is studied. New approximated expressions for the average missed-detection probability and the

average AUC over a generalized channel model are derived. The optimal detection threshold problem is formulated to minimize the total error rate subject to bounded false alarm and miss-detection probabilities. The exact optimal detection threshold for the AWGN channel is derived in closed form. Based on the low-SNR model, the approximated optimal detection threshold over Rayleigh fading channel is also given. Diversity combining techniques and cooperative spectrum sensing are shown to reduce the needed sensing time or sampling rate, enabling low-SNR detection in cognitive radio networks. The low-SNR detection is highly relevant to the emerging cognitive radio networks.

$\sim$

Chapter 8

Conclusion and Future Work

This thesis provides a rigorous analytical framework for the analysis of energy detection based spectrum sensing in cognitive radio networks.

- Chapter 3 provides the performance analysis of an energy detector under both multipath fading and shadowing effects. This analysis reveals that severe multipath fading or/and shadowing degrades the detection performance, and diversity receptions can help to boost the detection performance.

- Chapter 4 proposes the MG distribution to model the SNR of mobile radio channels. Although primarily intended to model composite shadowing/fading channels, this MG distribution is nevertheless effective for many other existing small-scale fading channels as well. For the scenarios where performance analysis is complicated or intractable with traditional mathematical tools, the MG model, a linear combination of gamma distributions, offers a solution. The MG distribution is not limited to energy detection analysis, but also useful for other wireless network performance as well.

- Although the ROC curves characterize the performance of an energy detector by using detection and false alarm probabilities, a single figure of merit is desirable. Chapter 5 thus introduces the measure AUC. The AUC value provides the insight of overall detection capability (combination of false alarm and detection probabilities), and also it can reveal some other properties that cannot be shown clearly by ROC curves, e.g., diversity order.

- Cooperative spectrum sensing which can mitigate the impact of multipath fading or/and shadowing effects is an effective way to improve the detection performance. Several cooperative spectrum sensing networks are introduced in Chapter 6, and a new set of results for the average detection probability is derived for multiple-node and multi-hop cooperative spectrum sensing networks based on either data or decision fusion strategy.

- The IEEE 802.22 standard requires spectrum-sensing techniques to identify primary signals in the very low SNR regime. An accurate low-SNR model for the energy detection and novel results on the average detection performance are provided in Chapter 7. The detection threshold, which is a key design parameter, is selected by considering false-alarm and missed-detection probabilities, and sensing time. The results reveal that the IEEE 802.22 requirements can be achieved with a simple (conventional) energy detector by using a higher sampling frequency, or with diversity combining/cooperative spectrum sensing by using a lower sampling frequency.

The system models and performance metrics introduced by this thesis, because of their simplicity and wide suitability for different fading/shadowing and environmental conditions, are already followed by other researchers. The proposed energy detection models, methodologies and results can be useful for other wireless research topics (e.g., UWB and radar communications). Overall, the research findings will eventually pave the way to design an energy detector in an implementable manner for cognitive radio networks.

However, there are still some open problems related to the topics of this thesis, which should be considered in future work.

- In this thesis, the MG model is determined by matching with SNR distribution of known channel models. Further research directions include the performance analysis of other wireless systems (such as cooperative relaying networks) and model fitting based on measured channel data (e.g., to find the parameters in the MG model when aggregate interference is considered).

- The conventional energy detector is typically optimal if the signal is impaired by the Gaussian noise, which comes from many natural sources, e.g., thermal effect. Moreover, in practice, the received signal may be impaired by a non-Gaussian noise (e.g., man-made impulsive noise) and interference (e.g., co-channel, out-of-band spectral leakage). Temperature, training sequence and known data pattern can help to estimate the noise variance. However, it has been shown that the noise variance estimation error referred to as noise uncertainty can make severe performance degradation of energy detector [135]. Similar to the noise power estimation, signal power is calculated based on the quantized signal levels which may also have an quantization error, δ. Since threshold and the number of samples of a conventional energy detector are selected by using estimated noise variance and signal power, the test statistic may be then defined as

$$\Lambda = \sum_{n=1}^{N} |\mathbf{y}(n) \pm \delta|^2 ,$$

which differs from the traditional modeling. The effects of noise estimation and signal quantization errors on detection performance are still unnoticed/unexplored in the literature. The analysis and design of an energy detector considering both signal quantization and noise estimation errors will be an interesting and challenging problem.

$\sim$

Bibliography

[1] E. Perahia, "IEEE 802.11n development: History, process, and technology," *IEEE Commun. Mag.*, vol. 46, no. 7, pp. 48–55, July 2008.

[2] Q. Spencer, C. Peel, A. Swindlehurst, and M. Haardt, "An introduction to the multi-user MIMO downlink," *IEEE Commun. Mag.*, vol. 42, no. 10, pp. 60–67, Oct. 2004.

[3] E. Charfi, L. Chaari, and L. Kamoun, "PHY/MAC enhancements and QoS mechanisms for very high throughput WLANs: A survey," 2013.

[4] F. Rusek, D. Persson, B. K. Lau, E. Larsson, T. Marzetta, O. Edfors, and F. Tufvesson, "Scaling up MIMO: Opportunities and challenges with very large arrays," *IEEE Signal Process. Mag.*, vol. 30, no. 1, pp. 40–60, Jan. 2013.

[5] A. Nosratinia, T. Hunter, and A. Hedayat, "Cooperative communication in wireless networks," *IEEE Commun. Mag.*, vol. 42, no. 10, pp. 74–80, Oct. 2004.

[6] S. Ramprashad, H. Papadopoulos, A. Benjebbour, Y. Kishiyama, N. Jindal, and G. Caire, "Cooperative cellular networks using multi-user MIMO: Trade-offs, overheads, and interference control across architectures," *IEEE Commun. Mag.*, vol. 49, no. 5, pp. 70–77, May 2011.

[7] D. Gesbert, S. Hanly, H. Huang, S. Shamai Shitz, O. Simeone, and W. Yu, "Multi-cell MIMO cooperative networks: A new look at interference," *IEEE J. Select. Areas Commun.*, vol. 28, no. 9, pp. 1380–1408, Dec. 2010.

[8] A. Damnjanovic, J. Montojo, Y. Wei, T. Ji, T. Luo, M. Vajapeyam, T. Yoo, O. Song, and D. Malladi, "A survey on 3GPP heterogeneous networks," *IEEE Wireless Commun.*, vol. 18, no. 3, pp. 10–21, June 2011.

[9] J. Mitola and G. Maguire, "Cognitive radio: Making software radios more personal," *IEEE Personal Commun.*, vol. 6, no. 4, pp. 13–18, Aug. 1999.

[10] S. Haykin, "Cognitive radio: Brain-empowered wireless communications," *IEEE J. Select. Areas Commun.*, vol. 23, no. 2, pp. 201–220, Feb. 2005.

[11] C. Cordeiro, K. Challapali, D. Birru, and S. S. N., "IEEE 802.22: An introduction to the first wireless standard based on cognitive radios," *J. of Commun. (JCM)*, vol. 1(1), pp. 38–47, Apr. 2006.

[12] S. J. Shellhammer, "Spectrum sensing in IEEE 802.22," in *Proc. 1st IAPR Workshop on Cognitive Information Processing*, June 2008.

[13] C. Stevenson, G. Chouinard, Z. Lei, W. Hu, S. Shellhammer, and W. Caldwell, "IEEE 802.22: The first cognitive radio wireless regional area network standard," *IEEE Commun. Mag.*, vol. 47, no. 1, pp. 130–138, Jan. 2009.

[14] ECMA-International, "MAC and PHY for operation in TV white space," June 2012. [Online]. Available: http://www.ecma-international.org/publications/files/ECMA-ST/ECMA-392.pdf

[15] F. Granelli, P. Pawelczak, R. Prasad, K. P. Subbalakshmi, R. Chandramouli, J. Hoffmeyer, and H. Berger, "Standardization and research in cognitive and dynamic spectrum access networks: IEEE SCC41 efforts and other activities," *IEEE Commun. Mag.*, vol. 48, no. 1, pp. 71–79, Jan. 2010.

[16] C.-S. Sum, H. Harada, F. Kojima, Z. Lan, and R. Funada, "Smart utility networks in TV white space," *IEEE Commun. Mag.*, vol. 49, no. 7, pp. 132–139, July 2011.

[17] P. Pawelczak, K. Nolan, L. Doyle, S. W. Oh, and D. Cabric, "Cognitive radio: Ten years of experimentation and development," *IEEE Commun. Mag.*, vol. 49, no. 3, pp. 90–100, Mar. 2011.

[18] J. Wang, M. Ghosh, and K. Challapali, "Emerging cognitive radio applications: A survey," *IEEE Commun. Mag.*, vol. 49, no. 3, pp. 74–81, Mar. 2011.

[19] C.-S. Sum, H. Harada, F. Kojima, and L. Lu, "An interference management protocol for multiple physical layers in IEEE 802.15.4g smart utility networks," *IEEE Commun. Mag.*, vol. 51, no. 4, pp. 84–91, Apr. 2013.

[20] T. Doumi, "Spectrum considerations for public safety in the United States," *IEEE Commun. Mag.*, vol. 44, no. 1, pp. 30–37, Jan. 2006.

[21] Connecting-America, "The National Broadband Plan," 2010. [Online]. Available: http://download.broadband.gov/plan/national-broadband-plan.pdf

[22] IEEE1900.1-2008. IEEE standard definitions and concepts for dynamic spectrum access: Terminology relating to emerging wireless networks, system functionality, and spectrum management. [Online]. Available: http://standards.ieee.org/findstds/standard/1900.1-2008.html

[23] Q. Zhao and B. Sadler, "A survey of dynamic spectrum access," *IEEE Signal Process. Mag.*, vol. 24, no. 3, pp. 79–89, May 2007.

[24] T. Yucek and H. Arslan, "A survey of spectrum sensing algorithms for cognitive radio applications," *IEEE Commun. Surveys Tutorials*, vol. 11, no. 1, pp. 116–130, 2009.

[25] Y.-C. Liang, Y. Zeng, E. Peh, and A. T. Hoang, "Sensing-throughput tradeoff for cognitive radio networks," *IEEE Trans. Wireless Commun.*, vol. 7, no. 4, pp. 1326–1337, Apr. 2008.

[26] A. Mariani, A. Giorgetti, and M. Chiani, "SNR wall for energy detection with noise power estimation," in *Proc. IEEE Int. Conf. Commun. (ICC)*, June 2011.

[27] H.-S. Chen, W. Gao, and D. Daut, "Signature based spectrum sensing algorithms for IEEE 802.22 WRAN," in *Proc. IEEE Int. Conf. Commun. (ICC)*, 2007, pp. 6487–6492.

[28] D. Cabric, S. M. Mishra, and R. W. Brodersen, "Implementation issues in spectrum sensing for cognitive radios," in *Proc. Asilomar Conference on Signals, Systems and Computers.*, Nov. 2004, pp. 772–776.

[29] W. Gardner, "Signal interception: a unifying theoretical framework for feature detection," *IEEE Trans. Commun.*, vol. 36, no. 8, pp. 897–906, Aug. 1988.

[30] ——, "Exploitation of spectral redundancy in cyclostationary signals," *IEEE Signal Process. Mag.*, vol. 8, no. 2, pp. 14–36, Apr. 1991.

[31] J. Lunden, V. Koivunen, A. Huttunen, and H. V. Poor, "Collaborative cyclostationary spectrum sensing for cognitive radio systems," *IEEE Trans. Signal Process.*, vol. 57, no. 11, pp. 4182–4195, Nov. 2009.

[32] Y. Zeng, Y.-C. Liang, A. T. Hoang, and R. Zhang, "A review on spectrum sensing for cognitive radio: Challenges and solutions," *EURASIP J. Appl. Signal Process. (USA)*, vol. 2010, 2010.

[33] B. H. Juang, G. Y. Li, and J. Ma, "Signal processing in cognitive radio," *Proc. IEEE*, vol. 97, no. 5, pp. 805–823, May 2009.

[34] Y. Zeng and Y. chang Liang, "Eigenvalue-based spectrum sensing algorithms for cognitive radio," *IEEE Trans. Commun.*, vol. 57, no. 6, pp. 1784–1793, June 2009.

[35] M. Naraghi-Pour and T. Ikuma, "Autocorrelation-based spectrum sensing for cognitive radios," *IEEE Trans. Veh. Technol.*, vol. 59, no. 2, pp. 718–733, Feb. 2010.

[36] B. Razavi, "Cognitive radio design challenges and techniques," *IEEE J. Solid-State Circuits*, vol. 45, no. 8, pp. 1542–1553, Aug. 2010.

[37] I. F. Akyildiz, W.-Y. Lee, M. C. Vuran, and S. Mohanty, "Next generation/dynamic spectrum access/cognitive radio wireless networks: A survey," *Computer Networks Journal (ELSEVIER)*, vol. 50, pp. 2127–2159, 2006.

[38] R. Prasad, P. Pawelczak, J. Hoffmeyer, and H. Berger, "Cognitive functionality in next generation wireless networks: standardization efforts," *IEEE Commun. Mag.*, vol. 46, no. 4, pp. 72–78, Apr. 2008.

[39] G. L. Stüber, *Principles of Mobile Communication (3rd ed.)*. Springer, 2012.

[40] S. Hirakawa, N. Sato, and H. Kikuchi, "Broadcasting satellite services for mobile reception," *Proc. IEEE*, vol. 94, no. 1, pp. 327–332, Jan. 2006.

[41] A. Abdi and M. Kaveh, "K distribution: An appropriate substitute for Rayleigh-lognormal distribution in fading-shadowing wireless channels," *Electron. Lett.*, vol. 34, pp. 851–852, Apr. 1998.

[42] P. Theofilakos, A. G. Kanatas, and G. P. Efthymoglou, "Performance of generalized selection combining receivers in K fading channels," *IEEE Commun. Lett.*, vol. 12, no. 11, pp. 816–818, Nov. 2008.

[43] P. M. Shankar, "Error rates in generalized shadowed fading channels," *Wireless Personal Commun.*, vol. 28, no. 3, pp. 233–238, 2004.

[44] P. S. Bithas, P. T. Mathiopoulos, and S. A. Kotsopoulos, "Diversity reception over generalized-K (K_G) fading channels," *IEEE Trans. Wireless Commun.*, vol. 6, no. 12, pp. 4238–4243, Dec. 2007.

[45] A. Laourine, M.-S. Alouini, S. Affes, and A. Stéphenne, "On the performance analysis of composite multipath/shadowing channels using the $\mathcal{G}$-distribution," *IEEE Trans. Commun.*, vol. 57, no. 4, pp. 1162–1170, Apr. 2009.

[46] S. Al-Ahmadi and H. Yanikomeroglu, "On the approximation of the generalized–K distribution by a gamma distribution for modeling composite fading channels," *IEEE Trans. Wireless Commun.*, vol. 9, no. 2, pp. 706–713, Feb. 2010.

[47] Z. Quan, S. Cui, A. H. Sayed, and H. V. Poor, "Optimal multiband joint detection for spectrum sensing in cognitive radio networks," *IEEE Trans. Signal Process.*, vol. 57, no. 3, pp. 1128–1140, Mar. 2009.

[48] H. Urkowitz, "Energy detection of unknown deterministic signals," *Proc. IEEE*, vol. 55, no. 4, pp. 523–531, Apr. 1967.

[49] R. Tandra and A. Sahai, "SNR walls for signal detection," *IEEE J. Select. Topics Signal Process.*, vol. 2, no. 1, pp. 4–17, Feb. 2008.

[50] A. Papoulis and S. U. Pillai, *Probability, Random Variables and Stochastic Processes*. McGraw-Hill Companies, Inc., 2002.

[51] V. Kostylev, "Energy detection of a signal with random amplitude," in *Proc. IEEE Int. Conf. Commun. (ICC)*, vol. 3, May 2002, pp. 1606–1610.

[52] F. F. Digham, M. S. Alouini, and M. K. Simon, "On the energy detection of unknown signals over fading channels," in *Proc. IEEE Int. Conf. Commun. (ICC)*, May 2003, pp. 3575–3579.

[53] ——, "On the energy detection of unknown signals over fading channels," *IEEE Trans. Commun.*, vol. 55, no. 1, pp. 21–24, Jan. 2007.

[54] S. Herath, N. Rajatheva, and C. Tellambura, "Energy detection of unknown signals in fading and diversity reception," *IEEE Trans. Commun.*, vol. 59, no. 9, pp. 2443–2453, Sep. 2011.

[55] J. Salt and H. Nguyen, "Performance prediction for energy detection of unknown signals," *IEEE Trans. Veh. Technol.*, vol. 57, no. 6, pp. 3900–3904, Nov. 2008.

[56] Y. Chen, "Improved energy detector for random signals in Gaussian noise," *IEEE Trans. Wireless Commun.*, vol. 9, no. 2, pp. 558–563, Feb. 2010.

[57] D. Cabric, A. Tkachenko, and R. W. Brodersen, "Experimental study of spectrum sensing based on energy detection and network cooperation," in *Proc. 1st int. Workshop on Technology and Policy for Accessing Spectrum (TAPAS)*, Aug. 2006, p. 12.

[58] P. Cheraghi, Y. Ma, R. Tafazolli, and Z. Lu, "Cluster-based differential energy detection for spectrum sensing in multi-carrier systems," *IEEE Trans. Signal Process.*, vol. 60, no. 12, pp. 6450–6464, Dec. 2012.

[59] D. Ramirez, J. Via, and I. Santamaria, "The locally most powerful test for multiantenna spectrum sensing with uncalibrated receivers," in *Proc. IEEE Int. Conf. Acoustics, Speech, and Signal Process. (ICASSP)*, Mar. 2012, pp. 3437–3440.

[60] J. Sala-Alvarez, G. Vazquez-Vilar, and R. Lopez-Valcarce, "Multiantenna GLR detection of rank-one signals with known power spectrum in white noise with unknown spatial correlation," *IEEE Trans. Signal Process.*, vol. 60, no. 6, pp. 3065–3078, June 2012.

[61] F. Lin, R. Qiu, Z. Hu, S. Hou, J. Browning, and M. Wicks, "Generalized FMD detection for spectrum sensing under low signal-to-noise ratio," *IEEE Commun. Lett.*, vol. 16, no. 5, pp. 604–607, May 2012.

[62] Z. Zhang, Z. Han, H. Li, D. Yang, and C. Pei, "Belief propagation based cooperative compressed spectrum sensing in wideband cognitive radio networks," *IEEE Trans. Wireless Commun.*, vol. 10, no. 9, pp. 3020–3031, Sep. 2011.

[63] M. Derakhshani, T. Le-Ngoc, and M. Nasiri-Kenari, "Efficient cooperative cyclostationary spectrum sensing in cognitive radios at low SNR regimes," *IEEE Trans. Wireless Commun.*, vol. 10, no. 11, pp. 3754–3764, Nov. 2011.

[64] T. Cui, F. Gao, and A. Nallanathan, "Optimization of cooperative spectrum sensing in cognitive radio," *IEEE Trans. Veh. Technol.*, vol. 60, no. 4, pp. 1578–1589, May 2011.

[65] L. Wei, P. Dharmawansa, and O. Tirkkonen, "Multiple primary user spectrum sensing in the low SNR regime," *IEEE Trans. Commun.*, vol. 61, no. 5, pp. 1720–1731, May 2013.

[66] G. Ganesan and Y. Li, "Cooperative spectrum sensing in cognitive radio, part I: Two user networks," *IEEE Trans. Wireless Commun.*, vol. 6, no. 6, pp. 2204–2213, June 2007.

[67] R. Fan and H. Jiang, "Optimal multi-channel cooperative sensing in cognitive radio networks," *IEEE Trans. Wireless Commun.*, vol. 9, no. 3, pp. 1128–1138, Mar. 2010.

[68] W. Zhang and K. B. Letaief, "Cooperative communications for cognitive radio networks," *Proc. IEEE*, vol. 97, no. 5, pp. 878–893, May 2009.

[69] V. I. Kostylev, "Energy detection of a signal with random amplitude," in *Proc. IEEE Int. Conf. Commun. (ICC)*, 2002, pp. 1606–1610.

[70] F. F. Digham, M. S. Alouini, and M. K. Simon, "On the energy detection of unknown signals over fading channels," in *Proc. IEEE Int. Conf. Commun. (ICC)*, 2003, pp. 3575–3579.

[71] A. Abdi and M. Kaveh, "Comparison of DPSK and MSK bit error rates for K and Rayleigh-lognormal fading distributions," *IEEE Commun. Lett.*, vol. 4, no. 4, pp. 122–124, Apr. 2000.

[72] P. M. Shankar, "Performance analysis of diversity combining algorithms in shadowed fading channels," *Wireless Personal Commun.*, vol. 37, no. 1, pp. 61–72, Apr. 2006.

[73] P. S. Bithas, N. C. Sagias, P. T. Mathiopoulos, G. K. Karagiannidis, and A. A. Rontogiannis, "On the performance analysis of digital communications over generalized-K fading channels," *IEEE Commun. Lett.*, vol. 10, no. 5, pp. 353–355, May 2006.

[74] I. S. Gradshteyn and I. M. Ryzhik, *Table of Integrals, Series and Products*, 7th ed. Academic Press Inc, 2007.

[75] Wolfram. The Wolfram functions site. [Online]. Available: http://functions.wolfram.com

[76] T. Sauter, "Computation of irregularly oscillating integrals," *Appl. Numer. Math.*, vol. 35, no. 3, pp. 245–264, Nov. 2000.

[77] M. Abramowitz and I. A. Stegun, Eds., *Handbook of Mathematical Functions: with Formulas, Graphs, and Mathematical Tables*. New York: Dover Publications, 1965.

[78] J. P. Egan, *Signal Detection Theory and ROC-Analysis*. Series in cognition and perception. New York: Academic press,, 1975.

[79] A. Laourine, M.-S. Alouini, S. Affes, and A. Stéphenne, "On the capacity of generalized-K fading channels," *IEEE Trans. Wireless Commun.*, vol. 7, no. 7, pp. 2441–2445, July 2008.

[80] G. Efthymoglou, N. Ermolova, and V. Aalo, "Channel capacity and average error rates in generalised-K fading channels," *IET Commun.*, vol. 4, no. 11, pp. 1364–1372, July 2010.

[81] C. Zhu, J. Mietzner, and R. Schober, "On the performance of non-coherent transmission schemes with equal-gain combining in generalized K fading," *IEEE Trans. Wireless Commun.*, vol. 9, no. 4, pp. 1337–1349, Apr. 2010.

[82] L. Wu, J. Lin, K. Niu, and Z. He, "Performance of dual-hop transmissions with fixed gain relays over generalized-K fading channels," in *Proc. IEEE Int. Conf. Commun. (ICC)*, 2009.

[83] K. P. Peppas, C. K. Datsikas, H. E. Nistazakis, and G. S. Tombras, "Dual-hop relaying communications over generalized-K (K_G) fading channels," *J. Franklin Inst.*, vol. 4, no. 1, pp. 116–124, Jan. 2010.

[84] J. Cao, L. L. Yang, and Z. Zhong, "Performance of multihop wireless links over generalized-K fading channels," in *Proc. IEEE Vehicular Technology Conf. (VTC)*, 2010.

[85] N. Ermolova, "Analysis of OFDM error rates over nonlinear fading radio channels," *IEEE Trans. Wireless Commun.*, vol. 9, no. 6, pp. 1855–1860, June 2010.

[86] M. Matthaiou, D. Chatzidiamantis, K. Karagiannidis, and A. Nossek, "On the capacity of generalized-K fading MIMO channels," *IEEE Trans. Signal Process.*, vol. 58, no. 11, pp. 5939–5944, Nov. 2010.

[87] S. Al-Ahmadi and H. Yanikomeroglu, "On the approximation of the PDF of the sum of independent generalized-K RVs by another generalized-K PDF with applications to distributed antenna systems," in *IEEE Wireless Commun. and Networking Conf. (WCNC)*, 2010.

[88] R. DeVore, L. Kuo, and G. Lorentz, *Constructive Approximation*. New York: Springer-Verlag, 1993.

[89] M. Wiper, D. R. Insua, and F. Ruggeri, "Mixtures of gamma distributions with applications," *J. Computational and Graphical Statistics*, vol. 10, no. 3, pp. 440–454, Sep. 2001.

[90] M. K. Simon and M. S. Alouini, *Digital Communication over Fading Channels*, 2nd ed. New York: Wiley, 2005.

[91] M. D. Yacoub, "The κ-μ distribution and the η-μ distribution," *IEEE Antennas Propagat. Mag.*, vol. 49, no. 1, pp. 68–81, Feb. 2007.

[92] D. B. da Costa and M. D. Yacoub, "Average channel capacity for generalized fading scenarios," *IEEE Commun. Lett.*, vol. 11, no. 12, pp. 949–951, Dec. 2007.

[93] N. Ermolova, "Moment generating functions of the generalized η-μ and κ-μ distributions and their applications to performance evaluations of communication systems," *IEEE Commun. Lett.*, vol. 12, no. 7, pp. 502–504, July 2008.

[94] ——, "Useful integrals for performance evaluation of communication systems in generalised η-μ and κ-μ fading channels," *IET Commun.*, vol. 3, no. 2, pp. 303–308, Feb. 2009.

[95] V. Asghari, D. da Costa, and S. Aïssa, "Symbol error probability of rectangular QAM in MRC systems with correlated η-μ fading channels," *IEEE Trans. Veh. Technol.*, vol. 59, no. 3, pp. 1497–1503, Mar. 2010.

[96] M. Nakagami, "The m-distribution - A general formula for intensity distribution of rapid fading," in *Statistical Methods in Radio Wave Propagation*, W. G. Hoffman, Ed. Oxford, England: Pergamon, 1960.

[97] Z. Wang and G. Giannakis, "A simple and general parameterization quantifying performance in fading channels," *IEEE Trans. Commun.*, vol. 51, no. 8, pp. 1389–1398, Aug. 2003.

[98] M. S. Alouini and A. J. Goldsmith, "Capacity of Rayleigh fading channels under different adaptive transmission and diversity-combining techniques," *IEEE Trans. Veh. Technol.*, vol. 48, no. 4, pp. 1165–1181, July 1999.

[99] H. Shin and J. H. Lee, "On the error probability of binary and M–ary signals in Nakagami–m fading channels," *IEEE Trans. Commun.*, vol. 52, no. 4, pp. 536–539, Apr. 2004.

[100] A. Annamalai and C. Tellambura, "Error rates for Nakagami-m fading multichannel reception of binary and M-ary signals," *IEEE Trans. Commun.*, vol. 49, no. 1, pp. 58–68, Jan. 2001.

[101] A. Maaref and S. Aïssa, "Exact error probability analysis of rectangular QAM for single and multichannel reception in Nakagami-m fading channels," *IEEE Trans. Commun.*, vol. 57, no. 1, pp. 214–221, Jan. 2009.

[102] S. Asmussen, *Applied Probability and Queues*. New York: Wiley, 1987.

[103] J. A. Swets, R. M. Dawes, and J. Monahan, "Better decisions through science." *Scientific American*, vol. 283, no. 4, pp. 82–87, Oct 2000.

[104] F. J. Provost and T. Fawcett, "Robust classification for imprecise environments," *Machine Learning*, vol. 42, no. 3, pp. 203–231, 2001.

[105] T. D. Wickens, *Elementary Signal Detection Theory.* New York: Oxford Univ. Press, 2002.

[106] J. A. Hanley and B. J. Mcneil, "The meaning and use of the area under a receiver operating characteristic (ROC) curve," *Radiology*, vol. 143, no. 1, pp. 29–36, Apr. 1982.

[107] J. H. Shapiro, "Bounds on the area under the ROC curve," *J. Opt. Soc. Am. A*, vol. 16, no. 1, pp. 53–57, Jan. 1999.

[108] E. Clarkson, "Bounds on the area under the receiver operating characteristic curve for the ideal observer," *J. Opt. Soc. Am. A*, vol. 19, no. 10, pp. 1963–1968, Oct. 2002.

[109] H. H. Barrett, C. K. Abbey, and E. Clarkson, "Objective assessment of image quality. III. ROC metrics, ideal observers, and likelihood-generating functions," *J. Opt. Soc. Am. A*, vol. 15, no. 6, pp. 1520–1535, June 1998.

[110] T. Fawcett, "An introduction to ROC analysis," *Pattern Recognition Lett.*, vol. 27, no. 8, pp. 861–874, June 2006.

[111] A. Liu, E. F. Schisterman, and C. Wu, "Nonparametric estimation and hypothesis testing on the partial area under receiver operating characteristic curves," *Communications in Statistics - Theory and Methods*, vol. 34, no. 9, pp. 2077–2088, Oct. 2005.

[112] S. G. Krantz, *Handbook of Complex Variables, 1st Ed.* Birkhuser Boston, 1999.

[113] J. N. Laneman, D. N. C. Tse, and G. W. Wornell, "Cooperative diversity in wireless networks: Efficient protocols and outage behavior," *IEEE Trans. Inf. Theory*, vol. 50, no. 12, pp. 3062–3080, Dec. 2004.

[114] M. O. Hasna and M. S. Alouini, "A performance study of dual-hop transmissions with fixed gain relays," *IEEE Trans. Wireless Commun.*, vol. 3, no. 6, pp. 1963–1968, Nov. 2004.

[115] G. Ganesan and Y. Li, "Cooperative spectrum sensing in cognitive radio, part II: Multiuser networks," *IEEE Trans. Wireless Commun.*, vol. 6, no. 6, pp. 2214–2222, June 2007.

[116] A. Ghasemi and E. S. Sousa, "Collaborative spectrum sensing for opportunistic access in fading environments," in *Proc. IEEE DySPAN*, Nov. 2005, pp. 131–136.

[117] S. M. Mishra, A. Sahai, and R. W. Brodersen, "Cooperative sensing among cognitive radios," in *Proc. IEEE Int. Conf. Commun. (ICC)*, vol. 4, June 2006, pp. 1658–1663.

[118] C. Tellambura, A. Annamalai, and V. K. Bhargava, "Closed form and infinite series solutions for the MGF of a dual-diversity selection combiner output in bivariate Nakagami fading," *IEEE Trans. Commun.*, vol. 51, no. 4, pp. 539–542, Apr. 2003.

[119] G. K. Karagiannidis, T. A. Tsiftsis, and R. K. Mallik, "Bounds for multihop relayed communications in Nakagami-m fading," *IEEE Trans. Commun.*, vol. 54, no. 1, pp. 18–22, Jan. 2006.

[120] G. K. Karagiannidis, "Moments-based approach to the performance analysis of equal gain diversity in Nakagami-m fading," *IEEE Commun. Lett.*, vol. 52, no. 5, pp. 685–690, May 2004.

[121] G. K. Karagiannidis, D. A. Zogas, N. C. Sagias, T. A. Tsiftsis, and P. T. Mathiopoulos, "Multihop communications with fixed-gain relays over generalized fading channels," in *Proc. IEEE Global Telecommn. Conf. (GLOBECOM)*, 2004, pp. 36–40.

[122] R. Mills and G. Prescott, "A comparison of various radiometer detection models," *IEEE Trans. Aerosp. Electron. Syst.*, vol. 32, no. 1, pp. 467–473, Jan. 1996.

[123] S. Ciftci and M. Torlak, "A comparison of energy detectability models for spectrum sensing," in *Proc. IEEE Global Telecommn. Conf. (GLOBECOM)*, Dec. 2008.

[124] J. Zhang and S. T. Mueller, "A note on ROC analysis and non-parametric estimate of sensitivity," *Psychometrika*, vol. 70, no. 1, pp. 203–212, Mar. 2005.

[125] A. Singh, M. Bhatnagar, and R. Mallik, "Cooperative spectrum sensing in multiple antenna based cognitive radio network using an improved energy detector," *IEEE Commun. Lett.*, vol. 16, no. 1, pp. 64–67, Jan. 2012.

[126] A. P. Prudnikov, Y. A. Brychkov, and O. I. Marichev, *Integrals and Series, vol. 2*. Gordon and Breach science Publishers, 1986.

[127] Q. Peng, P. Cosman, and L. Milstein, "Optimal sensing disruption for a cognitive radio adversary," *IEEE Trans. Veh. Technol.*, vol. 59, no. 4, pp. 1801–1810, May 2010.

[128] H. L. V. Trees, *Detection, Estimation, and Modulation Theory, Part I*. Wiley-Interscience, 2001.

[129] J. Shen, Y. Liu, S. Liu, J. Gao, G. Xie, and C. Chi, "Robust energy detection based on Bayesian estimation for cognitive radio," in *Proc. IEEE Global Telecommn. Conf. (GLOBECOM)*, Dec. 2008.

[130] F. Penna, Y. Sun, L. Dolecek, and D. Cabric, "Joint spectrum sensing and detection of malicious nodes via belief propagation," in *Proc. IEEE Global Telecommn. Conf. (GLOBECOM)*, Dec. 2011.

[131] P. Jia, M. Vu, T. Le-Ngoc, S.-C. Hong, and V. Tarokh, "Capacity- and Bayesian-based cognitive sensing with location side information," *IEEE J. Select. Areas Commun.*, vol. 29, no. 2, pp. 276–289, Feb. 2011.

[132] "IEEE standard for terminology and test methods for analog-to-digital converters," *IEEE Std 1241-2010 (Revision of IEEE Std 1241-2000)*, pp. 1–139, Jan. 2011.

[133] A. Verma and B. Razavi, "A 10-Bit 500-MS/s 55-mW CMOS ADC," *IEEE J. Solid-State Circuits,*, vol. 44, no. 11, pp. 3039–3050, Nov. 2009.

[134] T.-H. Yu, O. Sekkat, S. Rodriguez-Parera, D. Markovic, and D. Cabric, "A wideband spectrum-sensing processor with adaptive detection threshold and sensing time," *IEEE Trans. on Circuits and Systems I*, vol. 58, no. 11, pp. 2765–2775, Nov. 2011.

[135] A. Mariani, A. Giorgetti, and M. Chiani, "Effects of noise power estimation on energy detection for cognitive radio applications," *IEEE Trans. Commun.*, vol. 59, no. 12, pp. 3410–3420, Dec. 2011.

[136] L. C. Andrews, *Special Functions of Mathematics for Engineers*, 2nd ed. New York: McGraw-Hill, 1992.

[137] A. H. Nuttall, "Some integrals involving the Q_M function," Naval Underwater Systems Center (NUSC), Tech. Rep., May 1974.

$\sim$

Appendix A

Proofs for Chapter 3

A.1 Derivation of $\overline{P_d^K}$

the average detection probability over Rayleigh distribution, $\overline{P_d^K}$, can be evaluated as $\int_0^\infty P_d^{Fad}(y) f_Y(y)\,\mathrm{d}y$ where $f_Y(y)$ is in (3.3) can be evaluated as in [53, eq. (9)] which gives

$$\begin{aligned} P_d^{Fad}(y) =& e^{-\frac{\lambda}{2}} \sum_{n=0}^{N-2} \frac{1}{n!} \left(\frac{\lambda}{2}\right)^n \\ &+ \left(\frac{1+Ny}{Ny}\right)^{N-1} \left[e^{-\frac{\lambda}{2(1+Ny)}} - e^{-\frac{\lambda}{2}} \sum_{n=0}^{N-2} \frac{1}{n!} \left(\frac{\lambda N y}{2(1+Ny)}\right)^n\right]. \end{aligned}$$

After applying series summation for exponential function, and with some algebraic manipulations, $\overline{P_d^K}$ can be written as

$$\begin{aligned} \overline{P_d^K} =& e^{-\frac{\lambda}{2}} \sum_{n=0}^{N-2} \frac{1}{n!} \left(\frac{\lambda}{2}\right)^n \\ &+ \frac{N^{1-N}}{\Gamma(k)\Omega^k} \sum_{n=0}^{\infty} \frac{(-\frac{\lambda}{2})^n}{n!} \int_0^\infty y^{k-N} (1+Ny)^{N-n-1} e^{-\frac{y}{\Omega}}\,\mathrm{d}y \\ &- \frac{e^{-\frac{\lambda}{2}}}{\Gamma(k)\Omega^k} \sum_{n=0}^{N-2} \frac{N^{1-N+n}(\frac{\lambda}{2})^n}{n!} \int_0^\infty y^{n+k-N} (1+Ny)^{N-n-1} e^{-\frac{y}{\Omega}}\,\mathrm{d}y. \end{aligned}$$

$\overline{P_d^K}$ can be derived as (3.4) with the aid of (3.5).

A.2 Derivation of $\overline{P_d^{K_G}}$

$\overline{P_d^{K_G}}$ can be evaluated as $\int_0^\infty P_d^{Fad}(y) f_Y(y)\,\mathrm{d}y$ where $P_d^{Fad}(y)$ can be written using [53, eq. (7)]. We use series summation of ${}_1F_1(a;c;x) = \sum_{n=0}^{\infty} \frac{(a)_n x^n}{(c)_n n!}$ [136, eq. (10.1)] and $L_n(x) = \sum_{k=0}^{n} (-1)^k \binom{n}{n-k} \frac{x^k}{k!}$ [74, eq. (8.970.1)], where ${}_1F_1(\cdot;\cdot;\cdot)$ and $L_n(\cdot)$ are the confluent hypergeometric function and the Laguerre polynomial of degree n, respectively. After some algebraic manipulations, equivalent $P_d^{Fad}(y)$ can be expressed as [1]

$$\begin{aligned} P_d^{Fad}(y) = &\sum_{v=0}^{m-1} \frac{\binom{m-1}{m-v-1}\left(\frac{\lambda}{2}\right)^v}{v! m^{1-m}} e^{-\frac{\lambda}{2}\frac{m}{m+Ny}} (Ny)^v (m+Ny)^{1-m-v} \\ &+ \sum_{n=0}^{m-2}\sum_{a=0}^{n} \frac{\binom{n}{n-a}\left(\frac{\lambda}{2}\right)^a}{a! m^{-n}} e^{-\frac{\lambda}{2}\frac{m}{m+Ny}} (Ny)^{a+1} (m+Ny)^{-n-a-1} \\ &+ \sum_{s=0}^{\infty}\sum_{n=1}^{N-1} \frac{e^{-\frac{\lambda}{2}}\left(\frac{\lambda}{2}\right)^{n+s} m^m}{n! s!} \frac{(m)_s}{(n+1)_s} (Ny)^s (m+Ny)^{-s-m}. \end{aligned} \tag{A.1}$$

Applying series summation for exponential function and averaging it over $f_Y(y)$, (A.1) can be re-written as

$$\begin{aligned} \overline{P_d^{K_G}} = &\frac{1}{\Gamma(k)(\Omega)^k} \\ &\times \Bigg[\sum_{t=0}^{\infty}\sum_{v=0}^{m-1} \frac{(-1)^t (\frac{\lambda}{2})^{t+v} N^v \binom{m-1}{m-v-1}}{t! v! m^v} \int_0^\infty y^{v+k-1} \left(1+\frac{Ny}{m}\right)^{-t-m-v+1} e^{-\frac{y}{\Omega}}\,\mathrm{d}y \\ &+ \sum_{s=0}^{\infty}\sum_{n=0}^{m-2}\sum_{a=0}^{n} \frac{(-1)^s (\frac{\lambda}{2})^{a+s} N^{a+1} \binom{n}{n-a}}{a! s! m^{a+1}} \int_0^\infty y^{a+k} \left(1+\frac{Ny}{m}\right)^{-s-n-a-1} e^{-\frac{y}{\Omega}}\,\mathrm{d}y \\ &+ e^{-\frac{\lambda}{2}} \sum_{s=0}^{\infty}\sum_{n=1}^{N-1} \frac{\left(\frac{\lambda}{2}\right)^{n+s} N^s}{n! s! m^s} \frac{(m)_s}{(n+1)_s} \int_0^\infty y^{s+k-1} \left(1+\frac{Ny}{m}\right)^{-m-s} e^{-\frac{y}{\Omega}}\,\mathrm{d}y \Bigg]. \end{aligned} \tag{A.2}$$

Then, $\overline{P_d^{K_G}}$ can be evaluated as (3.6) with the aid of (3.5).

$\sim$

[1] The expression in [53, eq. (8)] has a typo. The power of the exponential term should be $-\frac{\lambda\beta}{2\sigma^2}$.

Appendix B

Proofs for Chapter 5

B.1 Necessary Integrations

Some integrations necessary for derivations in Chapter 5 are presented below.

First, $J_1(a, p, r, c)$ is defined as

$$J_1(a, p, r, c) \triangleq \int_0^\infty x^{a-1} e^{-px^2} I_r(cx)\ \mathrm{d}x \tag{B.1}$$

with parameters a, p, r, c, where $\mathrm{Re}[a] > 0 \wedge \mathrm{Re}[p] > 0$.[1] Although a closed-form solution for $J_1(a, p, r, c)$ is available in [126, eq. (2.15.5.4)], it can not be applied for negative integer values of r. Therefore, an alternative method is presented for any integer r, as follows.

After applying series expansion of $I_r(cx)$ in (B.1), and with transformation $t = x^2$, $J_1(a, p, r, c)$ can be written as

$$J_1(a, p, r, c) = \sum_{k=0}^{\infty} \frac{\left(\frac{c}{2}\right)^{2k+r}}{\Gamma(k + r + 1)k!} \frac{1}{2} \int_0^\infty t^{k+\frac{r+a}{2}-1} e^{-pt}\ \mathrm{d}t.$$

Further, $J_1(a, p, r, c)$ can be shown to be

$$J_1(a, p, r, c) = \frac{c^r}{2^{r+1}} p^{-\frac{a+r}{2}} \Gamma\left(\frac{a+r}{2}\right) \sum_{k=0}^{\infty} \frac{\left(\frac{a+r}{2}\right)_k p^{-k}}{\Gamma(k + r + 1)\ k!} \left(\frac{c^2}{4}\right)^k$$

where $(n)_k$ is the Pochhammer symbol defined as $(n)_k = \frac{\Gamma(n+k)}{\Gamma(n)}$ [74]. Given a hypergeometric or generalized hypergeometric function ${}_pF_q(a_1, ..., a_p; b_1, ..., b_q; z)$,

[1] Here $\wedge$ stands for AND.

the regularized hypergeometric function is defined as [75, eq. 07.32.02.0001.01]

$$\begin{aligned} {}_p\tilde{F}_q(a_1,...,a_p;b_1,...,b_q;z) &\triangleq \frac{{}_pF_q(a_1,...,a_p;b_1,...,b_q;z)}{\Gamma(b_1)...\Gamma(b_q)} \\ &= \sum_{k=0}^{\infty} \frac{\prod_{j=1}^{p}(a_j)_k\, z^k}{k!\ \prod_{j=1}^{q}\Gamma(k+b_j)}. \end{aligned} \tag{B.2}$$

Therefore, $J_1(a,p,r,c)$ can be evaluated as

$$J_1(a,p,r,c) = \frac{c^r p^{-\frac{a+r}{2}}\Gamma\left(\frac{a+r}{2}\right)}{2^{r+1}} {}_1\tilde{F}_1\left(\frac{a+r}{2}; r+1; \frac{c^2}{4p}\right). \tag{B.3}$$

Next, $J_2(a,p,b,d,c)$ is defined as

$$J_2(a,p,b,d,c) \triangleq \int_0^{\infty} x^{a-1}e^{-px}\,{}_1\tilde{F}_1\left(b;d;cx\right)\ \mathrm{d}x \tag{B.4}$$

with parameters a,p,b,d,c, where $\mathrm{Re}[a] > 0 \ \wedge\ \mathrm{Re}[p] > 0$. Using the definition of the regularized hypergeometric functions ${}_p\tilde{F}_q$ in (B.2), $J_2(a,p,b,d,c)$ can be solved as

$$J_2(a,p,b,d,c) = \sum_{k=0}^{\infty} \frac{(a)_k\, c^k}{k!\,\Gamma(b+k)} \int_0^{\infty} x^{k+a-1}e^{-px}\ \mathrm{d}x = \sum_{k=0}^{\infty} \frac{(a)_k c^k}{k!\,\Gamma(b+k)} \frac{\Gamma(k+a)}{p^{k+a}}.$$

With the relationship of $\Gamma(k+a) = (a)_k\Gamma(a)$ for integer values of a, $J_2(a,p,b,d,c)$ is shown to be

$$J_2(a,p,b,d,c) = p^{-a}\Gamma(a)\,{}_2\tilde{F}_1\left(a,b;d;\frac{c}{p}\right). \tag{B.5}$$

B.2 Derivation of $\mathcal{A}(\gamma)$ in (5.7)

(5.6) can be written as

$$\mathcal{A}(\gamma) = \frac{1}{2^{N-1}\Gamma(N)}\left(I_1 - I_2 + I_3\right) \tag{B.6}$$

where I_1, I_2 and I_3 are defined as follows

$$I_1 \triangleq \int_0^{\infty} t^{2N-1}e^{-\frac{t^2}{2}}\ \mathrm{d}t = 2^{2N-1}\Gamma(N)$$

$$I_2 \triangleq \int_0^\infty t^{2N-1} e^{-\frac{t^2}{2}}\, Q_N(t, \sqrt{2\gamma})\, \mathrm{d}t = 2^{2N-1}(N-1)!\, e^{-\frac{\gamma}{2}} \sum_{k=0}^{N-1} \frac{1}{k!} \left(\frac{\gamma}{2}\right)^k$$

$$I_3 \triangleq e^{-\gamma} \sum_{k=1-N}^{N-1} \left(\frac{1}{2\gamma}\right)^{\frac{k}{2}} \int_0^\infty t^{2N+k-1} e^{-t^2} I_k\left(\sqrt{2\gamma} t\right)\, \mathrm{d}t$$

$$= e^{-\gamma} \sum_{k=1-N}^{N-1} 2^{-(1+k)} \Gamma(N+k)\, {}_1\tilde{F}_1\left(N+k; 1+k; \frac{\gamma}{2}\right)$$

where the second equality of I_2 is from [137, eq. (28)], and the second equality of I_3 is from (B.1) and (B.3). ${}_1\tilde{F}_1(\cdot;\cdot;\cdot)$ is the regularized confluent hypergeometric function of ${}_1F_1$ [75].

After replacing I_1, I_2, and I_3 by the above definitions, (B.6) is exactly (5.7).

B.3 Derivation of $\bar{\mathcal{A}}_{Nak}$ in (5.13)

With (5.7), (5.12), (5.11) and the fact $\int_0^\infty f_\gamma(x)\, \mathrm{d}x = 1$, $\bar{\mathcal{A}}_{Nak}$ can be written as

$$\bar{\mathcal{A}}_{Nak} = 1 - \frac{1}{\Gamma(m)} \left(\frac{m}{\bar{\gamma}}\right)^m \sum_{k=0}^{N-1} \frac{1}{2^k\, k!} I_4 + \frac{1}{\Gamma(m)} \left(\frac{m}{\bar{\gamma}}\right)^m \sum_{k=1-N}^{N-1} \frac{\Gamma(N+k)}{2^{N+k}\Gamma(N)} I_5 \tag{B.7}$$

where I_4 and I_5 are defined as

$$I_4 \triangleq \int_0^\infty x^{m+k-1} e^{-\left(\frac{m}{\bar{\gamma}} + \frac{1}{2}\right)x}\, \mathrm{d}x = \Gamma(k+m) \left(\frac{m}{\bar{\gamma}} + \frac{1}{2}\right)^{-(k+m)} \tag{B.8}$$

and

$$I_5 \triangleq \int_0^\infty x^{m-1} e^{-\left(\frac{m}{\bar{\gamma}} + 1\right)x}\, {}_1\tilde{F}_1\left(N+k; 1+k; \frac{x}{2}\right)\, \mathrm{d}x.$$

Using the transformation $x = 2y$ and based on (B.4) and (B.5), I_5 can be evaluated for integer m as

$$I_5 = \frac{\Gamma(m)}{\left(\frac{m}{\bar{\gamma}} + 1\right)^m}\, {}_2\tilde{F}_1\left(m; N+k; 1+k; \frac{\bar{\gamma}}{2(m+\bar{\gamma})}\right). \tag{B.9}$$

After replacing I_4 by (B.8) and replacing I_5 by (B.9), (B.7) is exactly (5.13).

$\sim$

Appendix C

Expressions for Chapter 6

C.1 Calculation of Residue

If $g(z)$ has the Laurent series representation, i.e., $g(z) = \sum_{i=-\infty}^{\infty} a_i(z - z_0)^i$ for all z, the coefficient a_{-1} of $(z - z_0)^{-1}$ is the residue of $g(z)$ at z_0 [112]. For $g(z)$ given in (6.3), assume there are k different poles at $z = \eta_i$ $(i = 1, 2, ..., k)$ and n_i poles at $z = \eta_i$. Thus, $\overline{P_d}$ in 6.4 can be calculated as $\overline{P_d} = e^{-\frac{\lambda}{2}} \sum_{i=1}^{k} \text{Res}(g; \eta_i)$, where

$$\text{Res}\,(g; \eta_i) = \frac{D^{n_i-1}\left(g(z)(z-\eta_i)^{n_i}\right)\Big|_{z=\eta_i}}{(n_i-1)!},$$

and $D^n(f(z))$ denotes the nth derivative of $f(z)$ with respect to z.

Residues of equation (6.5)

$$\text{Res}\,(g; 0) = \frac{D^{N-\beta_i-1}\left(g(z)z^{N-\beta_i}\right)\Big|_{z=0}}{(N-\beta_i-1)!}$$

$$\text{Res}\left(g; \frac{N}{N+\zeta_i}\right) = \frac{D^{\beta_i-1}\left(g(z)(z-\frac{N}{N+\zeta_i})^{\beta_i}\right)\Big|_{z=\frac{N}{N+\zeta_i}}}{(\beta_i-1)!}.$$

Residues of equation (6.9)

$$\text{Res}\,(g; 0) = \frac{D^{N-K-1}\left(\frac{e^{\frac{\lambda}{2}z}}{(1-z)}\prod_{i=1}^{K}\left(\frac{1-\Delta_i}{z-\Delta_i}\right)\right)\Big|_{z=0}}{(N-K-1)!},$$

$$\text{Res}\,(g; \Delta_j) = \frac{e^{\frac{\lambda}{2}\Delta_j}}{\Delta_j^{N-K}}\prod_{i=1, i\neq j}^{K}\left(\frac{1-\Delta_i}{\Delta_j-\Delta_i}\right)$$

for $j = 1, ..., K$.

Residues of equation (6.11)

$$\text{Res}\,(g;0) = \frac{D^{N-K-2}\left(\frac{(1-\Delta)e^{\frac{\lambda}{2}z}}{(1-z)(z-\Delta)}\prod_{i=1}^{K}\frac{1-\Delta_i}{z-\Delta_i}\right)\Big|_{z=0}}{(N-K-2)!},$$

$$\text{Res}\,(g;\Delta) = \frac{e^{\frac{\lambda}{2}\Delta}}{\Delta^{N-K-1}}\prod_{i=1}^{K}\frac{1-\Delta_i}{\Delta-\Delta_i},$$

$$\text{Res}\,(g;\Delta_j) = \frac{(1-\Delta)e^{\frac{\lambda}{2}\Delta_j}}{(\Delta_j-\Delta)\Delta_j^{N-K-1}}\prod_{i=1,i\neq j}^{K}\left(\frac{1-\Delta_i}{\Delta_j-\Delta_i}\right),$$

for $j = 1, ..., K$.

Residues of equation (6.14)

$$\text{Res}\,(g_i;0) = \frac{1}{(N-2)!}D^{N-2}\left(\frac{e^{\frac{\lambda}{2}z}}{(1-z)\left(z-\frac{1}{1+p_i}\right)}\right)\Bigg|_{z=0},$$

$$\text{Res}\left(g_i;\frac{1}{1+p_i}\right) = \frac{e^{\frac{\lambda}{2}\frac{1}{1+p_i}}}{p_i(1+p_i)^{-N}}.$$

C.2 Cascaded BSC

The transition probability matrix T_i of the ith hop can be written using the singular value decomposition as $T_i = P^{-1}Q_iP$, where

$$P = \begin{pmatrix} 1 & 1 \\ 1 & -1 \end{pmatrix}, Q_i = \begin{pmatrix} 1 & 0 \\ 0 & 1-2p_{e,i} \end{pmatrix}, T_i = \begin{pmatrix} 1-p_{e,i} & p_{e,i} \\ p_{e,i} & 1-p_{e,i} \end{pmatrix}.$$

Then, the equivalent transition probability matrix T for n-cascaded binary symmetric channel (BSC)s can be evaluated as $T = \prod_{i=1}^{n} T_i$ to yield

$$T = \frac{1}{2}\begin{pmatrix} 1+\prod_{i=1}^{n}(1-2p_{e,i}) & 1-\prod_{i=1}^{n}(1-2p_{e,i}) \\ 1-\prod_{i=1}^{n}(1-2p_{e,i}) & 1+\prod_{i=1}^{n}(1-2p_{e,i}) \end{pmatrix}.$$

Therefore, the effective cross-over probability P_e is given as

$$P_e = \frac{1}{2}\left(1-\prod_{i=1}^{n}(1-2p_{e,i})\right).$$

$\sim$

Appendix D

Proofs for Chapter 7

D.1 Proof of Theorem 7.1

As λ varies from $-\infty$ to ∞, P_f varies from 1 to 0. Therefore, the area under P_d versus P_f curve can be written as

$$\begin{aligned}\mathcal{A} &= \int_{0}^{1} \frac{1}{2}\text{Erfc}\left(\frac{\sigma_0}{\sigma_1}\text{Erfc}^{-1}(2x) - \frac{m_1 - m_0}{\sqrt{2}\sigma_1}\right) \mathrm{d}x \\ &= \int_{-\infty}^{+\infty} \frac{1}{2}\text{Erfc}\left(\frac{\sigma_0}{\sigma_1}z - \frac{m_1 - m_0}{\sqrt{2}\sigma_1}\right) \frac{e^{-z^2}}{\sqrt{\pi}} \mathrm{d}z\end{aligned} \tag{D.1}$$

where the second equality comes after substituting $z = \text{Erfc}^{-1}(2x)$. Moreover, by using $\text{Erfc}(x) = \frac{2}{\sqrt{\pi}}\int_x^\infty e^{-w^2}\,\mathrm{d}w$, and with some algebraic manipulations, (D.1) can be re-written as

$$\mathcal{A} = \frac{1}{\pi}\int_{-\infty}^{+\infty}\int_{\frac{\sigma_0}{\sigma_1}z - \frac{m_1-m_0}{\sqrt{2}\sigma_1}}^{+\infty} e^{-(w^2+z^2)}\,\mathrm{d}w\,\mathrm{d}z.$$

Now, clockwise rotation to the (w, z) axis through angle θ is applied to generate the (u, v) axis, which is also equivalent to $\begin{bmatrix} u \\ v \end{bmatrix} = \begin{bmatrix} \cos\theta & -\sin\theta \\ \sin\theta & \cos\theta \end{bmatrix} \begin{bmatrix} w \\ z \end{bmatrix}$ axis transformation where $\tan\theta = \frac{\sigma_0}{\sigma_1}$. This result gives

$$\mathcal{A} = \frac{1}{\sqrt{\pi}}\int_{-\infty}^{+\infty} e^{-u^2}\,\mathrm{d}u \frac{1}{\sqrt{\pi}}\int_{-\frac{m_1-m_0}{\sqrt{2(\sigma_0^2+\sigma_1^2)}}}^{+\infty} e^{-v^2}\,\mathrm{d}v = \frac{1}{2}\text{Erfc}\left(-\frac{m_1 - m_0}{\sqrt{2(\sigma_0^2+\sigma_1^2)}}\right), \tag{D.2}$$

where the second equality is due to the fact that $\frac{1}{\sqrt{\pi}}\int_{-\infty}^{+\infty} e^{-u^2}\,\mathrm{d}u = 1$ and the definition of the Erfc$(\cdot)$ function. (7.11) can be obtained from (D.2) by using Erfc$(-x) = 2 - $ Erfc(x).

D.2 Optimal Threshold for AWGN Channel

For the optimal threshold, $\lambda^* = \arg\min_{\lambda} P_e(\lambda)$ is achieved when $\frac{\partial P_e(\lambda)}{\partial \lambda} = 0$. With the aid of (2.23), and $\frac{\partial}{\partial x}\text{Erfc}\left(\frac{x-a}{b}\right) = -\frac{2e^{-\frac{(x-a)^2}{b^2}}}{b\sqrt{\pi}}$, it can be written

$$\frac{\partial P_e(\lambda)}{\partial \lambda} = \frac{e^{-\frac{(\lambda - N(1+\gamma)\sigma^2)^2}{2N(1+2\gamma)\sigma^4}}}{\sqrt{2\pi N(1+2\gamma)\sigma^2}} - \frac{e^{-\frac{(\lambda - N\sigma^2)^2}{2N\sigma^4}}}{\sqrt{2\pi N\sigma^2}} = 0. \tag{D.3}$$

After some algebraic manipulations and taking the logarithm, (D.3) can be simplified into a quadratic equation of λ as

$$\lambda^2 - N\sigma^2\lambda - \frac{N\sigma^4}{2}\left(N\gamma + \frac{(1+2\gamma)\ln(1+2\gamma)}{\gamma}\right) = 0. \tag{D.4}$$

Thus, the solution for λ is given in (7.18) (here the negative root of (D.4) is omitted since $\lambda \geq 0$).

The second-order derivative of $P_e(\lambda)$ is given as

$$\frac{\partial^2 P_e(\lambda)}{\partial \lambda^2} = \frac{(\lambda - N\sigma^2)e^{-\frac{(\lambda - N\sigma^2)^2}{2N\sigma^4}}}{\sqrt{2\pi}N^{3/2}\sigma^6} - \frac{(\lambda - N(1+\gamma)\sigma^2)e^{-\frac{(\lambda - N(1+\gamma)\sigma^2)^2}{2N(1+2\gamma)\sigma^4}}}{\sqrt{2\pi}N^{3/2}\sigma^6(1+2\gamma)^{3/2}}. \tag{D.5}$$

It can be shown that $\frac{\partial^2 P_e(\lambda)}{\partial \lambda^2}|_{\lambda=\lambda^*} > 0$ at low SNR when λ_e^* is given in (7.18). Therefore, there is a minimum point of $P_e(\lambda)$ at $\lambda = \lambda_e^*$ for $\lambda \geq 0$.

$\sim$